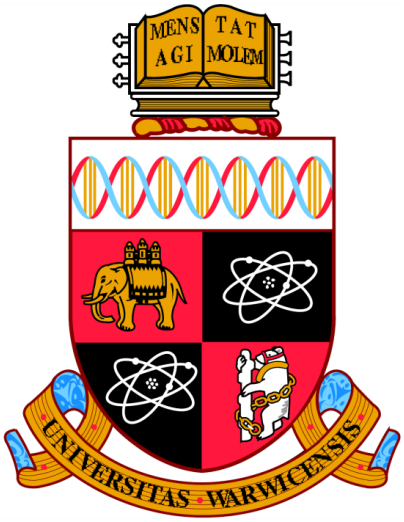

Superacid-based Passivation for Accurate Measurements of Bulk Carrier Lifetime in Silicon Wafers

by

Alex Ivan Pointon

A thesis submitted to the University of Warwick

for the degree of

Doctor of Philosophy in Engineering

Supervised by

Prof John D. Murphy & Dr Nicholas E. Grant

September 2022

Table of Contents

List of Tables

List of Figures

Declaration

I declare that this thesis contains an account of my research carried out at the University of Warwick between September 2016 and September 2022 under the supervision of Prof John D. Murphy and Dr Nicholas E. Grant. The research reported here has not been submitted, either wholly or in part, in this or any other academic institution for admission to a higher degree.

Abstract

This thesis investigates the treatment of silicon surfaces by the superacid bis(trifluoromethane)sulfonimide (TFSI). The aim is to develop high quality surface passivation with sufficient longevity for reliable use in the determination of accurate bulk carrier lifetimes in silicon wafers, particularly those used for solar cells.

The role of the solvent was first investigated and it was found that TFSI in hexane provides improved temporal stability, better passivation and improved solution longevity compared to solvents used previously. Sample storage conditions, particularly humidity, were found to strongly influence the passivation stability. The optimised TFSI-hexane passivation scheme was applied to a set of 3 Ωcm *n*-type wafers, and, at 10^{15} cm^{-3} injection, the best-case effective surface recombination velocity is 0.69±0.04 cm s^{-1}, with bulk lifetimes measured up to the intrinsic lifetime limit at high injection and > 43 ms at lower injection.

To elucidate the mechanisms of passivation, others solutions based on molecules containing a triflyl group, like TFSI, were used to passivate silicon. The study shows that the presence of CF_3SO_2 groups and not the solution's superacidity is critical for passivation, opening up the possibility of using the new solutions on materials more sensitive to acidic environments. Kelvin probe measurements established that the mechanism of passivation comprises both chemical and field effect passivation (from a negatively charged thin film).

Finally, the role of the silicon surface preparation was investigated. Lifetime measurements showed clean silicon surfaces can be temporarily passivated by a short treatment in both HF(2%):HCl(2%) and HF(50%) solutions. XPS and AFM showed treatment with strong HF solutions result in a roughened fluorine-terminated surface. Subsequent superacid-derived surface passivation on the different chemically-treated surfaces show considerably better passivation on surfaces treated with HF(2%) : HCl(2%) compared with HF alone, highlight the importance of surface pre-treatment in the creation of high quality functionalised surfaces.

Abbreviations

DCE	1,2-dichloroethane
AlOx	Aluminium Oxide
AFM	Atomic Force Microscopy
ALD	Atomic Layer Deposition
TFSI	Bis(trifluoromethanesulfonyl)imide
c-Si	Crystalline Silicon
DCM	Dichloromethane
FTIR	Fourier-transform infrared spectroscopy
HF	Hydrogen Fluoride (aq)
a-Si:H	Hydrogenated Amorphous Silicon
IBC	Interdigitated Back Contacted
IPA	Isopropanol
KP	Kelvin Probe
LED	Light Emitting Diode
MOSFET	Metal Oxide Semiconductor Field-Effect Transistor
NMR	Nuclear magnetic resonance
PERC	Passivated Emitter Rear Cell
PCD	Photoconductance Decay
PL	Photoluminescence
PV	Photovoltaic
PECVD	Plasma Enhanced Chemical Vapour Deposition
QSS	Quasi-Steady-State
QSS-PC	Quasi-Steady-State Photoconductance
RCA	Radio Corporation of America
RTO	Rapid Thermal Oxidation
RTO	Rapid Thermal Oxidation
SAM	Self Assembled Monolayer
SRH	Shockley-Read-Hall
SiNx	Silicon Nitride
SiOx	Silicon Oxide

sc-Si	Single Crystalline Silicon
SA	Superacid
SRV	Surface Recombination Velocity
TMAH	Tetramethylammonium hydroxide
TMAH	Tetramethylammonium Hydroxide
XPS	X-ray photoelectron spectroscopy

List of Publications

First author papers published as a direct result of the research in this thesis:

- A. I. Pointon, N. E. Grant, E. C. Wheeler-Jones, P. P. Altermatt, and J. D. Murphy, Superacid-derived surface passivation for measurement of ultra-long lifetimes in silicon photovoltaic materials. Solar Energy Materials and Solar Cells, 2018. 183: p. 164-172. [1]

- A. I. Pointon, N. E. Grant, R. S. Bonilla, E. C. Wheeler-Jones, M. Walker, P. R. Wilshaw, C. E. J. Dancer, and J. D. Murphy, Exceptional Surface Passivation Arising from Bis(trifluoromethanesulfonyl)-Based Solutions. ACS Applied Electronic Materials, 2019. 1(7): p. 1322-1329. [2]

- A. I. Pointon, N. E. Grant, S. L. Pain, J. T. White, and J. D. Murphy, Sub-2 cm/s passivation of silicon surfaces by aprotic solutions. Applied Physics Letters, 2020. 116(12): p. 121601. [3]

- N. E. Grant, A. I. Pointon, R. Jefferies, D. Hiller, Y. Han, R. Beanland, M. Walker, and J. D. Murphy, Atomic level termination for passivation and functionalisation of silicon surfaces. Nanoscale, 2020. 12(33): p. 17332-17341. [4]

Papers contributed towards and published during the period of study for this thesis:

- J. D. Murphy, A. I. Pointon, N. E. Grant, V. A. Shah, M. Myronov, V. V. Voronkov, and R. J. Falster, Minority carrier lifetime in indium doped silicon for photovoltaics. Progress in Photovoltaics: Research and Applications, 2019. 27(10): p. 844-855. [5]

- M. Al-Amin, N. E. Grant, A. I. Pointon, and J. D. Murphy, Iodine–Ethanol Surface Passivation for Measurement of Millisecond Carrier Lifetimes in Silicon Wafers with Different Crystallographic Orientations. physica status solidi (a), 2019. 216(17): p. 1900257. [6]

- N. E. Grant, J. R. Scowcroft, A. I. Pointon, M. Al-Amin, P. P. Altermatt, and J. D. Murphy, Lifetime instabilities in gallium doped monocrystalline PERC silicon solar cells. Solar Energy Materials and Solar Cells, 2020. 206: p. 110299. [7]

Chapter 1 Introduction

The ever increasing global demands placed on electrical energy, means that the output of greenhouse gasses, particularly CO_2, continues to increase year on year due to the widespread use of fossil fuels for generation [8]. At the same time governments are setting ever-stringent targets on the reduction of CO_2 production in order to prevent global warming. Renewable energy sources are being focused on, to bridge the gap between the demand for the needed electrical energy supply and reduction in greenhouse gas output. As part of a wide array of sources of renewable energy, the use of photovoltaics is becoming greater than ever and their market share continues to grow at an extreme rate each year [9].

Silicon based photovoltaic (PV) devices convert sunlight directly into usable electrical energy; the absorbed incident photons from the sun excite electrons from the valence band to the conduction band in the semiconductor material, generating a free electron-hole pair. This electron-hole pair can then be extracted from the material to produce externally available electrical power. As the sun currently provides the earth with around 10,000 times the present energy demand daily [10], this gives PV the potential to be an almost limitless source of cheap, environmentally friendly, carbon free electricity.

Despite the market for photovoltaics continuing to grow at a rapid pace [9], there are still challenges that need to be overcome in order to ensure this trend continues. For a long time photovoltaic generated electricity has been an expensive source of energy when compared with most forms of traditional fossil fuel based electricity generation [11, 12]. In order to compete on a larger scale the production costs must be brought to the level of other more traditional electrical generation methods. As silicon based technologies are now a mostly well understood, proven, reliable technology, and the materials used in the manufacture are naturally abundant and non-toxic, silicon photovoltaics are expected to remain the dominant solar cell technology [13].

1.1 Motivation

Photovoltaic (PV) cells are playing an ever-greater role in today's global energy network, as the focus is increasingly turning to cleaner, emission-free electricity production. The significance of the use of solar cells for energy production is substantial with several countries posting penetration rates above 10%[8].

In 2022 the total global PV capacity surpassed the 1,185 GW_{peak} mark (≈ 1,2 TW)[8], generating over 50% of generation from new renewable capacity and avoiding approximately 1,399 Mt of annual CO_2 emissions. The trends in PV energy capacity from 2015 to 2021 are presented in Figure 1.1.

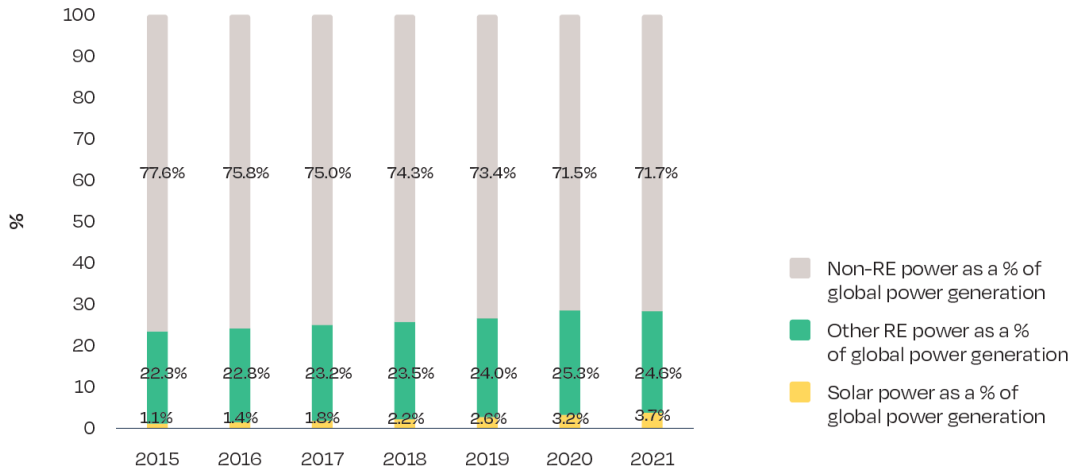

Figure 1.1 – Solar renewable power generation and capacity as a share of total global power generation for the years 2015 to 2021. Reproduced from reference [9].

Despite this dramatically increasing market [9], worldwide solar power generation still only makes up just 3.7% of all electricity generating capacity [14]. This is mainly due to the high initial costs of photovoltaic panels, meaning that traditional mechanically generated power can still often cheaper (before any government subsidy). This means that it is still a highly active ongoing area of research, looking to both lower the production costs of the cells and increase their efficiencies for greater outputs. Continuing research to overcome the drawbacks is well justified. Advances to increase the efficiencies of the technology, to reduce the cost per kWh of the generated electrical power, and greater cost reductions in the manufacture of the solar cells are essential to ensure solar generated electricity remains financially competitive.

In recent years due to continued research the industry has realised improved silicon ingot growth processes [15] and improved contamination control during cell fabrication processes has resulted in the bulk quality of silicon wafers being improved to the point that further device

advances are now reliant upon new innovative interface passivation technologies for improving efficiencies [16].

The requirement for higher efficiency solar cells is also driving industry into adopting different, better performing architectures [16]. The passivated emitter rear cell (PERC) [17] and the interdigitated back contacted (IBC) cell, which are some of the most promising cell designs for high efficiencies in PV in the coming decades [18]. The performance of these architectures are reliant on high quality passivation of the front and back wafer surfaces, as the cell efficiency of these architectures are strongly dependant on the passivation quality [16, 17, 19].

The efficiency in silicon solar cells is now often limited by the surface recombination of photo-generated carriers and this is one of the largest charge loss mechanisms in high efficiency solar cells.

One route towards future generations of lower cost plus higher efficiency PV cells is via improved surface passivation treatments. Silicon wafer surface passivation through the use of room temperature, solution processed, organic techniques is a relatively new area of research, and relatively little information is known on its mechanisms or abilities. In order to expand the possibilities for future high efficiency PV systems alternative surface passivation methods that do not require complex vacuum systems or high temperature steps are required due the costs and time involved. The aim of this thesis is to investigate whether excellent surface passivation can be achieved using organic solutions at low temperatures, for use in solar cell material testing, such as bulk lifetime characterisation. Whilst these processes currently afford only temporary passivation, the long-term aim of this research field, is to turn these short-term techniques into permanent passivation methods, with the potential to have a significant impact on the operational costs of manufacture.

1.2 Thesis Outline

The goal of this thesis is to study and improve the passivation levels and stability of organic solution-processed passivation methods, while developing a scientific understanding of the underlying mechanisms involved, in the hope of stabilising the techniques so they may able to be included at device level. A series of comprehensive studies were performed and the following outlines the information presented in this thesis.

Chapter 2 presents a brief explanation of the quantification of the quality of surface passivation and then reviews the current permanent passivation techniques used by industry in the production of silicon-based solar cells. This chapter then reviews the current state of the field of temporary low temperature silicon surface passivation including the organic solution-processed techniques being researched in this thesis.

In chapter 3, the key techniques required to characterise the quality of the passivating films are described, including the methods needed to accurately assess the surface recombination velocity of silicon wafers. The working principles behind the characterisation tools including contactless minority carrier lifetime measurements are also discussed. This chapter also includes outlines of all the techniques used in the characterisation of the solutions and films presented in this thesis including, X-ray photoelectron spectroscopy (XPS), nuclear magnetic resonance (NMR), liquid and surface based Raman microscopy and Fourier-transform infrared spectroscopy (FTIR).

Chapter 4 presents an empirical study of effects on superacid-derived passivation, including solvent dependence, storage humidity, ambient atmosphere degradation of the passivation scheme, degradation of the passivating solutions and research into the reproducibility of the chemical treatment. This provided initial understanding of how the passivation scheme could be improved and where to focus further research processes. The results presented in this Chapter are published in Reference. [1].

Chapter 5 describes the finding of several new passivating chemicals not previously reported and their effects on the properties of the surface passivation. The findings shown in this Chapter are published in Reference. [2].

Chapter 6 presents the research performed regarding the underlying surface physics, including the evolution and origin of the passivating species of the organic solution-based passivation treatments outlined in Chapter 6. The findings shown in this Chapter are published in Reference [4]

Chapter 7 summarises the key results from each chapter of the thesis, and outlines possible future avenues of research.

Chapter 2 Silicon Photovoltaic Surface Passivation Technologies

In this Chapter, some of the most common methods for surface passivation of silicon materials will be discussed, including the permanent passivation methods used industrially in the production of photovoltaic cells and the more temporary passivation methods used in laboratory settings in order to preserve the bulk properties of the material to enable accurate, fast and simple materials characterisation. Unless otherwise stated, for the purposes of this review the passivation of (100)-orientation silicon surfaces will be focused on and reported, as this is the monocrystalline silicon orientation of most interest to the silicon PV industry. Initially a short introduction section detailing the values used to quantify the levels of surface passivation will be presented.

2.1 Recombination and Carrier Lifetime in Silicon

Minority carrier lifetime is a key figure of merit for the silicon wafers used in the manufacture of photovoltaics; this is due to its effect on the potential cell efficiency, with increased carrier lifetimes generally leading to increased efficiencies in solar cells [20, 21]. Whilst a single value of carrier lifetime is often stated, more accurately the term refers to a complex parameter revealing much information about the overall quality of the sample undergoing measurement, and varies according to the doping level and type and also several other material parameters.

The carrier lifetime of a material falls into two categories: recombination lifetime and generation lifetime. When discussing lifetime values, the quantity being discussed is most often the recombination lifetime of excess minority carriers in the material caused by the decay in excess minority carriers due to recombination processes in the materials. These recombination effects can more generally be split into bulk and surface recombination [22], a brief overview of these is presented next. For a more in-depth review discussing the factors effecting recombination lifetime including the different recombination processes and the effect on lifetime they have please see references [23, 24].

2.1.1 Bulk Recombination

The recombination of minority carriers in the bulk of silicon semiconductors is generally based on the three following parameters:

- Radiative (band to band) recombination [25-27]
- Auger recombination [28-31]
- Shockley-Read-Hall recombination [32, 33]

In the bulk of a uniformly doped semiconductor the recombination lifetime is composed of the lifetime of the decay of excess carriers as a result of carriers recombining through all these processes, each having its own associated lifetime. A simplified band diagram is presented in Figure 2.1 outlining the pathways of each recombination method.

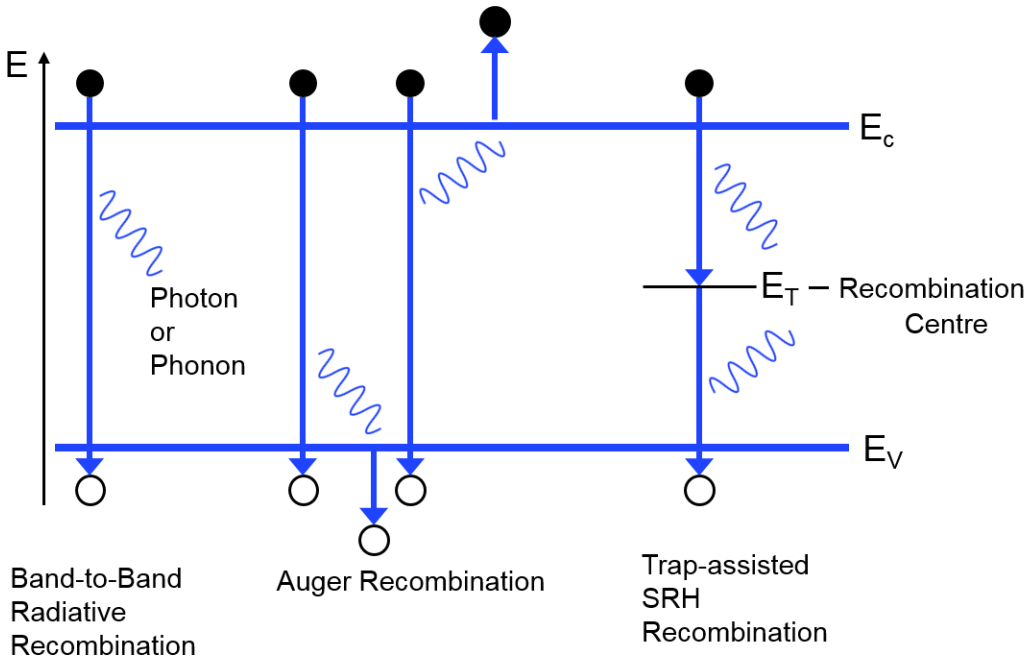

Figure 2.1 - A simplified energy band diagram showing the main carrier recombination processes in the bulk of a semiconductor material.

The average minority carrier lifetime in the bulk of the material (τ_{Bulk}) is made up of a combination of radiative (band-to-band) recombination lifetime (τ_{Rad}), Auger recombination lifetime (τ_{Auger}) and Shockley-Read-Hall recombination lifetime (τ_{SRH}) leading to the relation Equation 2.1.

$$\frac{1}{\tau_{Bulk}} = \frac{1}{\tau_{Rad}} + \frac{1}{\tau_{Auger}} + \frac{1}{\tau_{SRH}} \qquad \text{Equation 2.1}$$

Radiative (band-to-band) recombination occurs when free electrons from the conduction band directly recombine with a hole in the valence band, releasing the excess energy as a photon [25, 26]. This process does not require the presence of a phonon. As this produces light this can be a useful analysis technique (photoluminescence imaging tools and light emitting diodes - LEDs - rely on this phenomenon). This recombination mechanism dominates in direct band gap semiconductors. However as most current solar cells are made of from silicon which is an indirect band gap semiconductor, the lifetime of radiative recombination is very large - much bigger than recombination times from other effects - so can often be neglected [31].

Auger recombination is a process involving three carriers, where a conduction band electron and valance band hole combine giving the excess energy to a free hole or electron instead of releasing the excess as heat in the form of phonons or photons (light) [30]. In *n*-type materials the resulting energy is usually given to an electron raising further it into the conduction band (eeh), where as in *p*-type materials the energy is usually given to a hole which is forced lower into the valence band (ehh) [34]. Both types of carriers should eventually return to their original positions due to thermionic emission or the Auger electron could escape.

As Auger recombination relies on carrier interaction, it dominates in materials with high concentrations of free carriers (in heavily doped materials), longer recombination lifetimes or under high carrier injection levels when using light based measurement techniques [30].

Shockley-Read-Hall (SRH) recombination is a process caused by defects in semiconductor materials [32, 33]. It is a two-step process that occurs through defect interactions, and can occur even in a 100% pure material through intrinsic material defects (e.g. via the silicon divacancy [35]). For carriers to recombine via SRH first an electron (or hole) is trapped by an energy state in the forbidden region (which is introduced through defects in the crystal lattice structure). Then if a hole (or electron) moves to the same energy level (defect) before the first has had a chance to be thermally excited out of the level they will recombine. The rate of this recombination effect is determined by the distance of the defects energy level from either the conduction or valence band edge. If the defect state is close to either edge there is less chance of recombination, as for example an electron is more likely to be thermally excited back into the conduction band, rather than a hole being excited into the forbidden state to recombine with the electron that is in that state.

The recombination lifetime is measured through the analysis of the excess carrier density and the recombination rate experienced by the carriers in the material. That can be represented by Equation 2.2.

$$\tau = \frac{\Delta n}{U} \qquad \text{Equation 2.2}$$

Where τ is the minority carrier lifetime, Δn is the excess carrier concentration and U is the recombination rate. As discussed previously, the recombination rate in crystalline silicon is dependent on several summative recombination processes. The total recombination rate is therefore the sum of all the individual recombination processes and thus is expressed by Equation 2.3.

$$U_{eff} = U_{Radiative} + U_{Auger} + U_{SRH} + U_{Surface} \qquad \text{Equation 2.3}$$

The combined effects of all bulk and surface recombination result in an effective measured lifetime (τ_{eff}) which can be represented by Equation 2.4.

$$\frac{1}{\tau_{eff}} = \frac{1}{\tau_{Radiative}} + \frac{1}{\tau_{Auger}} + \frac{1}{\tau_{SRH}} + \frac{1}{\tau_{Surface}} \qquad \text{Equation 2.4}$$

This can be simplified into bulk and surface effects in wafers, represented by Equation 2.5.

$$\frac{1}{\tau_{eff}} = \frac{1}{\tau_{Bulk}} + \frac{1}{\tau_{Surface}} \qquad \text{Equation 2.5}$$

As discussed, there are various recombination mechanisms within a uniformly doped semiconductor. The recombination of the carriers can be calculated using theoretical models; using the improved 2022 parameterisation of Niewelt *et al.*[29] to model Auger recombination, and Nguyen *et al.* [27] to model the effects of radiative recombination. The graph presented in Figure 2.2 shows the limitations on the measurable lifetime in bulk silicon, due to the recombination mechanisms outlined above. The values are representative of the *n*-type (phosphorus doped) silicon wafers used in this study, with a nominal resistivity of 5 Ωcm.

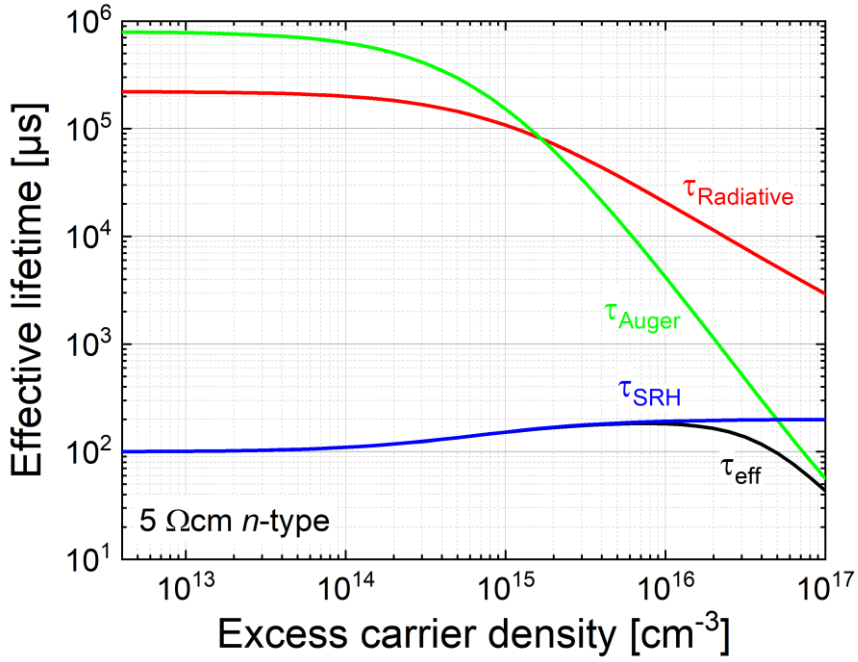

Figure 2.2 - Typical curves of effective carrier lifetime as a function of injection level, due to the variety of bulk recombination mechanisms in silicon; the intrinsic Auger and radiative recombination, as well as Shockley-Read-Hall. The modelled data is based on n-type silicon, with a nominal resistivity of 5 Ωcm.

2.1.2 Surface Recombination

In addition to the recombination mechanisms in the bulk of silicon semiconductors, the surfaces also play a very important part in the overall recombination rate as carrier recombination can also occur here [36].The surface of silicon is an area of high defect concentration, due to the disruption in the crystal lattice causing the presence of dangling bonds. As impurities or defects in semiconductors strongly increase recombination, recombination rates at the surface are also very high. Surface recombination effects complicate lifetime measurements, as during investigation of material properties it is the value of lifetime in the bulk of the material that is important.

Recombination at the surface is limited by the rate at which minority carriers are able to move towards the surface of the material. The parameter used to specify surface recombination is known as the surface recombination velocity (*S*). Through the use of suitable surface treatments, it is possible to electrostatically shield the charge carriers from the surface interface (field-effect passivation), and to tie up dangling bonds at the surface boundary, significantly reducing the

surface recombination rates. Surface recombination can be reduced to negligible levels by using suitable surface treatments. As this investigation is looking into passivating treatments, surface recombination will be our main focus.

2.1.3 Intrinsic Lifetime Limit

On some graphs presented in this thesis, an intrinsic lifetime limit has been calculated and presented alongside the experimental data. This shows the maximum theoretical carrier lifetime in the given material, to help visually represent the quality of the passivation level achieved.

The doping dependent intrinsic lifetime limits have been plotted on graphs using the advanced parameterisation presented in Ref. [28] to show the fundamental limits of the minority carrier lifetime in each case.

In order to calculate the overall effect of intrinsic lifetimes in this study the following enhanced model [28] has been used, with lifetimes calculated using Equation 2.6.

$$\tau_{intr,enh} = \frac{\Delta n}{(np)(2.5 \times 10^{-31} g_{eeh} n_0 + 8.5 \times 10^{-32} g_{ehh} p_0 + 3.0 \times 10^{-29} \Delta n^{0.92} + B_{low})}$$

Equation 2.6

Where *n* and *p* are concentrations of electrons and holes in the semiconductor, n_0 and p_0 are the density of electrons and holes at equilibrium, Δn is the excess carrier density, and $B_{low} = 4.73 \times 10^{-15}$ $cm^3 s^{-1}$ [26] is the radiative recombination coefficient for lowly doped and lowly injected silicon.

The enhancement factors g_{eeh} and g_{ehh} are given by Equation 2.7 and Equation 2.8.

$$g_{eeh}(n_0) = 1 + 13\left\{1 - \tanh\left[\left(\frac{n_0}{N_{0.eeh}}\right)^{0.66}\right]\right\} \qquad \text{Equation 2.7}$$

$$g_{ehh}(p_0) = 1 + 7.5\left\{1 - \tanh\left[\left(\frac{p_0}{N_{0.ehh}}\right)^{0.63}\right]\right\} \qquad \text{Equation 2.8}$$

Where $N_{0,eeh} = 3.3 \times 10^{17}$ cm^{-3} and $N_{0,ehh} = 7.0 \times 10^{17}$ cm^{-3}.

2.2 Measurement of Carrier Lifetime

Although the fundamentals of carrier lifetime in silicon are complex, performing the measurements to evaluate the minority carrier lifetime is relatively simple. Several different techniques exist for determination of the carrier lifetime in semiconductors – particularly in silicon [37, 38]. Technique types can be separated by time dependence, the method of illumination and the method of measurement of excess carrier density. One of the most common methods is to use contactless photoconductance decay (PCD) methods [39, 40], which can itself be split into two techniques; the transient technique and the quasi-steady-state photoconductance method (QSS-PC).

The photoconductance decay measurement techniques employed with the Sinton series of tools used within this study, use a flash lamp to generate electron hole pairs in the semiconductor material. The wafer is placed in close proximity to an eddy current sensor, so that it is inductively coupled to it, that enables contactless determination of the change in conductance of the material, as a function of illumination intensity [40, 41]. For QSS mode measurements the illumination intensity is also measured using a photodiode, mounted next to the wafer sample from which the generation rate (G) can be calculated.

When measuring samples with higher carrier lifetimes the transient method is used, which relies on the decay of carriers over time. For accurate results, the lifetime must be much longer than the pulse of the flash lamp which is used to inject carriers into the sample. As the minimum decay time for the flash lamp of the WCT-120 is roughly 30 μs this is limited to samples with lifetimes generally over approximately 200 μs. Using this method carriers are generated by a very short pulse of light and the decay of the carrier density is then measured over time. The longer the minority carrier lifetime the longer it takes for the carriers to decay back to equilibrium.

When measuring samples with lower lifetimes below approximately 200 μs, the QSS-PC method is generally used [41]. If a steady-state illumination method were to be used, then the sample being tested would suffer from heating which would change the lifetime of the semiconductor [37]. In order to avoid this, a quasi-steady-state method was first introduced by Sinton *et al.* [41]. During the QSS-PC test, the sample is flashed with a slowly decaying pulse of light in order to keep the recombination processes in the material in a quasi-steady-state, so that carrier populations can be assumed to be in steady-state where the minority carrier generation and

recombination rates are in balance. The generation rate is then calculated by measuring the amount of light falling onto the cell and then corrected for the reflectivity and the absorption coefficient of the Silicon wafer. In order for this process to be valid the decay constant of the flash needs to be more than 10 times slower than the carrier lifetime of the sample, which is why it is generally only valid for short carrier lifetimes [40, 41]. Both of the above photoconductance decay methods are the limiting circumstances for the general equation given by Equation 2.9 [42].

$$\tau_{eff} = \frac{n(t)}{G(t) - \frac{dn(t)}{dt}} \qquad \text{Equation 2.9}$$

Where n(t) is the time dependent excess minority carrier density in the wafer, G(t) is the generation rate of carriers, and τ_{eff} is the measured effective carrier lifetime.

When performing transient measurements only a short pulse of light is used to initially excite the carriers and is not on during the measurement, therefore G(t) = 0. This then simplifies to Equation 2.10.

$$\tau_{eff} = -\frac{\Delta n}{\frac{d(\Delta n)}{dt}} \qquad \text{Equation 2.10}$$

Which leads to the relation between lifetime and excess carrier density expressed in Equation 2.11.

$$\tau_{eff} = -\frac{\tau}{\ln(\Delta n)} \qquad \text{Equation 2.11}$$

In the case of QSS-PC measurements, is it assumed that the light is varying so slowly that $d(\Delta n)/dt = 0$ so that the equation becomes that presented in Equation 2.12.

$$\tau_{eff} = \frac{\Delta n}{G(t)} \qquad \text{Equation 2.12}$$

The minority carrier lifetime is determined as a function of the injection level of the carriers at specified injection levels, using these techniques it is possible to measure a large range of carrier lifetimes, from as low as 0.1 μs to tens of milliseconds [37].

2.3 Surface Recombination Velocity

The effective lifetime (τ_{eff}) of passivated silicon wafers is often presented in order to help quantify the levels of surface passivation achieved by the chosen method. In some circumstances, however, this can be misleading because the value of lifetime does not take into account the sample thickness (W) or wafer doping (N_{dop}) of each measured sample, which can greatly change the value of τ_{eff} measured. In order to quantify the effectiveness of surface passivation accurately, the value of surface recombination velocity (S) is used instead of τ_{eff}. This takes into account variations in both doping type and doping level, and also sample thickness.

Surface recombination velocity can be defined as the rate of recombination through surface defects; this strongly depends on the surface preparation and surface passivation method chosen.

The lifetime of recombination at material surfaces is denoted by surface lifetime $\tau_{Surface}$, and is a function of the surface recombination velocities ($S_1 + S_2$) at each surface, the thickness of the semiconductor material W, and the minority carrier diffusivity *D* [43-45]. The approximate solution [44] is given by the equation Equation 2.13.

$$S = \sqrt{D\left(\frac{1}{\tau_{eff}} - \frac{1}{\tau_{Bulk}}\right)} \tan\left[\frac{W}{2}\sqrt{D\left(\frac{1}{\tau_{eff}} - \frac{1}{\tau_{Bulk}}\right)}\right] \qquad \text{Equation 2.13}$$

where $\tau_{Surface}$ can be split into effects from the front and back surfaces of the wafers

$$\frac{1}{\tau_{Surface}} = \frac{S_{Front}}{W} + \frac{S_{Back}}{W} = \frac{1}{\tau_{eff}} - \frac{1}{\tau_{Bulk}} \qquad \text{Equation 2.14}$$

The two most common situations are materials with two identical surface recombination velocities or where the surfaces have been passivated to remove the dangling bonds at the surface. If the surfaces are identical ($S = S_1 = S_2$) the solution to the equation [45] is given by Equation 2.15.

$$\tau_{Surface} = \frac{W}{2S} + \frac{1}{D}\left(\frac{W}{\pi}\right)^2 \qquad \text{Equation 2.15}$$

If the surfaces are perfectly passivated ($S = S_1 = S_2 = 0$), then the solution to the equation [45] is given by Equation 2.16.

$$\tau_{Surface} = \infty \qquad \text{Equation 2.16}$$

2.4 Surface Passivation - Chemical vs. Field effect

There are two main complimentary approaches used to achieve surface passivation of silicon semiconductors: chemical and field-effect passivation [1].

Chemical passivation aims to reduce the level of recombination at the interfaces through optimising the surface properties, so as to reduce the surface interface state density (D_{it}). The method used to achieve this type of passivation is usually the deposition of a dielectric film on the surface of the silicon material – typically silicon nitride. By forming electron pairs between the Si interface and the passivating film ties up unpaired electrons at the silicon surface, dramatically reducing the number of silicon surface dangling bonds. This results in a reduction in Dit, and an accompanying decrease in surface recombination velocity.

The surface recombination rate ($U_{Surface}$) can also be reduced by decreasing the concentration of one of the two carrier concentrations at the surface of the material, typically the minority carrier. Field effect passivation achieves this by electrostatically shielding the generated charge carriers from the interface by an internal electric field in the material. This is often achieved by storing charge in an overlying film. The charges stored at the surface of the silicon interact with the charge carriers in the bulk of the material and induce a depletion or accumulation layer close to the crystalline silicon surface. If the charge density is great enough, it also has the possibility of creating an inversion layer at the silicon surface – this is dependant on the charge type (positive or negative) and the substrate type [46, 47]. Through these characteristics, the surface is able to repel the generated carriers from the silicon surface interface, reducing the ability of the carriers to recombine here and resulting in a reduction of the surface recombination velocity.

Surface passivation is becoming increasingly more important as the crystalline silicon-based PV industry moves toward lower substrate thicknesses – hence increasing the surface to volume ratio – in order to reduce costs. A decreased surface recombination velocity means higher carrier

lifetimes and thus higher efficiency cells. Next, some of the most common methods of surface passivation and the state of the field will be reviewed.

2.5 Permanent Dielectric Based Surface Passivation

Currently in the photovoltaics industry the most important materials used for surface passivation are silicon oxides (SiO_x), silicon nitride (SiN_x), aluminium oxide (AlO_x) and hydrogenated amorphous silicon (a-Si:H).

2.5.1 Thermal Silicon Oxide (SiO_x)

Traditionally, high quality surface passivation of crystalline silicon was achieved through the use of thermal oxidisations [48, 49]. This process typically occurs at temperatures greater than 800 °C [49]. However, thermally-processed oxides are falling out of favour largely due to the negative impacts on carrier lifetimes in the bulk of silicon material that can be associated with high temperature processing steps [50, 51]. Additionally, high temperature processing is expensive and acts to increase thermal budget of cell manufacturing.

Thermally-grown silicon oxides were one of the first and most universally used dielectric films for surface passivation of silicon, with research dating back to the 1960s in the integrated circuit industry [52] – originating from the development of metal oxide semiconductor field-effect transistors (MOSFETs) in the integrated circuit industry using silicon dioxide films (SiO_2) during the 1970s, before being applied to surface passivation of silicon for photovoltaics more recently. The properties of this film have been extensively researched and more in-depth summaries relating to its use in the context of the PV industry can be found in the following references [19].

One of the most successful passivation methods was reported by Kerr and Cuevas in 2001 [53]. By performing oxidations on silicon at 1050 °C, they were able to obtain extremely high-quality surface passivation of silicon. This resulted in exceptionally low values of SRV of 0.46 cm s^{-1} and 0.63 cm s^{-1} on *n*-type and *p*-type silicon, respectively [53].

The advantages of thermally-grown SiO_x for passivation are that it provides very effective passivation of both *n*-type and *p*-type silicon surfaces – meaning exceptionally low values of SRV are possible – and that the processing methods make it suitable for batch wafer processing which is valuable to the PV industry. The disadvantage of thermal SiO_x is that it requires very high temperatures (greater than 800 °C) [53] in order to provide good levels of surface passivation;

for the PV industry this greatly increases the fabrication cost of solar cells because of the large thermal budget. The high temperature steps involved in the processing limit the use of this technique to higher quality silicon, as there is a risk of degrading the bulk lifetime when processing lower quality silicon.

2.5.1.1 Rapid Thermal Oxidation (RTO)

In the 1980s, the thermal oxidation technique was improved upon with the use of rapid thermal oxidation systems [54]. These systems use halogen lamps to heat the material being processed rapidly. This process helped to reduce the fabrication cost over traditional furnace-based oxidation due to a lower overall thermal load and increased productivity due to reduced oxidation times. However, this method still requires processing steps at a very high temperature and can result in a poorer oxide uniformity.

The disadvantages offered by thermal SiO_x passivation methods resulted in a large effort being put into researching lower temperature passivation methods suitable for the PV industry. The most successful of these currently in use is plasma-enhanced chemical vapour deposition (PECVD).

2.5.2 Plasma Enhanced Chemical Vapour Deposition of Silicon Nitride (PECVD SiN_x)

The difficulties with high temperature thermal oxides led to the hunt for a lower temperature deposition technique, one of the most successful being plasma enhanced chemical vapour deposition (PECVD). Currently, plasma-enhanced chemical vapour deposition (PECVD) is one of the most widely used deposition techniques in the photovoltaic industry. The origins of the technique can be first dated back to 1963 when it was used to deposit silicon oxides [55].

PECVD systems are able to deposit a range of surface passivation treatments including SiN_x, SiO_x, a-Si:H and AlO_x [56] at temperatures from 200 °C to 500 °C. The development of this lower temperature deposition method enables very effective surface passivation treatments, the most notable of which is SiN_x; as this is the most common PECVD passivation treatment in use industrially, this will be focused upon here.

Surface passivation is achieved through PECVD deposition of SiN_x with ammonia (NH_3) and silane (SiH_4) precursor gases, often using argon (Ar) as a carrier gas. The deposition is performed at temperatures between 250 °C and 450 °C – much lower than thermal silicon oxidations.

Initial work on the properties of SiN_x as a passivation method for silicon was performed in the 1990s [57-59]; this initial research helped to set PECVD SiN_x as the go-to passivation method in the commercial production of silicon based solar cells. Throughout its history, PECVD SiN_x passivation has always been of very high quality, offering very low values of SRV (< 10 cm s^{-1}) [60, 61]. However, recent developments by Wan *et al.* [62, 63] showed that it was possible to obtain exceptionally low values of SRV using this technique, reporting SRV as low as 0.67 cm s^{-1} in *p*-type silicon and immeasurably low SRV in *n*-type silicon.

This technique is preferred by industry today for passivating silicon wafer surfaces for several reasons: it is performed at lower temperatures – which can reduce fabrication costs – and fast deposition rates can be achieved with high through put industrial inline PECVD systems whilst still providing exceptional levels of surface passivation. It is also a very good antireflection coating, which removes the need for an additional processing step during the manufacturer of photovoltaic cells. A significant problem with the technique is that, because it must be performed under vacuum, these complex systems add to setup and running costs. In addition, the gases used for the deposition are both toxic and have harmful effects on the environment; exhaust gases must be processed, which further increases the cost of this deposition method.

It should be noted that the results presented in laboratory situations might not always mirror those in industry. As the solar cell industry grows ever larger, there is a need for very large throughput systems, which may not be able to produce as high a quality passivation layer as can be produced using laboratory equipment.

2.5.3 Atomic Layer Deposition of Aluminium Oxide (ALD AlO_x)

A more recent technique introduced to the industry is atomic layer deposition (ALD) of dielectric thin films. This method has attracted significant attention recently and can be used to deposit many different thin films for passivation – the most popular of these are currently aluminium oxides. For a more in-depth review of the technique and the different dielectrics possible please see review reference [19]. Here it will be discussed relating to the deposition of

aluminium oxide (AlO_x) as this appears currently to be the most promising alterative passivation material.

Plasma-assisted ALD was developed in order to enable the deposition of dielectric thin films at lower temperatures (< 400 °C), with the ability to precisely control the parameters of the deposition over large surface areas, resulting in excellent passivation uniformity [46].

Atomic layer depositions are performed under vacuum, in a reaction chamber with accurate control of the substrate temperature. The film is deposited by exposing the silicon substrate to precursor gases in millisecond pulses; for example ALD deposition of AlO_x most commonly uses trimethylaluminium (TMA) gas as the precursor. By cycling the precursor and carrier gases, an AlO_x layer is formed in a self-limiting layer-by-layer growth [46]. The desired layer thickness is very accurately controlled by the number of deposition cycles.

The main breakthrough for AlO_x came in 2006 when Hoex *et al.* [64] and Agostinelli *et al.* [65] reported aluminium oxide films deposited using the atomic layer deposition. These initial films achieved SRVs lower than 10 cm s^{-1} in both *n*-type and *p-type* silicon substrates, making them of great interest to the photovoltaics industry. Slightly later these results were improved upon by Hoex *et al.* [66] in 2008 when they reported SRV values below 2 cm s^{-1} on both *n*-type and *p*-type silicon.

ALD-deposited layers of AlO_x can provide extremely high levels of surface passivation; the best performing AlO_x passivation to date was reported by Richter *et al.* [28] using plasma-enhanced ALD, resulting in exceptionally low SRV of 0.26 cm s^{-1} and 0.95 cm s^{-1} on *n*-type and *p*-type silicon, respectively.

The ALD deposition of AlO_x has several advantages: depositions can be performed at lower temperatures (less than 400°C) compared to other passivating materials. The ALD technique allows the precise control of the thickness of the passivating layer and results in high film uniformity available over large surface areas. However, the ALD process has a very slow deposition rate resulting long deposition times, as the method deposits the films a single monolayer at a time. The deposition is performed under a vacuum like PECVD – this increases equipment complexity and cost. Moreover, expensive – and often toxic – precursor gases are used in the deposition process which further increases processing costs. Additionally, a key step for AlO_x passivation is often a post-deposition elevated temperature anneal (around 350 °C to

450 °C) in order to "activate" the passivation [46], which may result in a degradation in the lifetime of the samples.

All of the discussed techniques can offer excellent levels of surface passivation for silicon substrates. However due to the elevated temperatures involved in the growth of thermal oxides and deposition of dielectrics, the processing can modify the properties in the bulk of the material being analysed.

2.6 Temporary Surface Passivation

Heat treatments are undesirable when looking to characterise materials because of the possibility of affecting the bulk lifetime of the material under analysis. For this reason, low temperature processes are an important development for material characterisation. Room temperature temporary passivation by wet chemical treatment provides a quick solution for passivating silicon surfaces to enable measurements to be performed with reduced influence from recombination at the surface. In this review the more established temporary passivation schemes will be discussed; for a more in depth review please refer to reference [67].

Of the more established temporary passivation schemes, the techniques can largely be separated into two categories. The first are liquid immersion-based passivation schemes, where the silicon must be constantly immersed in the passivating solution whilst measurements are performed, and the passivation is mostly either reduced or lost once the silicon is removed from the solution. The other are thin film-based passivation methods where, once applied, the passivation is generally stable on the surface for a limited period of time.

2.6.1 Liquid Immersion Passivation

Several liquid immersion passivation techniques exist and three of the most common will be reviewed here.

2.6.1.1 Acid Based Passivation Treatment

Several acids have been found to offer some passivation to the surfaces of silicon including sulphuric acid (H_2SO_4), and hydrochloric acid (HCI) [68]. However, as hydrofluoric acid (HF)-based passivation is the most heavily researched, this will be the focus of this review.

2.6.1.1.1 HF Passivation

It has long been known that HF etching of silicon terminates the dangling bonds at the surface [68, 69], leaving behind a hydrogen terminated surface [70]. This property makes HF particularly effective at temporarily passivating silicon surfaces and research has been performed using HF to passivate the surface of silicon since the 1980s.

The most commonly-reported procedure is to fully immerse the silicon surfaces to be measured in a concentrated HF solution in order to take measurements; this is generally performed in a sealed container or in an extracted fume hood. As far back as 1986 this method was used to achieve exceptionally low values of SRV of less than 0.4 cm s^{-1} [68] on un-doped (100) orientation silicon materials.

The same technique provided even better passivation when performed on (111) orientation silicon surfaces, with SRV values measured as low as 0.25 cm s^{-1} [68].

More recently in 2012 Grant *et al.* developed a light-enhanced HF passivation technique [71] that allows low SRV on silicon with doping levels of those more conventionally used by the photovoltaic industry. By illuminating the samples being analysed prior to performing measurement, Grant *et al.* reported SRV values of less than 2.7 cm s^{-1} for highly doped (1 ohm-cm) *n*-type silicon [71]. Figure 2.3 shows the type of setup used to measure the carrier lifetimes in silicon through this passivation method.

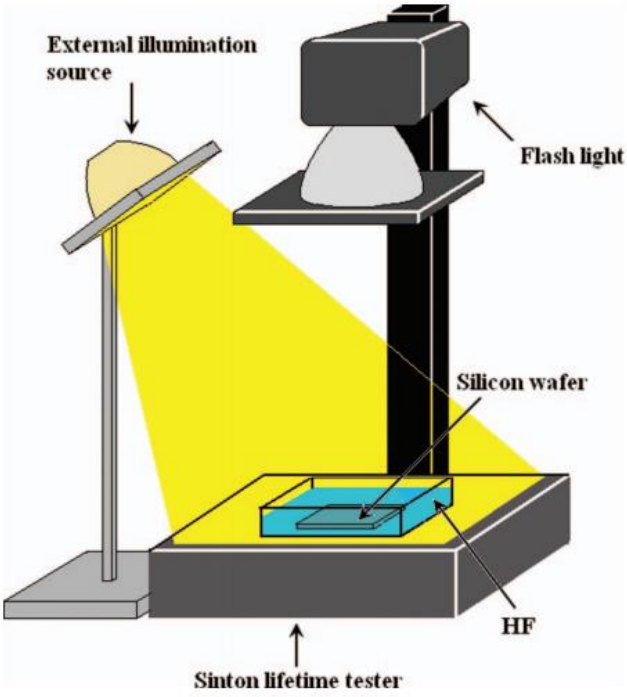

Figure 2.3 - Schematic showing the measurement setup used to perform the light enhanced HF passivation performed by Grant *et al.* The whole measurement setup should be placed inside a fume hood for adequate safety. Figure reproduced from [71].

This use of this method for performing measurements has several practical issues because of the high safety risk associated with the use of HF. One of the largest drawbacks with HF passivation of silicon is that the samples must remain submerged in the HF solution for measurements with low SRV. Experimentally this poses issues; as can be seen by Figure 2.3 the whole measurement setup should be kept in a fume hood for adequate safety and space requirements may not allow this.

The use of HF poses large safety risks to both people and equipment because of the use of concentrated (generally 48% reference) acidic HF solutions. Extreme care must be taken not to splash equipment with the liquid, as there is risk of damaging the – often expensive –equipment due to the use of acidic solutions. In addition, adequate safety measures must be taken to protect the people working with HF solutions.

2.6.1.2 Halogen-Alcohol Passivation

One of the first investigations performed into the passivating ability of halogen-alcohol solutions on silicon was completed by Horanyi *et al.* [72] in 1992. Here the silicon sample was immersed in a solution of iodine and ethanol (IE) in a plastic container in order to provide the chemical surface passivation, and then standard measurements were performed. During this study, they were able to achieve SRV values of less than 10 cm s^{-1}, on *n*-type (111) orientation silicon.

This result was later improved upon in 1996 by Maekawa and Shima [73], who managed to reduce the SRV to below 5.5 cm s^{-1} when performing the measurements on *n*-type silicon with a resistivity of 6.7 Ωcm [73].

Several other halogen and alcohol solutions have been tested since the discovery of the technique, including bromine and methanol (Br-M) and iodine methanol (IM) [74, 75]. In 1994, M'saad *et al.* successfully used IM passivation, which gave an improved surface passivation quality reducing the level of SRV to less than 0.75 cm s^{-1}.

In order to make performing measurements using standard laboratory techniques simpler the silicon samples can be sealed inside transparent plastic bags along with the halogen-alcohol solution to be used. This is demonstrated in Figure 2.4. The samples can then be easily analysed using PCD, QSSPC and PL imaging methods.

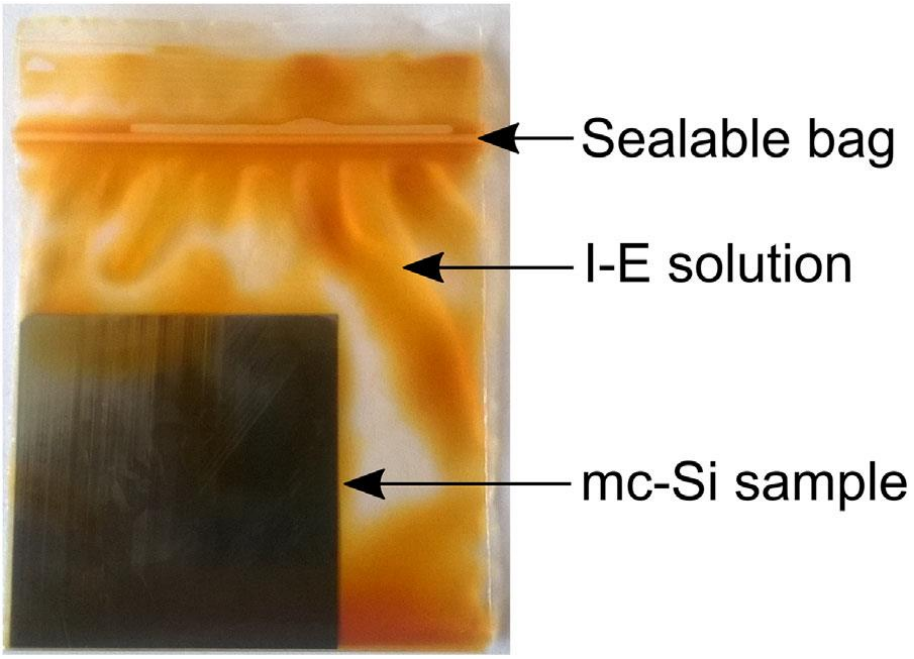

Figure 2.4 – Silicon sample to be measured passivated using an iodine ethanol solution sealed inside a plastic bag to enable measurements to be made using PCD techniques. Figure reproduced from [67].

Halogen-alcohol solutions are much safer to use than HF passivation and have been shown to provide relatively low levels of surface recombination. This technique however does still require the samples to be immersed in solution for the entire measurement process. Additionally the levels of SRV offered by halogen-alcohol passivation may not be good enough to accurately measure the lifetime in lower resistivity/higher lifetime materials.

2.6.1.3 Benzyl-Alcohol Passivation

Similarly to halogen alcohol passivation in order to passivate the surface of silicon using benzyl-alcohol mixtures samples are immersed in a solution of benzene-based chemicals dissolved with alcohols, upon which the standard measurement techniques can be performed.

Most of the research currently available has been performed on three type of benzene-derived molecule: hydroquinone (HQ) [76], p-benzoquinone (BQ) [76] and quinhydrone (QHY) [77-79], which comprises a mixture of HQ and BQ. To perform the passivation, these chemicals are dissolved in either ethanol or methanol alcohols.

Takato *et al.,* who performed QHY passivation using both ethanol and methanol, presented one of the earliest reports. Utilising this method, they managed to show low SRV values of around 4 cm s^{-1} when the treatment was applied to 5 ohm-cm *p*-type silicon wafers [78, 79]. The findings presented so far generally show that the mixture QHY provides the best levels of surface passivation.

When compared with HF and halogen-alcohol passivation, schemes based on benzyl-alcohol passivation generally provides worse surface passivation, which results in higher levels of SRV. To the knowledge of this researcher a SRV for benzyl-alcohol passivation below 1 cm s^{-1} has not yet been reported [67].

As all the methods outlined so far rely on the sample being submerged during the experimental measurements, there is a question over suitability for measuring low lifetime samples (< 200 µs). As low lifetime samples require the use of quasi-steady-state photoconductance (QSSPC) measurements [39, 40]. QSSPC measurements are performed under constant illumination (unlike photoconductance decay measurements) and require an accurate measurement of the surface illumination of the silicon samples in order to measure the generation rate of carriers in the silicon and hence the lifetime. When immersed in solution this may introduce errors in the measurement and an accurate calibration of generation rate in the sample is important for high accuracy measurements results [80].

Currently all of the outlined temporary passivation techniques are not stable enough in air to enable measurements to be taken and therefore must be in-solution for measurements to be taken (a particular issue in terms of safety when performing HF passivation).

2.6.2 Thin Film Passivation

Alongside the immersion based temporary passivation techniques, the surface passivation of silicon can also be accomplished by forming thin films on the surface of the samples using various solution-based processes. One of the most exciting areas developed so far is using organic polymers to form a thin passivating film at the surface and several different polymer films have been researched [81, 82]. One of the most promising of these currently appears to be the use of poly (3,4- ethylenedioxythiophene):poly (styrenesulfonate) (PEDOT:PSS) [83, 84].

During research on the formation of organic heterojunction cells Schmidt *et al.* found that PEDOT:PSS gave high levels of surface passivation. The method used was to spin coat a later of PEDOT:PSS onto the surface of silicon that is followed by a curing step at 130 °C for 30 seconds

on a hot plate. This research performed by Schmidt *et al.* resulted in high quality surface passivation of the silicon with a low SRV of 4.5 cm s^{-1} [67, 84]. Additional research presented by Zielke *et al.* using similar methods also resulted in good SRV values of less than 6 cm s^{-1} for the treatment [67, 85].

Polymer film based processing can often sometimes require the use of curing processes at elevated temperatures (around 100-200 °C [82-84]) so care should be taken to ensure this does not affect the bulk lifetime of the silicon material by keeping temperatures low and curing times short.

One major benefit of thin film passivation is of the increased short term stability, this enables samples to be measured using the standard techniques in ambient conditions, without the need for the silicon material to remain immersed in solutions and without the need for fume hoods and extracted characterisation equipment particularly in the case of HF acid passivation.

Long-term degradation of the surface passivation quality of thin polymer films in ambient conditions has been found to be a common problem. Schmidt *et al.* [84] measured the significant efficiency degradation (around 4 % absolute) of silicon solar cells using a PEDOT:PSS passivating film on the front surface whilst being stored in ambient conditions. This was reported to be due to interaction with moisture in the air [84]. Additionally Chen *et al* [82] examined the stability of PSS-based passivating films alone and demonstrated that in ambient conditions high levels of degradation of the passivating polymer films quality occurred. The literature shows that thin organic films tend to have short-term stability in ambient conditions and are therefore useful for semiconductor material characterisation. Relatively little research into increasing the stability of the films in the long term has been performed. This is required in order to make these passivation schemes suitable for device-based applications.

Other temporary passivation techniques do exist which can provide good surface passivation for silicon materials, but they have not been widely investigated and only the more established schemes have been discussed here. Also included in the thin film category is the recently discovered superacid derived passivation, as this is the focus of the research in this PhD superacid-based passivation will be discussed in more detail alone in the next section.

To enable easier comparison between the different temporary passivation methods an overview of the upper ranges of possible of surface recombination offered by temporary passivation schemes is reproduced in Figure 2.5.

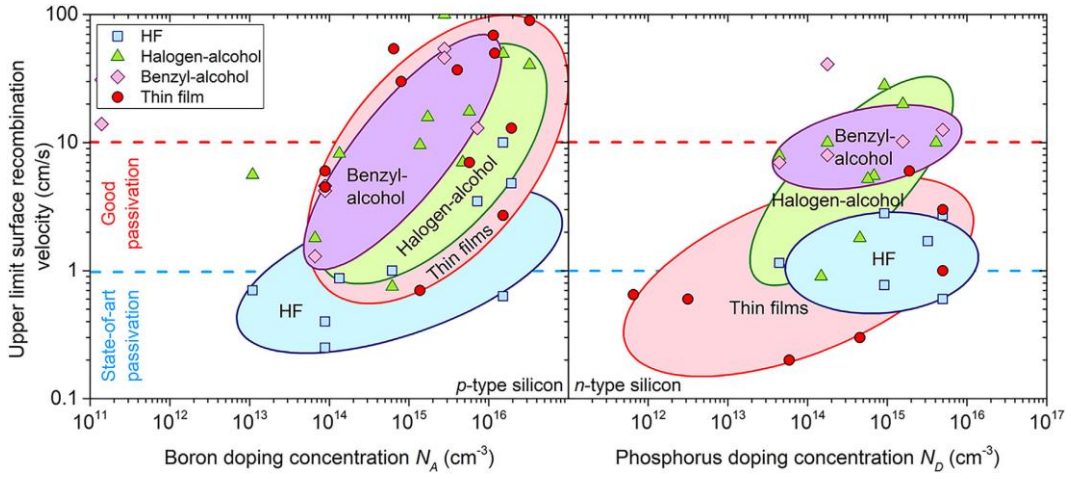

Figure 2.5 - Upper limits of surface recombination velocity (S) offered by the most prevalent temporary passivation schemes on both *p*-type and *n*-type silicon surfaces, plotted by doping level. The coloured regions indicate a rough range of the possible surface recombination values offered by that particular passivation scheme. Reproduced from reference [67].

A summary is presented in Table 2.1 of an overview of some of the best results that have been obtained from the wide range of permanent dielectric methods and temporary techniques. For comparison the best result from this work is also included. All data is from tests done on *n*-type (100) orientation silicon wafers comparable to the sample wafers used in this thesis.

Passivation Type	Chemical/Material	Deposition Method	SRV (cm s^{-1})	Reference
Dielectric	SiO_2	PECVD	2.6	[86]
	HfO_x	ALD	1.92	[87]
	SiO_2	Alnealed Thermal SiO_2	1.72	[53]
	amorphous-SiO_x:H	PECVD	1.5	[86]
	SiN_x	Catalytic-CVD	0.6	[88]
	AlO_x	Plasma-enhanced ALD	0.26	[28]
Acid	HF (20%)	Immersion	2.7	[71]
	HF(15%) + HCl	Immersion	0.6	[89]
Halogen	Iodine + Methanol	Immersion	25	[90]
	Bromine + Methanol	Immersion	20	[91]
	Iodine + Ethanol	Immersion	5.2	[92]
Benzyl	Quinhydrone + Methanol	Immersion	7	[93]
	Benzoquinone + Methanol	Immersion	1.6	[94]
Organic	Polystyrenesulfonate	Spin Coated	6	[95]
Superacid	TFSI-Hexane	Dip Coated	0.69	This work

Table 2.1 – Summary of significant passivation materials and methods on n-type (100) orientation silicon wafers. Passivation levels can be considered good if < 10 cm s^{-1}, can be considered state of the art if < 1 cm s^{-1}.

2.7 Organic Superacid-Derived Passivation

The first application of organic superacid solutions to passivate semiconductor surfaces was in 2015 by Amani *et al.* [96]. An air-stable, solution-based chemical treatment by an organic superacid was found to uniformly enhance the photoluminescence and minority carrier lifetime of MoS_2 monolayers by more than two orders of magnitude. The method reported used bis(trifluoromethane)sulfonimide (TFSI) superacid based solutions to passivate the surface of molybdenum disulfide (MoS_2) [96] and produced an increase in the quantum yield from the material under analysis. Superacids are solutions with an acidity greater than that of 100% pure

sulfuric acid (H_2SO_4) [97]. The technique using TFSI was later also applied to more transition metal dichalcogenides (TMDs) including; the surfaces of tungsten disulfide (WS_2) in 2016 [98] and copper indium disulfide ($CuInS_2$) in 2018 [99].

Following on from the successful surface passivation of 2D transition metal dichalcogenides by Amani *et al.* [96, 98, 100] using a liquid superacid, the first application of this method to crystalline silicon materials was performed by Bullock *et al.* in 2016 [101], carrying on from that groups initial work on TMDs. They developed the organic passivation method in which silicon wafers are dipped into a nonaqueous superacid solution, demonstrating the potential of this technique to provide high quality, room temperature surface passivation of c-Si surfaces.

In their study Bullock *et al.* [101] researched the solvent dependence of the treatment quality using 5 different solvents:

- 1,2,4 Trichlorobenzene (TCB)
- 1,2 Dichloroethane (DCE)
- Octane
- 2 Propanol (IPA)
- Acetonitrile (CAN)

In their initial paper on the treatment scheme their data showed that the passivation quality was highly dependent on the choice of solvent used [101]. After trialling several superacid solutions DCE was shown to offer the highest quality passivating film. However, these are the only five solvents that have been tested in all the currently available literature.

The method used was to dissolve crystalline TFSI using 1,2-dichloroethane (DCE) as a solvent – DCE is now widely thought to be a carcinogen [102]. Chemically cleaned and HF etched silicon samples are then dipped into the superacid solution for a short time (reported as being 60 seconds). They are then removed and allowed to dry, leaving behind a thin passivating film on the surface of the silicon. Measurements can then be performed with standard lab methods. Through the use of this this procedure Bullock *et al.* reported achieving surface recombination velocities of 3 cm s^{-1} on *n*-type silicon [101]. Figure 2.6 gives an overview of the treatment and the results obtained on *n*-type silicon by Bullock *et al.*

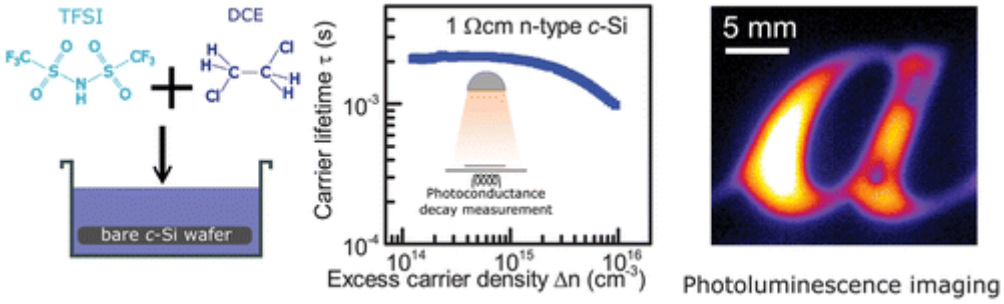

Figure 2.6 – Schematic showing the chemicals used for the superacid treatment of silicon, along with excess minority carrier density results measured on a 1 ohm-cm *n*-type silicon sample after undergoing the treatment procedure. Also included is a PL image showing how the solution can be used to treat specific areas of a sample. Figure reproduced from [101].

These levels of surface passivation were not yet good enough for the technique to compete with the levels of passivation offered by state of the art dielectric films (< 1 cm s^{-1}) [19]. This was possibly due to the lack of controlled pre-treatment cleaning, as Bullock *et al.* only performed an HF dip prior to passivation using the TFSI-DCE solution.

This initial work done by Bullock *et al.* was improved upon by Grant *et al.* [103] in 2017. Through optimising the silicon sample cleaning and pre-treatment processes, Grant *et al.* was able to develop the passivation method further in order to reduce the SRV. This resulted in a reported upper limit SRV of below 1 cm s^{-1} on both *n*-type and *p*-type materials [103], demonstrating the excellent surface passivation made possible by the use of this technique. Utilising this method Grant *et al.* demonstrated its ability to measure exceptionally high lifetimes in high resistivity silicon (up to 75 ms) [103], the lifetime data for this experiment is presented in Figure 2.7.

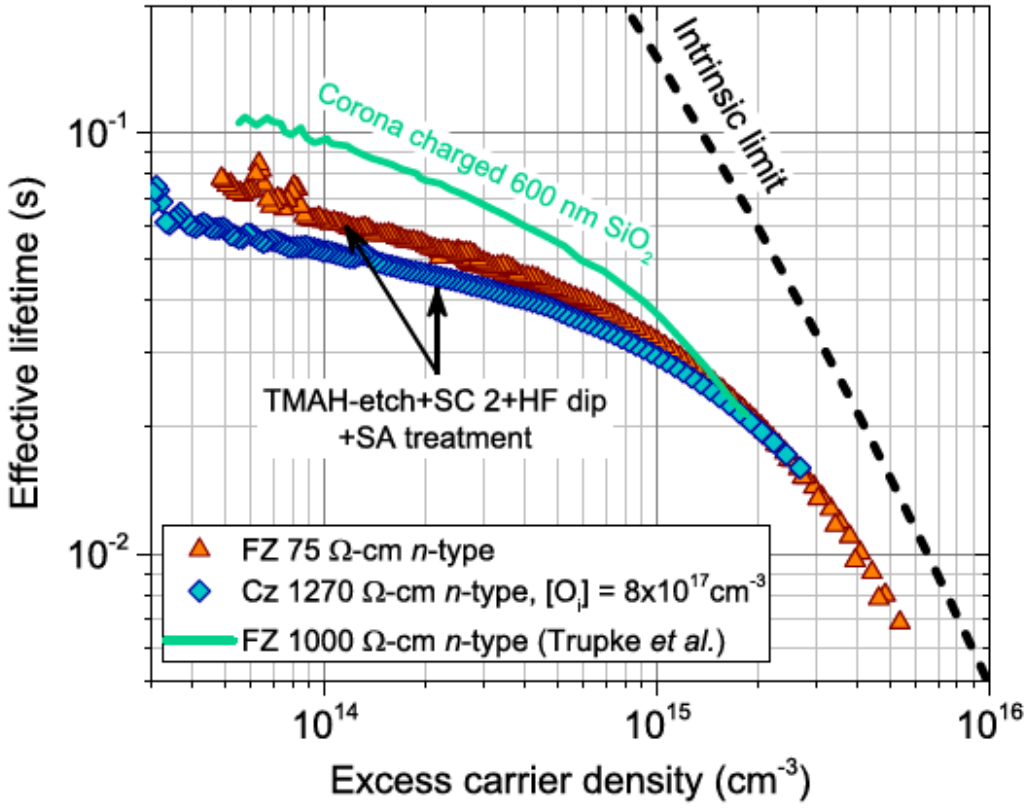

Figure 2.7 – Plot of injection-dependent lifetime of high quality silicon, treated with superacid-derrived solution and optimised cleaning process. The maximum lifetime of 75 ms is represented by the orange triangle data points. Figure reproduced from [103].

Also presented on the graph for comparison purposes, is the lifetime data for a thermally oxidized (600 nm) and corona charged 525 μm thick FZ 1000 Ω·cm n-type silicon by Trupke et al. [104], having measured lifetimes exceeding 100 ms.

Corona discharge is a technique routinely used to deposit positive or negative charge on the surface of materials, in order to enhance the surface passivation through the field-effect mechanism [105]. The use of appropriate charge can repel either holes or electrons from the surface, and so helps to prevent their recombination by repelling the mobile charge carriers from recombination sites at the interface. Despite the fact that extremely effective passivation is possible, corona discharges are largely only used in research settings due to the lack of stability of that deposited charge [106, 107].

2.7.1 Stability

One benefit of organic superacid passivation is the relative stability of the film once it has been applied. Unlike several of the other temporary passivation schemes discussed, when using superacid based passivation the sample can be removed from the solution it has been dipped in and allowed to dry, allowing measurements to be performed in ambient conditions. However, like thin polymer films after increased time periods the passivation quality does start to degrade in ambient atmosphere.

Both Bullock *et al.* [101] and Grant *et al.* [103] examined the stability of silicon samples after performing the superacid treatment, like most organic films it was demonstrated that the treatment was not fully stable in ambient conditions and degrades in the presence of air. Despite knowing this Bullock *et al.* do not control the treatment atmosphere during application of the TFSI-DCE solution, performing the passivation method in varying ambient conditions.

The reported results show the film stays relatively stable in ambient conditions for the first hour following the application of the passivating film. After this time, a significant increase in the degradation of the film was reported in both cases. Grant *et al.* showed a roughly 30% degradation in the initial measured lifetime of the sample was observed over the next 2 to 3 hour time period [101].

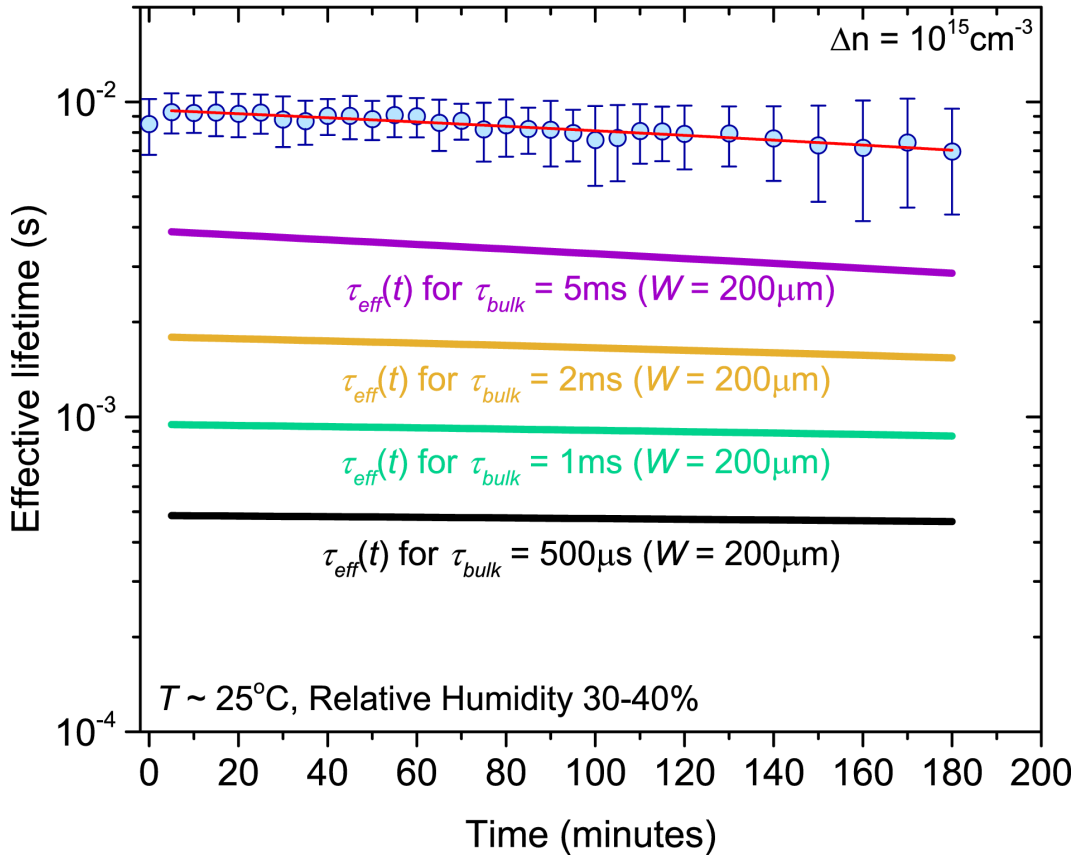

Figure 2.8 – Effective lifetime plotted over time in minutes for *n*-type silicon samples having undergone superacid treatment, showing the trends in degradation of the sample in ambient conditions. Figure reproduced from [103]. The solid lower four lines are modelled data.

Grant *et al.* went on to analyse the in air degradation of *n*-type silicon that had undergone the treatment process and this data is presented in Figure 2.8. They calculated the degradation rate in ambient conditions of the SRV of the samples and reported the reduction rate of S to be 0.0052 cm s^{-1} per minute [103].

The cause of the degradation has not been reported so far in the literature, but is thought to be due to moisture reacting with the film. One of the aims of this thesis is to further understanding in this area.

2.7.2 Superacid Passivation Mechanism

Despite research that is currently available in this field, the underlying mechanism behind the passivating ability of TFSI superacid solutions is still not fully understood, and the exact passivant/chemical structure of the film is unknown. Both the initial studies performed on TMDs [96, 98, 100, 108], and the following first study performed on silicon materials by Bullock *et al.* [101] could not pinpoint the exact reason for the improved surface passivation offered by the treatment.

Grant *et al.* [103] and Bullock *et al.* [101] analysed the injection dependence of the lifetime for the treatment on both *n*-type and *p*-type silicon but neither found any substantial evidence for charge at the surface from the treatment solution providing field effect passivation.

Bullock *et al.* suggested the passivation mechanism was based on the saturation of silicon dangling bonds by protonation of the silicon surface providing chemical passivation [101]. However, the exact mechanism by which TFSI passives the surfaces of semiconductors is still not fully understood. In order to try to determine the origin of the passivation mechanism Bullock *et al.* performed FTIR measurements in both solution and on silicon surfaces, and performed XPS measurements on silicon surfaces treated with the liquid passivation technique. These results from reference [101] have been presented in Figure 2.9.

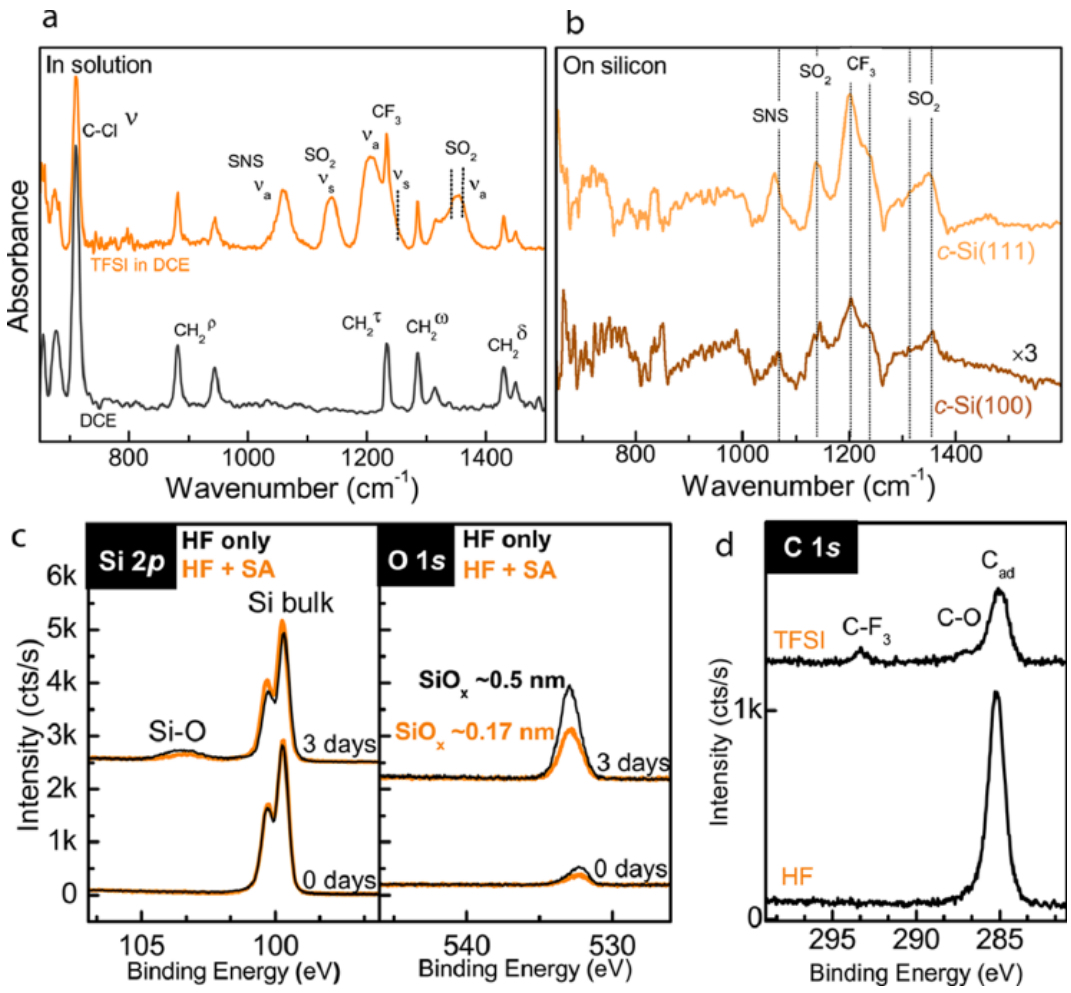

Figure 2.9 – a) FTIR spectrum of DCE and TFSI-DCE solutions, with the characteristic peaks labelled. b) ATR-FTIR spectrum of TFSI-DCE treated silicon, performed on (100) and (111) orientation silicon wafers. c) XPS spectrums of Si and O peaks for HF treated and TFSI-DCE treated (100) orientation silicon samples. d) XPS spectrums of C peaks for HF treated and TFSI-DCE treated (111) orientation silicon samples. Figure reproduced from [101].

Some flaws exist with the tests performed by Bullock *et al.* to understand the origin of the passivation mechanism. Both FTIR and XPS data are presented with no untreated control samples to compare the data against, so it is difficult to say for certain if the data is due solely to the passivation treatment or possibly other contamination.

FTIR and XPS data is also reported for both (100) and (111) orientation silicon surfaces. While it is known that changes in surface orientation can greatly affect the passivation ability of surface treatments, particularly temporary passivation schemes [67], Bullock *et al.* does not report any data to show the TFSI-DCE treatment successfully passivates (111) orientation surfaces. Only

that it successfully passivates (100) orientation silicon surfaces, so it is unknown whether this data is a true representation of the passivation scheme reported.

Lastly whilst it is known that the superacid-derived passivation scheme is moderately stable in air in the short term (< 3 hours), it is not known whether the treatment is stable in vacuum. Because of this and the high vacuum conditions required for performing XPS measurements it is unclear whether the silicon surfaces will remain passivated using the TFSI-DCE solution whilst XPS measurements are performed and whether this measurement technique is suitable for investigating this surface passivation method.

2.8 Summary

In this chapter, existing literature and state of research on superacid-based passivation schemes has been reviewed. As this is such a new area of research, a very limited amount of literature is available. However, from the studies it is clear that organic films derived from superacid-based solutions can provide exceptional silicon surface passivation that can compete with the state of the art dielectric films [103], whilst being cheaply and simply deposited at room temperature without the need for expensive and complicated vacuum equipment. Whilst the literature available demonstrates the ability of the TFSI passivation method to give very low levels of surface recombination, more work is required in the field to gain a greater understanding of both the composition and thickness of the passivating film.

Future developments to enhance the long-term stability of the current temporary passivation scheme are crucial in order to enable their use in devices. Encapsulation has been shown to work initially on metal dichalcogenides [100], therefore superacid based passivation schemes may also be a suitable for encapsulation for use in silicon based photovoltaics.

Chapter 3 Experimental Methods

This chapter specifies the materials used throughout this work. It also outlines the general sample preparation sequences, experimental methods and analysis techniques used.

3.1 Sample Wafers

The passivation schemes outlined in this thesis were generally developed and evaluated on *n*-type (phosphorus doped), (100) and (111)-orientation float-zone (FZ) silicon wafers, which were obtained from Topsil Semiconductor Materials. The wafers had an initial diameter of either 100 mm (4 inches) or 150 mm (6 inches), unless otherwise stated the wafers used had a nominal resistivity of 5 Ωcm and a starting thickness of 750 μm. If the resistivity and starting thickness of the sets varied, the exact details will be listed alongside each data set. For most experiments, wafers were cleaved into quarters using a diamond scribe and wafer-breaking tool, to make processing and treatment more manageable.

Tests performed to analyse the SRV of specific treatments were done on a set of whole 100 mm (4 inch) diameter wafers cut from the same ingot to have different thicknesses. These were also provided by Topsil, had a nominal resistivity of 3 Ωcm and had initial thicknesses of 1500 μm, 1000 μm, 500 μm, and 250 μm.

3.2 Sample and Chemical Preparation

The following sections aim to outline the exact procedures used in the preparation of samples.

3.2.1 Gloveboxes

It was already known that contamination with water of solutions containing bis(trifluoromethane)sulfonimide (TFSI) impaired the treatment and resulting passivation [101], and the crystalline form of TFSI is known to be hygroscopic [109]. Therefore, accurate control and knowledge of the treatment conditions that each experiment was performed in was vital to both ensure repeatability and to produce valid results, including not only the composition of the starting solution but also potential further contamination from water in the atmosphere - measured as humidity - during both sample treatment and storage.

In order control atmospheric conditions as well as possible, the use of two atmospherically controlled gloveboxes were key to the research performed during this thesis. These two

gloveboxes will be referred to as the low specification and high specification gloveboxes from here onwards when noting the location where experiments were prepared and performed.

3.2.1.1 Low Specification Glovebox

The low specification glovebox shown in Figure 3.1 was a Cole-Palmer supplied glovebox (model 34788) which was manually filled with BOC supplied oxygen-free nitrogen working gas of greater than 99.9% purity, and is located in lab A408B in the School of Engineering and is vented into a fume hood. This glovebox contained a digital thermohygrometer (Testo Model 610) and the main goal of this glovebox was to control the atmospheric humidity when performing experiments. During use, the relative humidity in this glove box was kept below 25%, unless noted otherwise.

Figure 3.1 – Image showing the low specification glovebox used during sample processing.

3.2.1.2 High Specification Glovebox

The high specification glovebox shown in Figure 3.2, located in the D030 chemical lab in the School of Engineering that was used during these studies consisted of a MBRAUN NIlab closed loop glovebox workstation connected to an MBRAUN LMF II inert gas purifier with solvent trap option. Monitoring equipment on the glovebox ensured that during use the levels of O_2 and H_2O contamination inside the system stayed below 0.1 ppm. The glovebox also featured two high vacuum-capable feedthrough antechambers (small and large) allowing materials to enter and exit the glovebox chamber without compromising the integrity of controlled atmosphere inside.

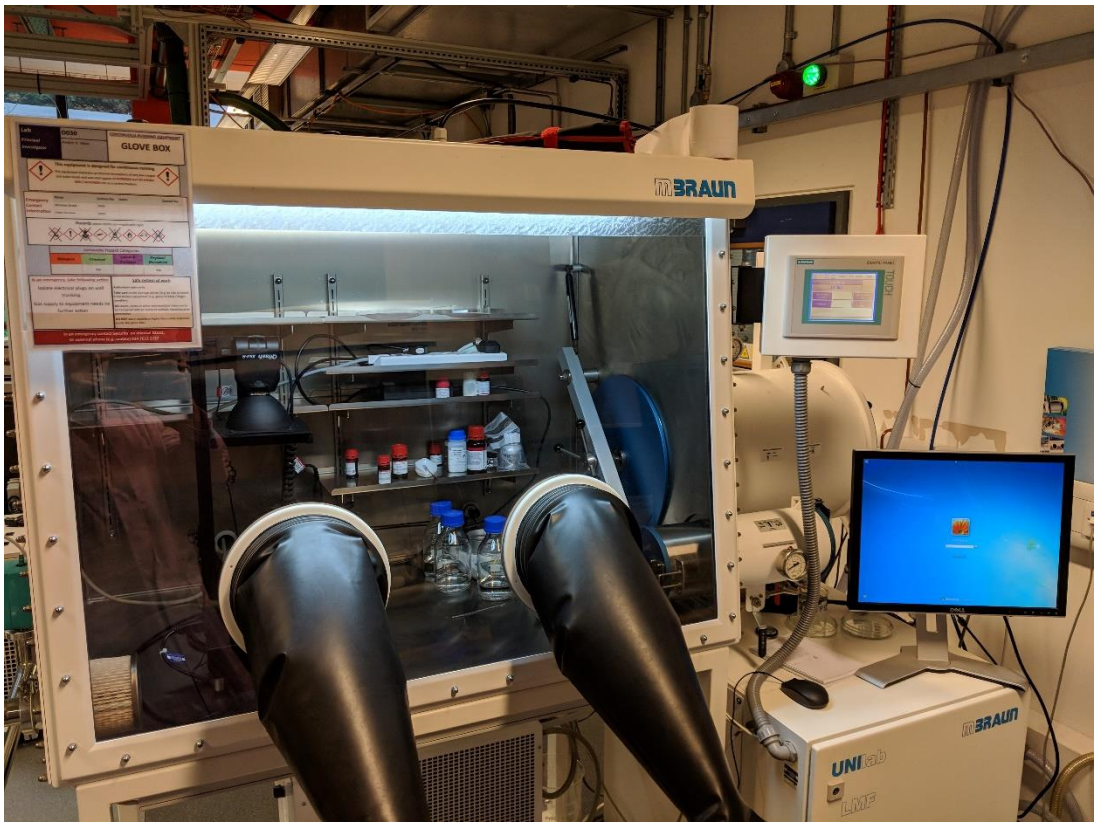

Figure 3.2 – Image showing the high specification MBRAUN glovebox used during the experimentation.

3.2.2 Sample Cleaning

In the pursuit of the highest possible quality surface passivation, any samples required chemical cleaning and processing before application of any of the solution based surface passivation methods. The silicon sample wafer cleaning routines used during the research for this thesis were initially based on the optimised procedure as outlined by Grant *et al.* [103]. This standard sample preparation procedure relies heavily on RCA cleaning, which was developed by Werner Kern while working for the Radio Corporation of America in 1965 [110]. This type of cleaning is divided into two distinct steps depending on the type of contaminant to be removed.

3.2.2.1 RCA 1 Cleaning

The first RCA clean is used to remove organic contaminants and particle contamination. The cleaning solution is made up of a 5:1:1 ratio of deionised (DI) water, aqueous ammonium hydroxide (NH_4OH) and aqueous hydrogen peroxide (H_2O_2) mixture. The "RCA 1" solution is heated to a temperature of 80 ˚C, before the sample to be cleaned is placed in it and left for 10 minutes, at a constant temperature. After which the samples are removed and rinsed in DI water.

3.2.2.2 RCA 2 Cleaning

The second RCA clean is used to remove metallic contaminants from the sample surface. The cleaning solution is made up of a 5:1:1 ratio of deionised (DI) water, aqueous hydrochloric acid (HCl) and aqueous hydrogen peroxide (H_2O_2). This "RCA 2" solution is heated to a temperature of 80 ˚C, before the sample to be cleaned is placed in it and left for 10 minutes, at a constant temperature. After which the samples are removed and rinsed in DI water.

3.2.2.3 Standard Cleaning Procedure

The standard procedure used for sample preparation consisted of the following steps:

1) A thorough rinse in 18.2 MΩ deionised (DI) water.
2) A dip in 1% HF for one minute to remove the native oxide.
3) An initial RCA 2 clean.
4) A thorough rinse in 18.2 MΩ DI water.

5) A dip in 1% HF for one minute to remove the native oxide.
6) An etch in 25% Tetramethylammonium hydroxide (TMAH) solution

   The item to be etched is submerged in the TMAH solution for 10 minutes held at a constant temperature of 80 ˚C.
7) A thorough rinse in 18.2 MΩ DI water.
8) A dip in 1% HF for one minute to remove any possible native oxide.
9) A second RCA2 clean.
10) A thorough rinse in 18.2 MΩ DI water.
11) Samples were then soaked in a mixture of 2% HF diluted with DI H2O for 1 minute, before being pulled dry from the solution ready for treatment.

Only acid-resistant plastic tweezers were used for any sample manipulation during all cleaning and treatment procedures. For safety and in order to accurately hold the temperature of the cleaning solutions throughout the whole cleaning process, beakers containing solutions were placed into a heated water bath, a bath temperature setting of 84 °C resulted in a measured chemical solution temperature of 80 °C. As the volume of the TMAH solution beaker was too large for the water bath, this was instead heated on an acid resistant ceramic hot place, and the solution temperature constantly monitored with a thermometer during processing.

3.2.2.4 Cleaning Modifications

In certain circumstances, this standard method was modified by the addition of other processing steps for the required outcome.

Pre-used samples often have organic contamination of the surface which needed to be removed in order to gain the optimal surface passivation upon treatment. In order to remove this an initial RCA1 cleaning step was added before the standard procedure outlined previously.

Etch back experiments on PV cells results in a lot of metal contamination at the surface (because of etching the cell contacts) which results in poor surface passivation when treated if this was not properly removed. To accomplish this any samples with heavily metallic contamination were subject to an initial aqua regia metal etch consisting of a 3:1 ratio of HCl (37%) and HNO_3 (69.5%). This was left to react and warm exothermically from room temperature for 15 min before adding the samples, which were then etched for 15 min.

An alternate planar etch process was used in some circumstances. Unlike the TMAH etch which acts to texture the surface partially at the nanometre scale, the planar etch smooths the surface acting as a chemical polish. The planar etch process consists of an etch solution comprised of, HNO_3 (69.5%) and HF (50%), mixed at a ratio of 10:1 respectively. This mixture was left for 15 minutes without external heating before use.

Where other special processing was required (such as different etch times) or alternate pre-treatments were used, this information will be specified alongside the results.

3.2.3 Avoiding Contamination of Glassware and Tools

All organic based treatments are exceptionally sensitive to any contamination, the methods used to characterise solutions (such as NMR) during this thesis are also very sensitive to even low ppm values of foreign chemicals. Due to this, it was crucial to keep any equipment and all glassware used during the research contamination free and spotless. To ensure this, all glassware (beakers, bottles, petri dishes and containers) as well as all manipulating instruments (tweezers) were subjected to a rigorous cleaning scheme between uses.

This consisted of:

1) A thorough rinse in 18.2 MΩ deionised (DI) water.
2) A 24 hour soak in a solution of 5% Decon 90, to 95% 18.2 MΩ DI water at room temperature.
3) A thorough rinse in 18.2 MΩ DI water.
4) An RCA1 clean in order to remove solvent contamination. (To ensure complete removal of all solvent residue which is particularly important for solution analysis).

   The item to be cleaned is submerged in the "RCA 1" solution for 10 minutes at a temperature of 80 ˚C. This solution is comprised of a 5:1:1 ratio of DI water, aqueous ammonium hydroxide (NH_4OH) and aqueous hydrogen peroxide (H_2O_2).
5) A thorough rinse in 18.2 MΩ DI water.
6) An RCA2 clean to remove any possible metallic contamination. (To ensure removal of any metallic contaminants which is crucial to the high quality of the resulting surface passivation).

The item to be cleaned is submerged in the "RCA 2" solution for 10 minutes at a temperature of 80 ˚C. This solution is comprised of a 5:1:1 ratio of DI water, aqueous hydrochloric acid (HCl) and aqueous hydrogen peroxide (H_2O_2).

7) A thorough rinse in 18.2 MΩ DI water.
8) Excess water is then removed using nitrogen (N_2) gas.

The item is then left in a heated drying cabinet held at 75 ˚C, for at least 24 hours before use, to ensure that all traces of water are removed.

3.2.4 Passivating Solution Preparation

Several different chemical passivating solutions were tested and used during this research, comprising of different solute bases added to various solvents. Each of the differing treatments were prepared using a similar process.

To prepare the passivating solutions the starting chemical (to be dissolved or diluted with solvent) was weighed out inside the high specification glovebox. Solid chemical solutes were weighed into antistatic polystyrene weigh boats (Fisher Scientific P/N: 11533432) to avoid sample loss and contamination, using stainless steel spatulas – a new weigh boat was used each time and spatulas for different chemicals kept separate. Liquid chemical solutes were measured out into borosilicate glass scintillation vials with PTFE lined caps using a pipette pump and glass pipette (Pasteur No. 612-1701) - a new pipette was used each time and changed any time different chemicals were used. All chemical weights were measured using a Kern PCB 100-3 weighing scale with 0.001 g resolution.

The solute chemical was then transferred into a graduated 500 ml bottle inside the high specification glovebox, the lid placed on and sealed tightly before being withdrawn through the airlock system on the glovebox. The bottles used for mixing and storage of the solutions were Simex reagent bottles (model 2070/500) made of borosilicate glass bottle with polypropylene (PP) caps, these were used to ensure no reaction occurred (and thus contamination) between some of the more highly acidic chemicals used during experimentation and the storage containers. The mixing bottle was then transferred to the low specification glovebox, which was then pumped down to a relative humidity < 25% using N_2 gas before the cap was removed. The chosen liquid solvent was then poured in from its container to dissolve the solute, marked graduations on the sides were used to measure the amount of solvent poured in. The air-tight

glass bottles were then used to store the chemicals while waiting for the solutes to dissolve and while the solutions were not in use; these were kept inside in a specialist solvent fridge programmed to maintain a temperature of 12 °C. Before performing tests the chemical bottles were removed from the fridge and placed inside the low specification glovebox and allowed to come up to room temperature before use.

To prepare the solutions, chemicals were mixed in the ratio of 100 mg of solute to 50 ml of solvent, due to the small quantities of measured solute a ±5% tolerance was allowed for all mixtures. This mixture was scaled according to the volumes required for the experiment, for example when testing 4-inch wafers 400 ml of solution was required. When preparing the main chemical solute in this study, bis(trifluoromethane)sulfonimide (TFSI), 800 mg of crystals were measured out and then dissolved in 400 ml of a chosen anhydrous solvent. When testing quarters of 4-inch wafers 200 ml of solution was acceptable.

Most chemicals generally dissolved in the solvents fairly rapidly, any exceptions will be detailed in the relevant section. Upon the development of the newer standard TFSI-based solutions using pentane and hexane these were allowed to stand for at least 24 hours before their first use, as these solvents reduced the speed of dissolving compared with the relatively instantaneous dissolving in the originally used 1,2-dichloroethane (DCE) solvent.

3.2.5 Solution Based Passivation

Immediately following their surface cleaning and pre-treatment, as described in Section 3.2.2.3 above, each silicon sample in its petri dish was kept inside the sealed dark transport box until needed – samples were used as quickly as possible and any further information will be provided alongside the results of that experiment. When being treated they were then transferred from the box into the low specification glovebox when which was continually purged with N_2 to maintain a RH below 25%.

For each type of treatment, the pre-prepared passivating solution was poured into a borosilicate glass beaker and a borosilicate watch glass placed over the top whilst it was not in use. When testing quarters of 4-inch wafers a 250 ml capacity beaker was adequate; for tests of whole 6-inch wafers a 2 L total capacity beaker was required.

To be treated, the sample was removed from its petri dish using a pair of Lerloy 61 Celcon copolymer acid and solvent resistant tweezers, and all subsequent sample handling was performed with these tweezers – a different, cleaned and prepared set of tweezers was used for each change of treatment solution. The sample was transferred into the beaker containing the treatment solution and left immersed in the solution timed for around 60 s. After this immersion the sample was withdrawn from the solution and held in the glovebox N_2 ambient atmosphere whilst waiting for the sample to dry (until visible residual solvent had evaporated off the surface), whilst still being held in the plastic tweezers. The treated and newly passivated sample was then placed back inside its petri dish and the lid placed back on before removal from the glovebox atmosphere for characterisation and testing. If the samples were not allowed to dry adequately and were placed back into the plastic petri dish too soon, this could, depending on the solvent used, result in reactions with the plastic, often ruining the experiment.

3.3 Characterisation Methods

A combination of several characterisation techniques is required in order to try to develop a complete understanding of the possible mechanisms and the exact nature of the absorbed surface layer resulting from various treatments. These include photoconductance decay lifetime measurements, Raman spectroscopy, nuclear magnetic resonance spectroscopy and X-ray photoelectron spectroscopy among others. This section gives a brief description of the techniques used to characterise the passivating films being studied during this thesis.

3.3.1 Photoconductance Decay Lifetime

Injection dependent bulk lifetime spectroscopy is one of the most important characterisation techniques used in silicon photovoltaics, and the photoconductance measurement methods are some of the most widely used. A contactless method of determining carrier lifetime was developed by Sinton and Cuevas [39, 40].

The PCD lifetime system (shown in Figure 3.3) comprises of a flash lamp, which is used to generate excess carriers in the silicon wafers and therefore to increase its conductance (σ). The silicon wafer under test is placed over a conductive coil, which measures this change in a

contactless manner, by measuring the sample conductivity using a bridge circuit and a coil located in close proximity to the sample. The coil's impedance varies as the conductivity of the sample changes, the resulting change in conductivity (Δσ) (which is measured by the Sinton tool) can be expressed as Equation 3.1.

$$\Delta\sigma = \frac{\Delta p}{q(\mu_n + \mu_p)} \qquad \text{Equation 3.1}$$

Where μ_n and μ_p, are the mobility of electrons and holes respectively in the semiconductor, and q is the electron charge of 1.6×10^{-19} coulomb.

The effective lifetime can be measured in several different modes that were discussed previously in Section 2.2.

Effective minority carrier lifetimes were measured using one of two Sinton WCT-120 photoconductance lifetime measuring tools (see Figure 3.3). One standard tool with 40 mm diameter measurement coil or one "small coil" with 10 mm diameter measurement coil were available to use. For each measurement it was made sure that the size of sample analysed on each tool was large enough to avoid the negative impact from edge effects during measurement [111], and care was always taken to locate the coil in the same place in centre of the sample each time.

To reduce the degradation of the passivating films in the ambient atmosphere (as well as from transport and handling), measurements were often performed with samples in plastic petri dishes (sometimes with the lid remaining on). This required the lifetime testers to also be calibrated to mitigate the effect of the petri dish moving the samples away from immediately above the coil. This calibration was achieved using a method developed by Black and Macdonald [112] to minimise any errors associated with measuring thicker silicon samples or samples further away from the sample stage.

It was sometimes required to relocate the small coil tester into either the cleanroom facility itself (to perform more immediate measurements after surface cleaning/treatment) or inside the high specification glovebox (to exactly control the atmospheric conditions of treatment and/or measurement). Equipment was passed into the glovebox using the feedthrough to preserve the controlled atmosphere inside. These experimental conditions will be outlined alongside the results for the data.

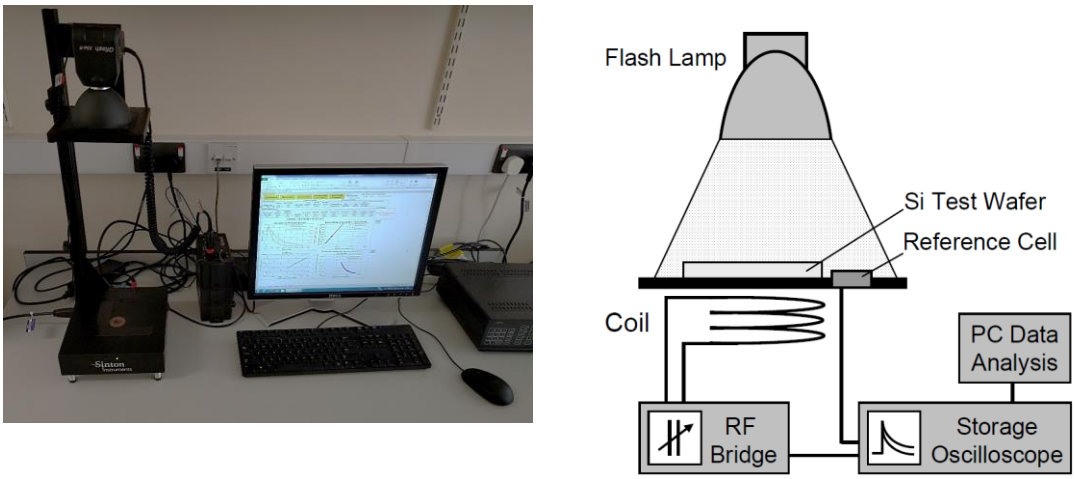

Figure 3.3 Left – Picture showing the experimental setup used for measuring minority carrier lifetime. The Sinton WCT-120 photoconductance tool is based in the School of Engineering at The University of Warwick. Right – Schematic diagram of the internal configuration of the system used to acquire the data. Reproduced from [47].

Lifetime measurements are recorded over a wide range of injection levels, however when quoting a single value for lifetime it is common in literature to specify this at a minority carrier injection level (Δp) of 1×10^{15} cm^{-3}, therefore any values quoted in this thesis will be at this injection level (unless stated otherwise). The measured lifetime values in this paper will be quoted as "lifetime" to separate them from bulk lifetime results. The error of a lifetime measurement performed on a Sinton tool has been determined to be ± 5 % when performed on one sample [113] and this value will be used during analysis. During this research the transient method was always used for samples with a high carrier lifetime any lifetime ≥ 200 μs) and for lower lifetime samples (a lifetime less than 200 μs) the quasi-steady-state (QSS) lifetime measurement method was used [40]. The majority of the treatments performed and samples presented in this thesis were much greater than 200 μs (often several ms), hence in most cases the transient mode is used when measuring bulk lifetime. For the solution-based passivation treatments performed during this study, an optical constant of 0.7 was used, as apart from the thin film of the passivating treatment on the surface the wafers were bare, with no anti-reflection coating.

3.3.2 Photoluminescence Imaging

Photoluminescence (PL) imaging is a spatially-resolved method for performing minority carrier measurements of silicon wafers and solar cells [114, 115]. By detecting photons released by the relaxation of conduction band electrons to the valence band (known as radiative recombination), the carrier lifetime across a silicon wafer can be quantified. In the BT imaging system used in these studies, the luminescence signal is generated by external illumination (photoluminescence, PL). In silicon wafers which have a uniform doping density, brighter regions in a photoluminescence image indicates regions of higher effective minority carrier lifetime. When passivating treatments have been performed, this can indicate areas of lower recombination, therefore this is an important technique for monitoring surface passivation quality and uniformity.

In order to assess both the quality and uniformity of the different surface treatments performed on the silicon wafers, photoluminescence (PL) measurements were made using a BT Imaging LIS-L1 photoluminescence imaging tool in the School of Engineering. The set-up used is shown in Figure 3.4, with the internal setup of the system presented in the diagram.

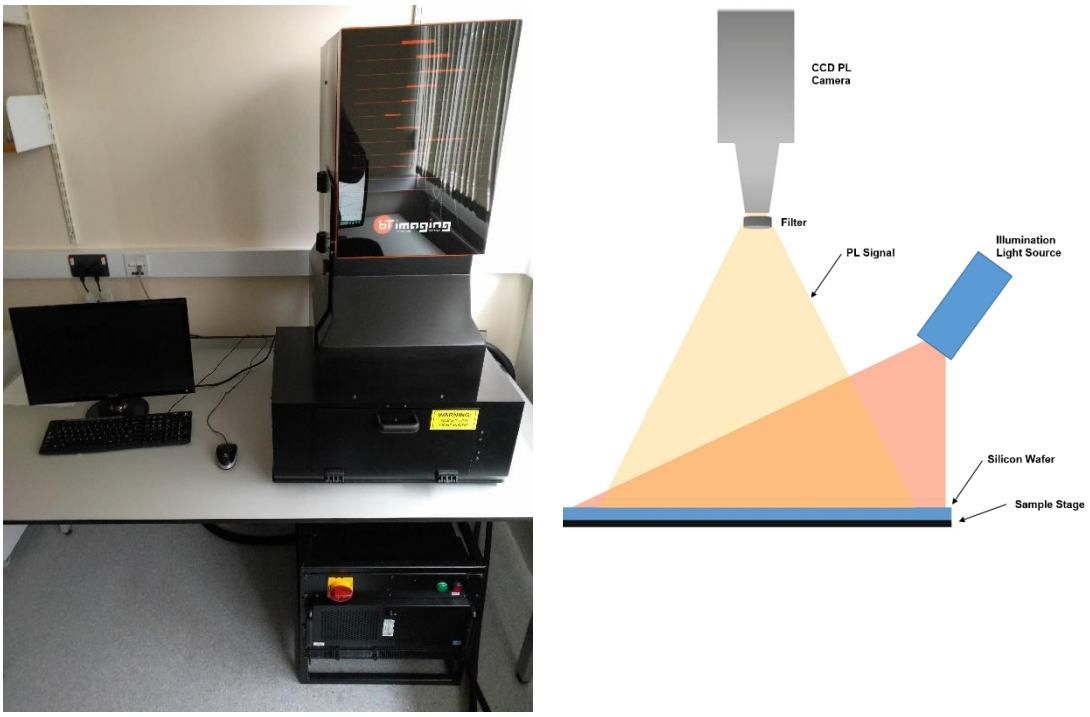

Figure 3.4 Left – Picture showing the BT Imaging iLS-L1 system used at Warwick to obtain photoluminescence images of the different passivating treatments performed during this research. Right – Simplified schematic diagram presenting the internal parts used to obtain the photoluminescence image.

The system makes use of the band-to-band radiative recombination effects [114], generating carriers by illuminating the samples from the top with an array of 630 nm light emitting diodes (LEDs). A Si CCD camera is then used to measure the intensity of the resulting luminescence of the material, producing an image of the sample being analysed. The system can produce an image with an area of up to 165 mm by 165 mm making it suitable for even larger 6-inch wafer samples.

The generation rate in the samples can be changed by varying the photon flux produced by the LED array – the maximum values this system is capable of is 3.56×10^{17} cm^{-2} s^{-1}. Photoluminescence images for the samples were gathered under a range of different generation rates and exposure times to produce quality images without over exposing the samples; these values will be specified alongside the images. Some samples were measured inside Petri dishes with their lids still on, to reduce any surface treatment degradation, however due to the type of plastic the dishes were manufactured from not fluorescing; this did not affect the measurements. Because this system does not contain a built in carrier lifetime measurement system, when calibrated lifetime images were required the minority carrier lifetime of the sample was first quantified using the standard PCD lifetime technique outlined above. A value for the carrier

lifetime in the sample is then taken from this measurement, at a specific injection level, which matches the level of illumination (generation rate) to be used when taking the PL image. A relationship between the power output of the LED array and the photon flux equivalent in Suns was known due to the linear relationship between LED power and photon flux – at the highest power level (100%), the illumination provided by the LEDs is equivalent to 1.42 Suns.

3.3.3 Raman Microscopy

All Raman microscopy measurements made in this thesis were performed on one of three Renishaw inVia Raman spectrometers, these were based in the Millburn House at The University of Warwick.

Figure 3.5 – Picture showing the Renishaw inVia spectrometer "Gonzo" with 532 nm laser used to collect some of the data presented in this thesis.

All Raman experiments presented were performed at room temperature, with raw data collected using the Renishaw provided "WiRE 3.1" software. All data were recorded the spectrometers in high confocal mode. Several different objective lenses were available for each spectrometer from

5X to 100X. Data presented measured on the 532 nm spectrometer was performed with a 50X objective lens, and point spectra data displayed are summed over 10 individual acquisitions of 1 s (unless otherwise specified). 100% laser power recorded at sample position with the 50X objective lens was measured at 18 mW; this was performed using a Thor Labs C - Series power meter equipped with a calibrated S120VC Photodiode.

Samples were transported from treatment in plastic Petri dishes with libs on; these lids were removed for data collection only to ensure minimal degradation of surfaces between treatment and analysis.

3.3.4 Nuclear Magnetic Resonance (NMR) Spectroscopy

Selected solutions in this thesis were studied in their as-prepared states by nuclear magnetic resonance (NMR) performed on a Bruker Avance III HD 400 MHz spectrometer equipped with 5mm BBFO probe with Z gradients. The equipment is based in the Department of Chemistry at the University of Warwick, with ^{1}H NMR or ^{19}F NMR spectra recorded at 400 or 376 MHz, respectively.

Bruker standard pulse sequences were used, 16 scans for ^{1}H observation and 64 scans for ^{19}F observation with inverse gated ^{1}H decoupling and without decoupling.

Chloroform-d ($CDCl_3$) was used as the NMR solvent, chemical shifts (δ) are reported in parts per million (ppm) relative to the internal standard tetramethylsilane (TMS, δH 0.00 ppm) for ^{1}H NMR and relative to external α,α,α-trifluorotoluene (δF, −63.72 ppm) reference standard for ^{19}F NMR. ^{19}F NMR is presented as hydrogen coupled.

All air and moisture sensitive chemical manipulations as well as sample tube filling were carried out under a nitrogen ambient atmosphere inside a glovebox to help prevent any external contamination. New, clean glass syringes were used to transfer each solvent or chemical solution independently.

All samples were analysed in 5 mm NMR tubes from Norell. All dry and deuterated solvents were purchased from Sigma Aldrich and used as supplied with no further purification. All data acquisition and initial processing was performed using Topspin 2.1, all post acquisition processing was performed with NMR Spectroscopy Software from Advanced Chemistry Development.

3.3.5 X-ray Photoelectron Spectrometry

The X-ray photoelectron spectroscopy (XPS) data presented in this thesis were collected and analysed by Dr Marc Walker on a Kratos Axis Ultra DLD, in the photoemission facility based at the University of Warwick.

The samples under analysis needed to be mounted to copper sample studs using electrically conductive carbon tape shown in Figure 3.6.

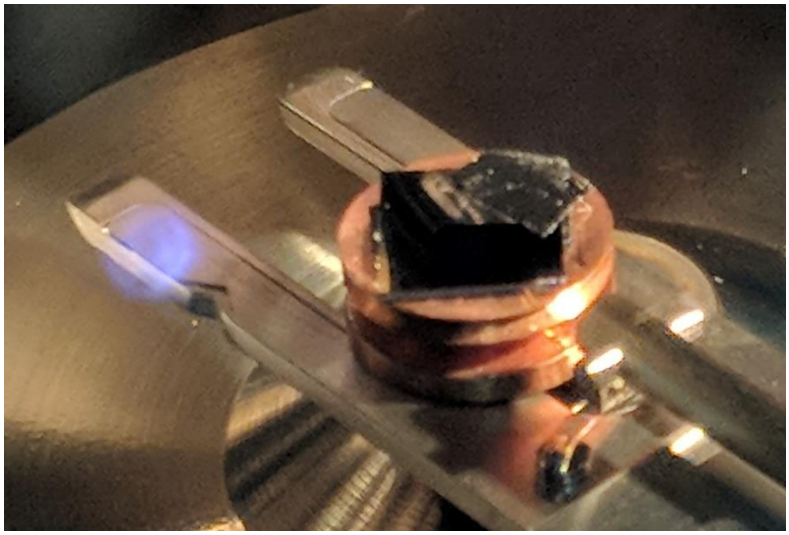

Figure 3.6 – Picture showing one of the samples mounted to copper stub inside the transfer chamber of the XPS system before being moved into the analysation chamber for measurement.

Samples were treated and mounted to the copper stub before being placed inside a transfer tube and sealed shut for transport to the XPS system. Depending on where the samples were treated different sample tube loading processes were used; for samples with a final treatment which was performed inside the high specification glovebox the whole tube assembly was transferred through the airlock into the glovebox chamber and the copper stud mounted in the transfer tube here, the tube was then sealed shut before removal back through the airlock in order to seal the sample in the inert atmosphere of the high specification glovebox during transport and while waiting to be loaded. When a sample was being processed in the low specification glovebox, the transfer tube was placed into the glovebox before the glovebox was purged and processing started, once the sample sub has been loaded additional N_2 gas was used to purge the small chamber of the transfer tube before being sealed shut, it was then removed from the low specification glovebox for transport. Finally samples which were processed in the open air (such

as at the wet benches used for chemical cleaning) were mounted to the copper stub and loaded into the tube in the ambient air of the lab, before the tube was sealed shut a N_2 gas spray gun located in the wet bench was used to purge the loading tube chamber containing the sample for 30 s before it was sealed shut. Purging with nitrogen was done to ensure samples were held in an inert atmosphere while being transported from the lab where treatments were performed to the lab containing the XPS equipment, in order to try to prevent any sample or surface degradation.

Sample stubs were moved from the transfer tube to the load lock under negative pressure where they were then pumped down for approximately one hour to achieve a base pressure of around $1x10^{-8}$ mbar. Once transferred to the analysis chamber a pressure of around $1x10^{-10}$ mbar is held whilst the measurements are taken.

XPS measurements were conducted with the sample being illuminated using a monochromated Al Kα X-ray source. The measurements were conducted at room temperature and at a take-off angles of both 90° (greater penetration depth) and 15° (more surface focused) with respect to the surface parallel.

The photoelectrons were detected using the Kratos delay-line detector, comprising a multi-channel plate stack above a delay-line anode. The core level XPS spectra were recorded using pass energy of 20 eV (resolution approximately 0.4 eV) from an analysis area of 300 μm × 700 μm. The spectrometer work function and binding energy scale were calibrated using the Fermi edge and 3d5/2 peak recorded from a polycrystalline Ag sample prior to the commencement of the experiments. Fitting procedures to extract peaks positions and relative stoichiometries from the XPS data were carried out using the Casa XPS software suite , using Shirley backgrounds and mixed Gaussian-Lorentzian (Voigt) line shapes.

3.3.6 Kelvin Probe

Surface charge calculations performed during this thesis were obtained through the Kelvin probe method, which uses non-contact methods to quantify levels of charge on a sample surface.

The macroscopic Kelvin technique was developed in 1898 by Kelvin [116] for the measurement of surface potentials. The probe is typically a small pin which acts as one plate and is held 0.1-1 mm above the sample. The sample constitutes the other plate of a parallel plate capacitor, with a known metal forming the probe plate, which is vibrated at a given frequency. This vibration changes the distance between the plates, which results in a capacitance change, and therefore produces an alternating current in the circuit connecting the two plates. The probe vibrates perpendicular to the sample plane forming a parallel plate capacitor; this setup can be seen in Figure 3.9.

The concentration of any surface charge that may be present can then be calculated through the use of the zero current method [117], where, by applying a dc-voltage to one of the plates this current is reduced to zero, this known voltage then corresponds to the contact potential difference of the two materials.

Kelvin probe measurements made during this thesis were performed on a KP technology single-point Kelvin probe system model KP020. This equipment was based in The University of Oxford's Department of Materials.

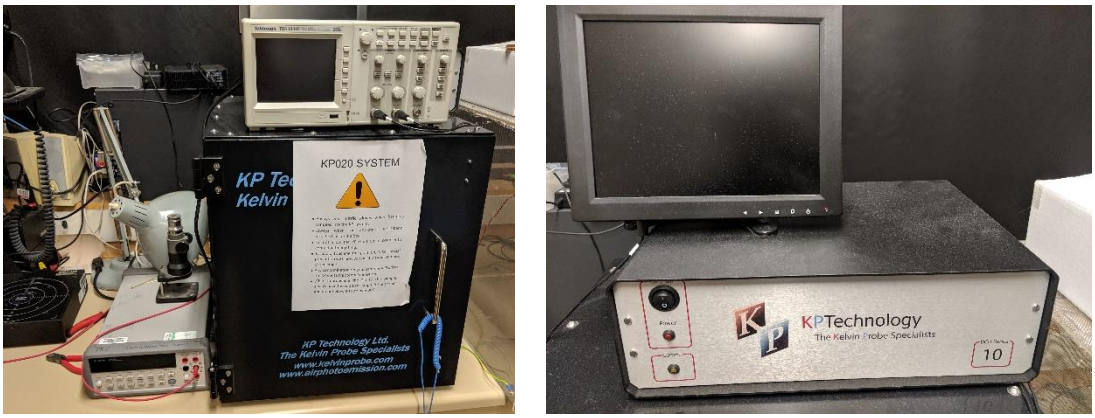

Figure 3.7 – Pictures showing the experimental setup used for measuring surface charge. The KP Technology KP020 tool was based in the Department of Materials and the University of Oxford.

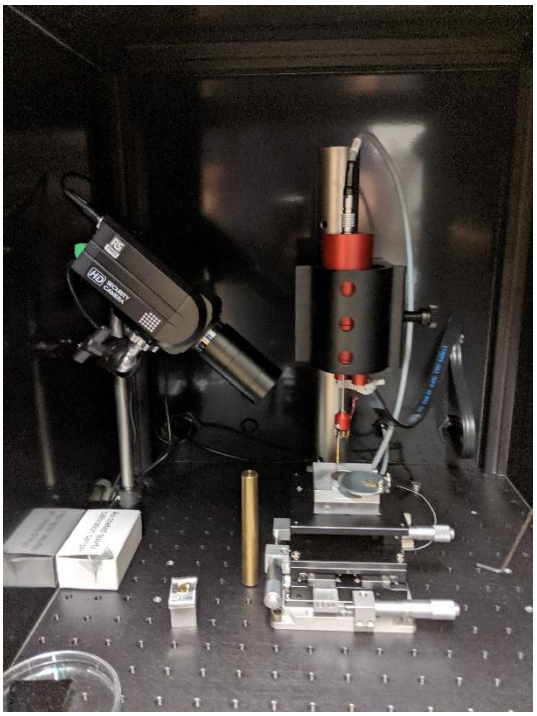

Figure 3.8 – Picture showing internals of the KP Technology KP020 measurement tool

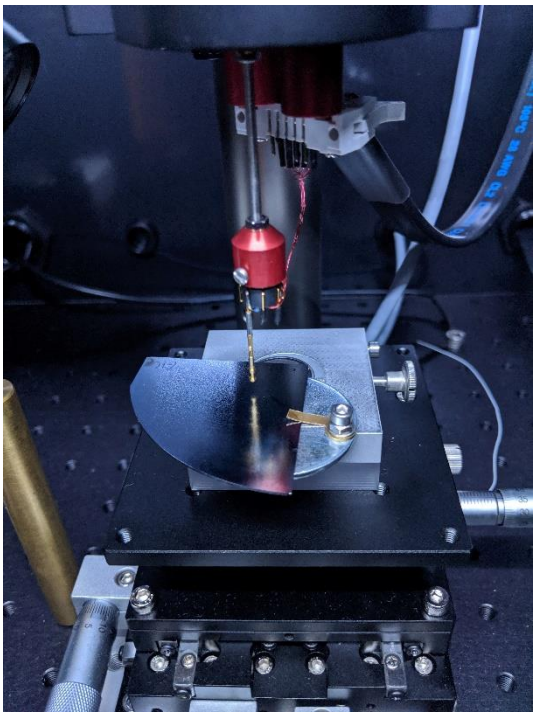

Figure 3.9 - Image showing sample in situ under Kelvin probe analysis tip.

Due to the distance and time taken to get to the instrument from Warwick it was vital to protect the samples from the atmosphere as much as possible. After preparation using the standard methods outlined, samples were placed into plastic petri dishes with their lids on. These were then sealed inside an airtight, lightproof flight case for transport to the measurement equipment. Samples were measured after preparation (before leaving Warwick) and upon arrival at Oxford and never lost more than 10% of their starting lifetime – the time between these two sets of measurements (dictated by the time taken to travel by car from Warwick to Oxford) was between 1 hour and 1 hour 30 minutes.

3.3.7 Atomic Force Microscopy (AFM)

The AFM data in this thesis were collected by Prof. Neil Wilson, based in the Department of Physics at the University of Warwick.

The silicon surface microtopography was measured using a Bruker Icon AFM operating in PeakForce Tapping mode.

3.4 Summary

In this chapter the sample and chemical treatment preparation procedures and experimental techniques employed in order to obtain the data presented in this study have been described.

Chapter 4 Solvent Dependence of Superacid-derived Passivation

In this chapter, an empirical study into how the choice of solvent for the super-acidic solution affects the passivation is presented. The effect of the environmental storage conditions on passivation quality and longevity is also studied. Finally, some applications of the passivation approach are demonstrated.

4.1 Motivation

The use of a new class of temporary passivation has been reported relatively recently in the literature [101] where thin films of superacid-containing solutions are deposited onto the surface of silicon samples to passivate their surface. This preliminary work by Bullock *et al.* examined various superacids and showed that bis(trifluoromethane)sulfonimide (TFSI) crystals dissolved in 1,2-dichloroethane (DCE) gave rise to the best levels surface passivation. Follow-on work performed at the University of Warwick, showed, that with optimised surface cleaning and pre-treatment, it is possible to use this approach to give effective surface recombination velocities of less than 1 cm s^{-1} [103]. This is exceptional when compared with other temporary passivation techniques, with most other temporary treatments providing surface recombination levels well in excess of 1 cm s^{-1} and as high as at least 100 cm s^{-1}; typically only HF acid based treatments being able to offer velocities below 1 cm s^{-1}. A more in depth review of temporary surface passivation has been published by Grant and Murphy [67].

However, the study by Bullock *et al.* [101] has shown that this technique has drawbacks when it comes to passivation longevity– particularly if the treatment is contaminated with water or exposed to air. Literature previously reviewed in this thesis, reported the passivation staying relatively stable during the first hour after treatment but rapidly degrading after this. Both studies used highly hazardous chemicals, with DCE being particularly problematic as it has been classified as a human carcinogen [102].

Therefore, there is strong motivation to seek alternative compositions to the solution used for the passivation treatment. By changing the solvent used in the creation of the solution it may be possible to improve its long-term stability, which may unlock the ability to turn this currently

temporary surface passivation scheme into something more permanent. Additionally, the underlying chemical mechanism by which the treatment solutions create the passivating thin film is not currently known – gaining a greater understanding of the effect the solvent has on the passivating solution may help to improve the fundamental understanding of the technique.

This work will present a study into alternative solvents to DCE, looking to improve the treatment properties while also reducing the chemical risks. The following sections will present the results obtained performing these studies.

4.1.1 Principle of Superacid-derived Passivation

The general experimental details and chemicals used for the solution-based treatment were outlined in Chapter 3; further details on the exact processes used for this part of the study will be given alongside the results for each experiment below.

All solvents used in this section of work are given in Table 4.1. The solvents chosen have a wide range of relative polarities with values obtained from Ref. [118].

Label	Solvent name used	Chemical name	Formula	Relative Polarity	Supplier (product number)	Purity
A	Acetone	2-propanone	C_3H_6O	0.355	VWR (83683)	99.9%
B	Chlorobenzene	Chlorobenzene	C_6H_5Cl	0.188	Sigma Aldrich (284513)	99.8%
C	Cyclohexane	Cyclohexane	C_6H_{12}	0.006	Sigma Aldrich (227048)	99.5%
D	Dichloroethane (DCE)	1,2-dichloroethane	$C_2H_4Cl_2$	0.327	Sigma Aldrich (284505)	99.8%
E	Dioxane	1,4-dioxane	$C_4H_8O_2$	0.164	Sigma Aldrich (296309)	99.8%
F	Dichloromethane (DCM)	Dichloromethane	CH_2Cl_2	0.309	Alfa Aesar (41835)	99.7%
G	Hexane	n-hexane	C_6H_{14}	0.009	Sigma Aldrich (296090)	95.0%
H	Isopropanol (IPA)	2-propanol	C_3H_8O	0.546	Sigma Aldrich (278475)	99.5%
I	Octane	n-octane	C_8H_{18}	0.012	Sigma Aldrich (296988)	> 99 %
J	Toluene	Toluene	C_7H_8	0.099	Sigma Aldrich (244511)	99.8%

Table 4.1 – List of solvents used during the study performed in this Chapter, with identifying labels. All the solvents purchased were in their anhydrous forms. The relative polarities provided are taken from Ref. [119].

4.2 Results & Discussion

4.2.1 Passivation Dependence on Solvent for TFSI

A series of experiments was performed passivating silicon wafers with TFSI dissolved in the different solvents listed in Table 4.1, in order to gain further understanding of the chemical mechanism of the passivating treatments and the variations the solvent itself causes.

For each new solvent, 200 ml of passivating solution was prepared using the standard procedure outlined in Chapter 3. The TFSI crystals generally dissolved in the solvents fairly rapidly, with the exception of chlorobenzene, hexane, and octane, in which the crystals took several hours or even days to dissolve fully. The test samples were treated using the solutions as soon as possible after the TFSI crystals had dissolved sufficiently in order to ensure treatments were performed with as fresh a mixture as was possible. The point of complete dissolution of the crystals was determined by eye, as it could clearly be seen whether TFSI crystals remained at the bottom of the solutions. For example, TFSI-DCE mixtures were ready almost instantaneously, with the crystals dissolving as soon as the solvent was added to the bottles. Conversely, when mixing TFSI-Hexane this solution needed to be left for around 24 hours before being ready to use, with no more visible TFSI crystals remaining.

When the solutions were ready, samples were treated using the standard procedure outlined in Chapter 3. It was important to take great care to ensure that bulk lifetime variations – which could occur even between float-zone wafers within the same batch [89] – did not influence the results gained from results across several test wafers. This was done by routinely cross-checking quarter samples taken from the same wafer (hence assumed to have the same bulk lifetime) with different passivation schemes. For example, the toluene and acetone results shown in Figure 4.1 were acquired from quarters taken from the same wafer, so it can be reasonably assumed that the different injection-dependence observed with acetone arises from the passivation and not from a bulk defect. Other pairs of samples were DCM and DCE, and chlorobenzene and octane. For other solvents cross-referencing was made to DCE as this passivation scheme was well understood from the previous work performed on this treatment scheme [103].

The injection-dependent lifetimes, measured immediately after passivation are all presented in Figure 4.1. This shows that the change in solvent for the treatment solution has a significant effect on the levels of surface passivation that can be achieved with the solution treatment. The dependence of lifetime on excess carrier density has similar characteristics in all cases, with the exception of TFSI-acetone, TFSI-cyclohexane and possibly TFSI-dioxane, with the last of these giving a much lower lifetime than all the other solvents studied.

There appears to be no immediate correlation between the lifetime achieved by the treatment and the relative polarity of the solvent used for the solution (as given in Table 4.1). DCE and DCM both have high relative polarities; whereas the polarities of toluene and hexane are relatively low, when used as a solvent for TFSI the lifetimes measured by all four different solutions appear to be very similar in each case, which will be discussed in greater depth in later sections.

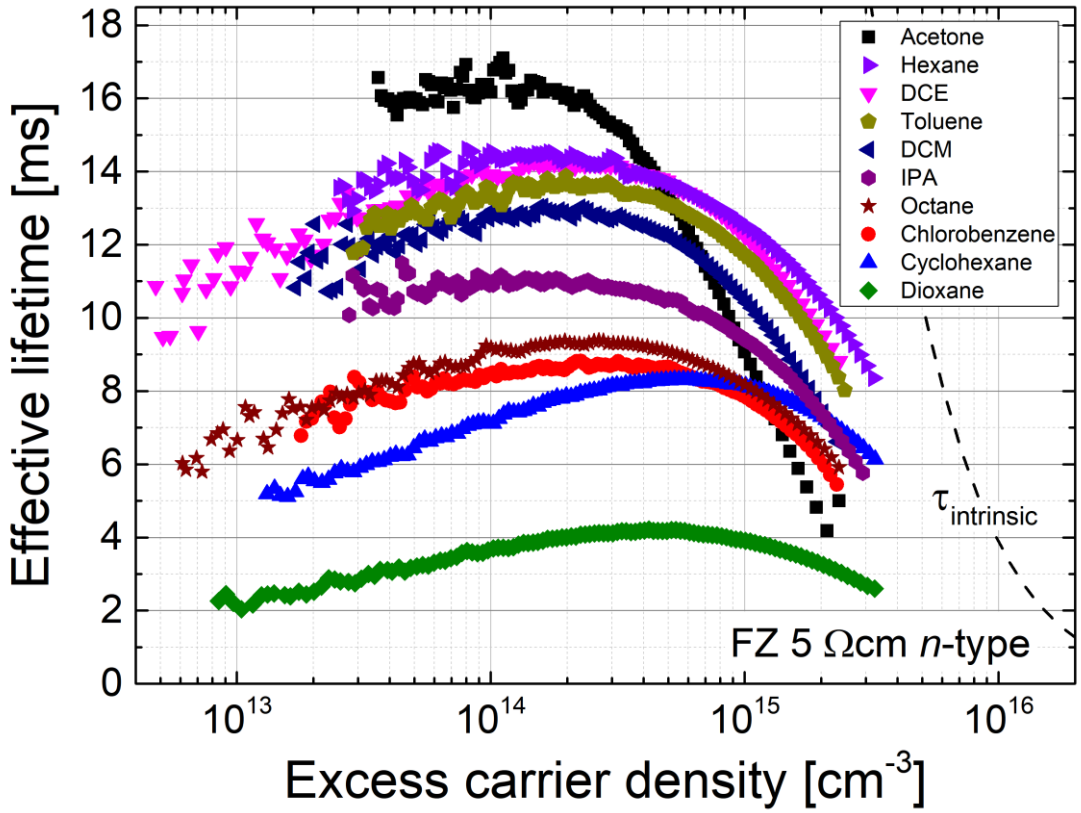

Figure 4.1 – Effective lifetime versus s excess carrier density plotted for 5 Ωcm *n*-type float-zone silicon wafers all with a thickness of 740 µm which have been passivated with TFSI dissolved in different solvents. The properties of the solvents are given in Table 4.1. The intrinsic lifetime limit given by Richter *et al.* [28] is also plotted, the calculation is discussed in Section 2.1.3.

In order to be a successful alternative to TFSI-DCE, the requirement for any new treatment is that it achieve similarly high lifetimes, whilst also offering other improvements. Initially the results presented in Figure 4.1 reveal TFSI-acetone, TFSI-hexane, TFSI-toluene and TFSI-DCM could be possible candidates when compared with TFSI-DCE (indicated with the data points denoted by ▼). Whilst the treatment based on TFSI-acetone does result in the highest measured lifetime, it must be noted that this is at lower injection levels, and that at high injection levels this treatment causes a much greater injection-dependence than some of the other treatments tested here, which could be undesirable when performing materials characterisation with the technique.

If during the course of treatment the superacid-containing solution induces a significant amount of negative charge at the surface of the silicon samples (the underlying mechanism of passivation will be discussed in greater detail later in this Chapter and throughout the thesis), an inversion layer may exist near the surface with sufficiently low sheet resistivity, so that holes could travel to the quarter wafer sample's edge as majority carriers and recombine there. This phenomenon was reported in Ref. [120] to cause a continuous decrease in effective lifetime with decreasing injection density in low-injection. This phenomenon may be the cause for the decrease in effective lifetime that can be observed in the results towards $\Delta n = 10^{13}$ cm^{-3}.

Furthermore, it is noted that the injection dependence following a treatment based on TFSI-acetone, is similar to that observed in the work of Bullock et al. [101] for acetonitrile (relative polarity 0.460 [119]) based treatments. Unlike standard hydrocarbon solvents, acetone also contains oxygen, so this difference may be attributed to the solvent molecules being incorporated into the thin passivating film, or the solvent influencing the break-up of the TFSI ion in some way. The change in the injection dependency could suggest that the films which form with acetone and acetonitrile solvents have different inbuilt charge densities from the other films tested, and this therefore could result in a field effect modifying the effective surface passivation.

While from this initial lifetime data there appeared to be little effect on the passivation from the chemical makeup of the other non-basic hydrocarbon solvents used, this was later shown not to be a complete picture and more crucial differences were found; these will be discussed in the following section.

4.2.2 Degradation of Passivation

A series of experiments was performed in order to assess the stability of the passivation achieved by the different TFSI-containing solvent solutions when applied to the test wafers. Once treated, the effective lifetime of the treated samples was recorded over a one hour period and this is plotted as a function of time post-superacid treatment, as shown in Figure 4.2. These data have been normalised by the starting lifetime of the sample to account for variances between the treatments. In between each measurement the samples were stored in the dark in their petri dishes, loosely covered by a lid. Figure 4.2 (a) shows the lifetime arising from TFSI dissolved in solvents shown to have a relatively high starting lifetime from Figure 4.1, and Figure 4.2 (b) shows the results for the relatively low-lifetime cases.

When considering the passivation schemes that were shown to provide relatively high lifetimes shown in Figure 2 (a) the most relatively stable treatments (i.e. within 10 % of the initial lifetime over 1 hour) appear to be TFSI-toluene and TFSI-hexane solutions, both appearing to offer some additional stability when compared with TFSI-DCE. The other systems offering comparable lifetimes to TFSI-DCE are less stable.

When considering the alternative low-lifetime results shown in Figure 2 (b), TFSI-chlorobenzene and TFSI-cyclohexane exhibit very good stability (again within 10% of the starting lifetime), offering some additional stability when compared to TFSI-DCE but with a lower effective lifetime, and thus passivation quality. The other lower lifetime treatments TFSI-IPA, TFSI-octane and TFSI-dioxane were seen to be less stable.

During testing the degradation of the passivation offered by the range of different solvent chemicals it was noted that while solvents which contained other elements (in this case, oxygen and nitrogen) could compete with the initial passivation levels and therefore with measured lifetimes of solutions using straight hydrocarbons (compounds containing only carbon and hydrogen) as the solvent, when it came to the degradation of the resulting surface passivation there were marked negative differences.

In general, the passivation achieved when using mixtures of TFSI dissolved in oxygen-containing or nitrogen-containing solvents (in this study acetone, dioxane and IPA), show a faster decay in the effective lifetime compared to those passivated using a standard hydrocarbon as the solvent (e.g. TFSI-Hexane, TFSI-toluene etc)

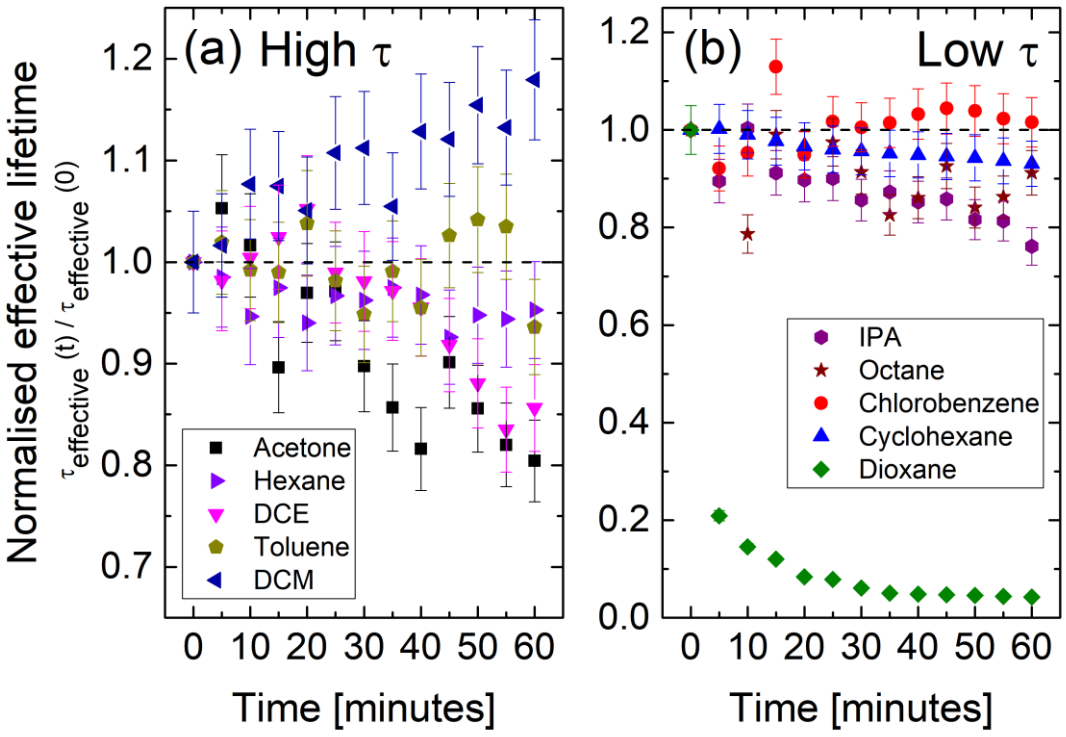

Figure 4.2 – Normalised effective lifetime at an excess carrier density of 10^{15} cm^{-3} vs time since first measurement (the lifetimes are normalised to the first measurement taken for that sample) on samples passivated with TFSI dissolved in the solvents being studied. Graph (a) contains the results from solvents which give high absolute lifetimes, while graph (b) shows results for lower absolute lifetimes in Figure 4.1. Samples for this experiment were 5 Ω cm *n*-type float-zone silicon with a thickness of 750 µm.

It should be noted that the passivation provided by TFSI-DCM treatment actually improves significantly with time after application, but this would not be desirable for a reproducible measurement in a lab setting. Further to this in the search for a safer treatment methodology compared to TFSI-DCE, it is also desirable to try and avoid the use of other chlorinated solvents.

The results presented in Figure 4.2 show that a TFSI-hexane based treatment is favourable over the TFSI-toluene treatment as it is seen to give slightly superior effective lifetimes, in addition to greater stability of prepared solutions as will be discussed in greater detail in Section 4.2.4. It is noted, however, that given the complexity of the surface chemistry (formation and stability), the exact mechanism by which the chemical treatment passivates the surface is unknown at this point. One hypothesis could be that the solvent, or some of its constituent atoms, are contained within the thin film that forms on the silicon surface, hence the passivation dependence on the solvent. It could also be that the TFSI molecule breaks up via specific routes depending on its

interaction with the solvent with which it is mixed, leading to the changes in passivation quality and passivation degradation as observed in Figure 4.1 and Figure 4.2.

4.2.3 Effects of Storage Conditions

It was known from existing literature [101, 103] that exposure of samples to air leads to a degradation in the surface passivation of prepared samples, and that any contamination of treatment solutions with water also degraded the performance of a subsequent treatment. In order to understand how atmospheric conditions affect the surface passivation, experiments were conducted to establish the influence of storage humidity on the level of surface passivation achieved as a function of time.

A single float-zone silicon wafer (5 Ωcm *n*-type) was cleaved into four quarter-wafer samples, which were all passivated with TFSI-hexane using the previously established method (see Chapter 3). The as-passivated lifetimes for the quarters were all within the interval 13.3 ± 0.1 ms, which demonstrates that the samples' initial states are identical within experimental error. After passivation, two samples were stored in ambient laboratory conditions (room relative humidity: 39 ± 2 %); one with the lid off the petri dish; another with its lid on. The two other samples were stored in conditions deliberately engineered to deviate from ambient humidity. The "dry" sample was stored in a desiccator containing silica gel in which the relative humidity was measured to be below 20 %. The "wet" sample was stored in a container with an open vessel of water, for which the relative humidity was measured to be above 70 % during the tests. When performing each lifetime measurement, samples were removed from their low or high humidity environments for as short a time as possible (typically < 2 minutes for each measurement), and returned to their storage conditions until the next measurement.

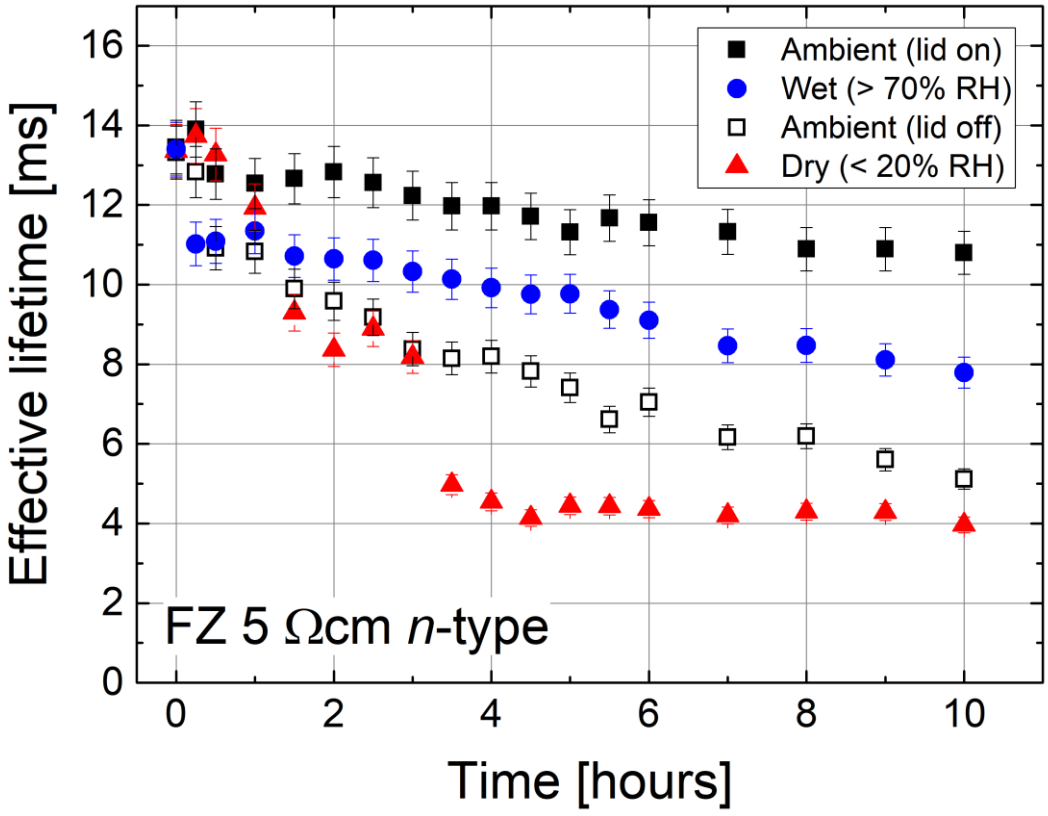

Figure 4.3 – The effect of humidity on effective lifetime at an excess carrier density of 10^{15} cm^{-3} for four quarters of a 5 Ωcm *n*-type float-zone silicon wafer. Samples were passivated with TFSI-hexane and were stored under the conditions indicated in the legend. Ambient relative humidity (RH) in the laboratory was 39 ± 2 %, and the laboratory temperature was 24 ± 1 °C. Samples for this experiment were 5 Ω cm *n*-type float-zone silicon with a thickness of 740 µm.

The results from this experiment are presented in Figure 4.3; the data show that the temporal dependence of lifetime varies strongly according to the storage conditions of the treated samples e.g, ambient (lid-on), ambient (lid-off), wet (>70% RH) and dry (<20% RH).

From Figure 4.4, it is apparent that exposing the superacid treated silicon surfaces to varying environmental conditions, that the degradation rate increases as the relative humidity decreases (excluding the ambient (lid-on) case). This suggests that the presence of some moisture in the storage atmosphere after treatment is actually beneficial for retaining the best surface passivating effect for the longest time. For the driest condition (e.g. <20% RH), which initially exhibits the fastest degradation rate, there may be a driving force for evaporation from the passivating film on the surface of the sample – whether that be from the treatment film itself or moisture from the film – which could reduce the level of passivation offered. As the composition of the films is as yet unknown, it is not yet possible to know the exact driving mechanism of this. It can be

noted that the dry case in Figure 4.3 appears to reach a plateau after 4 hours; this could be due to some form of equilibrium being established between the surface film and the surrounding environment, which would appear to support the idea of the passivating film drying out or evaporating. When in a more humid environment there should be less of a driving force for evaporation from the sample surface and passivating film, however it might then be that water from the surrounding environment becomes absorbed into the passivating film, effectively diluting the chemical passivation effects. This dilution effect is supported by the degradation seen in the TFSI-DCE study by Bullock *et al.* [101], which found that adding water to the passivating solution decreases the level of surface passivation achieved.

Now considering the storage condition that exhibited the most stable behaviour, ambient (lid-on), it is apparent this condition is rather unique, as the local environment beneath the lid (i.e. inside the container) can be approximated as a closed system. In this case, no additional moisture can access the film to dilute the passivation, and the possibility of any evaporation of the film is reduced as equilibrium will soon be reached due to the small volume of the storage container. Any degradation which does occur in the lid-on sample could occur when the lid is removed for lifetime measurement purposes or due to any leaks which occur due to the relatively loose fitting of the lid. Much more experimental work is needed to understand these effects further, and may only be fully understood when the detailed chemical composition and passivation mechanism of the films is known.

4.2.4 Solution Degradation

During the course of research, as well as passivation quality degrading with time (in the order of a few hours) it was also discovered that the age of the passivating solution appeared to be an important factor affecting the resulting quality of the passivation treatments, with chemical reactions being observed to occur in various TFSI-solvent systems once prepared, which was evidenced by a colour change of the solution.

In order to achieve the optimal passivation possible with the superacid-containing solutions it was necessary to quantify this behaviour and to understand which chemical mixtures were affected by reactions between the chemicals making up the solutions. In order to do this standard mixtures were prepared for each of the different solvents used in this section. These were

carefully decanted into sterile 50 ml scintillation vials and left without being opened, with regular images being taken of the set of vials under consistent lighting conditions. These images are composed in Figure 4.4, which shows a time series of the photographs of small sealed vials of TFSI-solvent solutions. Colour changes are visible to the eye for acetone, DCE, dioxane and toluene, even in the sealed sterile storage vials depicted.

The colour changes that have been observed in sealed containers of unused passivating solutions (shown in Figure 4.4) give evidence of reactions occurring between the solvent and TFSI alone, even when not in the presence of silicon. This is not surprising given the extreme acidity of the TFSI superacid ion, and the plethora of acid-catalysed organic reactions that are known to exist.

In the simplest case when using acetone as the solvent, it is most likely that a self-condensation or cross-condensation [121] reaction has occurred in this solution; the speed of the reaction and progression of the solution to it's final dark black colour is also expected because of the ease with which aldol reactions typically take place when acetone is in the presence of an acid. Further to this, recent studies have shown that more complex reactions can take place when DCE [122] and toluene [123, 124] react with a variety of superacids as well. Dioxane, like TFSI, is hygroscopic – the accumulation of water from the atmosphere after mixing may explain the reaction that is observed, and it could be reasonably assumed that this absorption of water would lead to increased degradation of the passivating film if this were a suitable treatment mixture. Additionally dioxane is Lewis-basic and so is able to undergo typical acid-base reactions.

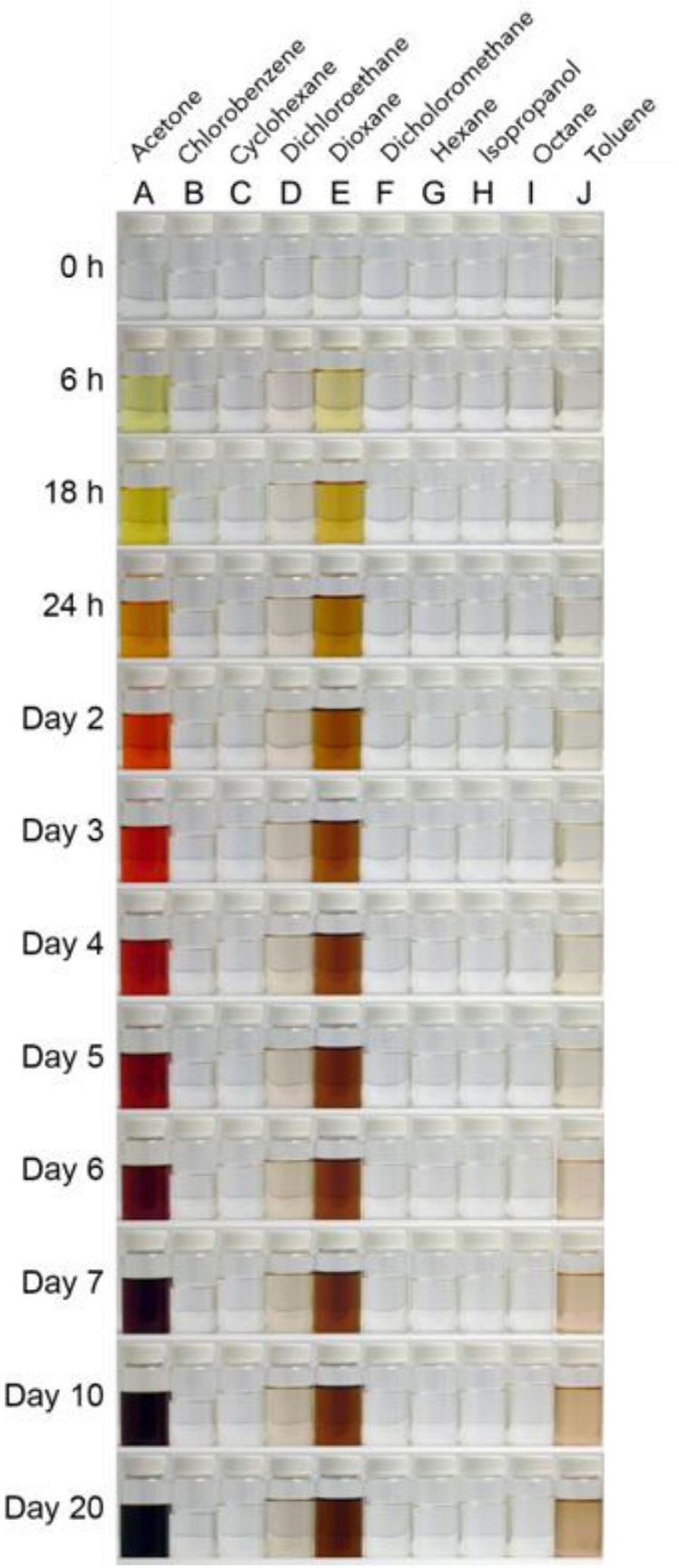

Figure 4.4 – Time series photographs showing vials containing solutions of TFSI in different solvents. The vials are labelled corresponding to additional chemical data provided in Table 4.1. Colour changes were observed in the vials containing acetone (A), DCE (D), dioxane (E) and toluene (J).

In order to identify the products that are created, individual characterisation of the solutions that appear to react when mixed would need to be done, but even without explicit characterisation it can be suggested that the solutions that undergo noticeable changes and the solvents that make them up are probably largely unsuitable for the passivation of silicon because these side reactions and the by-products that are created will most likely hinder the underlying passivation mechanism of superacid solutions, if not just through a reduction in the reagents available for surface passivation due to being used up in the unwanted side reactions. Moreover, even if these side reactions and by-products did not directly hinder the passivation treatments, when used for testing in order to ensure the passivation would be reproducible across a range of experiments an entirely new solution would need to be made each time which would be a waste of chemicals and time, and be more expensive.

With one of the main aims of this study being to find a suitable replacement passivating solution for TFSI-DCE, it is interesting to note from the colour changes evident in Figure 4.4 that in fact the TFSI-DCE solutions are amongst those that undergo a chemical reaction between the TFSI and solvent components even in the absence of silicon. It therefore seems likely that this chemical change, given time, may also affect the quality of the resulting surface passivation.

Even though TFSI-hexane did not appear to experience a noticeable colour change it is important to assess its long-term passivation ability and solution longevity once prepared. In order to evaluate if there are improvements offered by using unreactive solvents, the TFSI-DCE (which was seen to react) and the most promising seemingly unreactive alternative TFSI-hexane were compared to see if to see if the reactions occurring in solution effects their passivation ability. To understand this in greater detail an experiment was performed passivating 5 Ωcm FZ silicon samples with new solutions and with solutions that have been stored in air-tight bottles for 21 days since mixing. The results from these tests are presented in Figure 4.5. After the passivation treatment, the samples were stored in the dark in their petri dishes loosely covered by a lid between each measurement. New solutions of TFSI-hexane and TFSI-DCE gave initially the same lifetimes within typical measurement errors [113].

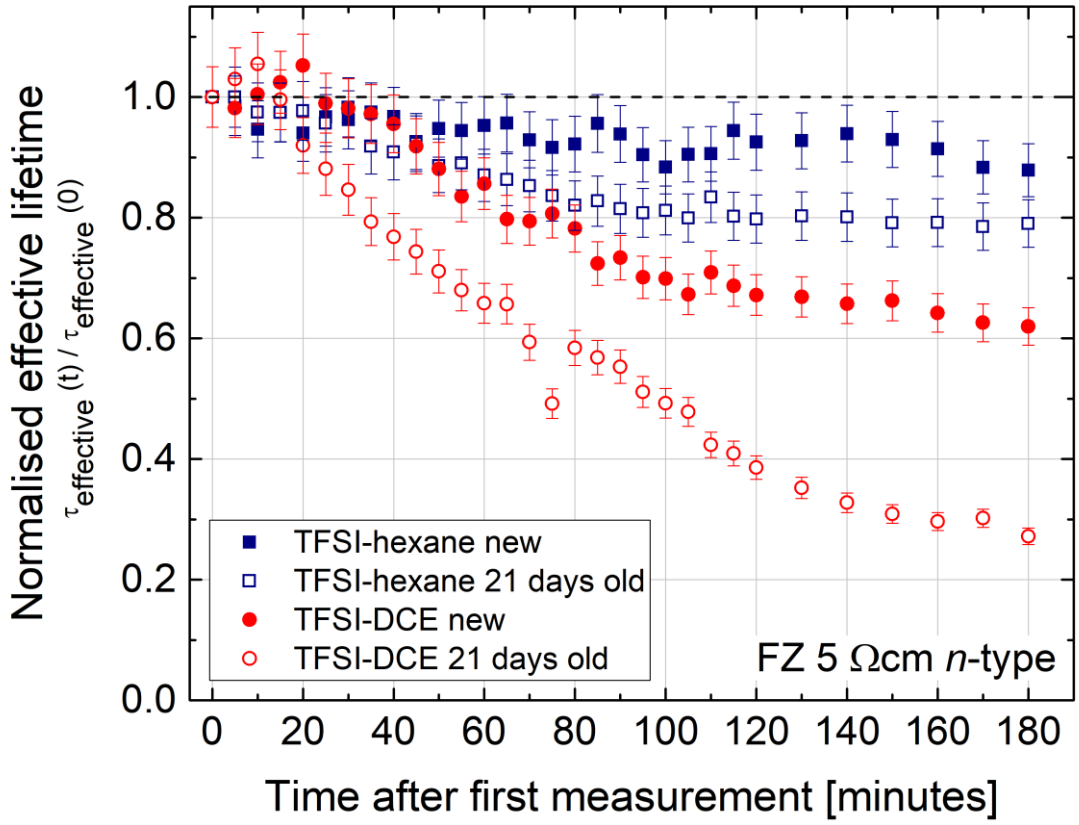

Figure 4.5 – A comparison of the time stability of TFSI-hexane and TFSI-DCE solutions in the (new) fresh state and after 21 days of sealed storage. The effective lifetime at an excess carrier density of 10^{15} cm^{-3} at each time step was normalised by that of the first measurement.

Upon testing, the solution ageing results (presented in Figure 4.5) indicate that better initial passivation results are achieved with new solutions for both the TFSI-DCE and TFSI-hexane treatments. Whilst the results from both new solutions do initially provide similar levels of surface passivation after approximately 1 hour, there is a distinct deviation between the passivation quality of the two, with the passivation offered by the TFSI-hexane treatment remaining noticeably more stable on the surface of the silicon wafer.

When the same test is repeated but using solutions which have aged for 21 days (open symbols in Figure 4.5), the trend is similar, however this time the degradation suffered by the TFSI-DCE solution is significantly worse than that when treated with a new solution, while the passivation arising from the aged TFSI-hexane solution shows only slightly worse degradation when compared with a freshly-made solution.

These changes in passivation would only occur if the films slightly differ in either their composition or charge state, both of which must stem directly from the change in solvent, as this

is the only variable. It can thereby be inferred that the solvent used in creating the passivating solution plays a significant role in both the passivation level and the stability of the film, which is also supported by the data in Figure 4.1

It could be suggested that the degradation rate is determined by water moisture contamination of the passivating solutions. At 25 °C the solubility of water in DCE is 0.1262 M [125], whereas in hexane it has a much lower value of 0.00362 M [126]. This could mean more water could be incorporated into the film when using the DCE-based treatment and so this could explain differences. Additionally from Figure 4.4, it is evident that TFSI-DCE undergoes some self-reaction and this could also explain the increased degradation with the older solution.

4.2.5 Extraction of Bulk Lifetime and Effective Surface Recombination Velocity

Having now established the apparent superiority of the passivation scheme arising from a solution of TFSI with hexane used as the solvent instead of DCE, a set of experiments was conducted in order to separate the contributions to effective lifetime arising from surface and bulk effects, in order to understand the true levels of surface recombination velocity that is possible with the improved treatment scheme.

For a symmetrically-passivated lowly-doped sample with relatively low surface recombination velocity, the injection-dependent effective lifetime, $\tau_{effective}$, varies according to Equation 4.1.

$$\frac{1}{\tau_{effective}} = \frac{1}{\tau_{bulk}} + \frac{2S}{W} \qquad \text{Equation 4.1}$$

Where τ_{bulk} is the injection-dependent bulk lifetime, S is the injection-dependent effective surface recombination velocity, and W is the sample thickness. By measuring $\tau_{effective}$ in a set of samples with variable W and constant τ_{bulk} it is possible to determine both τ_{bulk} and S as a function of excess carrier density using Equation 4.1.

A set of 3 Ωcm *n*-type FZ silicon wafers with different thicknesses were specially sourced from the same ingot for this experiment. These 4" diameter wafers were not cleaved and were measured whole, as supplied, to minimise edge effects. The wafers were passivated using the TFSI-hexane solution, and the best-case effective lifetime data are shown in Figure 4.6 (a).

As expected, the effective lifetime increases with increasing wafer thickness due to the reducing influence of the surfaces. The assumption is that τ_{bulk} is approximately the same in all these wafers, so any change in effective lifetime is due to differences in surface recombination. Figure 4.6 (b) shows plots in accordance with Equation 4.1 used to extract S and τ_{bulk} at two different excess carrier densities. The fits to the data shown are very good with R^2 values of 0.978 and 0.990 at 10^{14} cm^{-3} and 10^{15} cm^{-3} injections, respectively. S is extracted as 0.68 ± 0.06 cm s^{-1} and 0.69 ± 0.04 cm s^{-1} for 10^{14} cm^{-3} and 10^{15} cm^{-3} injections, respectively, and τ_{bulk} being 41 ± 2 ms and 34 ± 2 ms, respectively. Equation 4.1 is used at each level of averaged injection to extract the τ_{bulk} as a function of excess carrier density and this is also plotted in Figure 4.6 (a).

Figure 4.6 (c) shows an uncalibrated photoluminescence image of the thinnest wafer, characterised when 179 μm thick, which demonstrates the passivation is uniform across the wafer, and that there are no unusual bulk lifetime features in the samples studied, such as concentric ring-like features which are sometimes observed in silicon lifetime images [51].

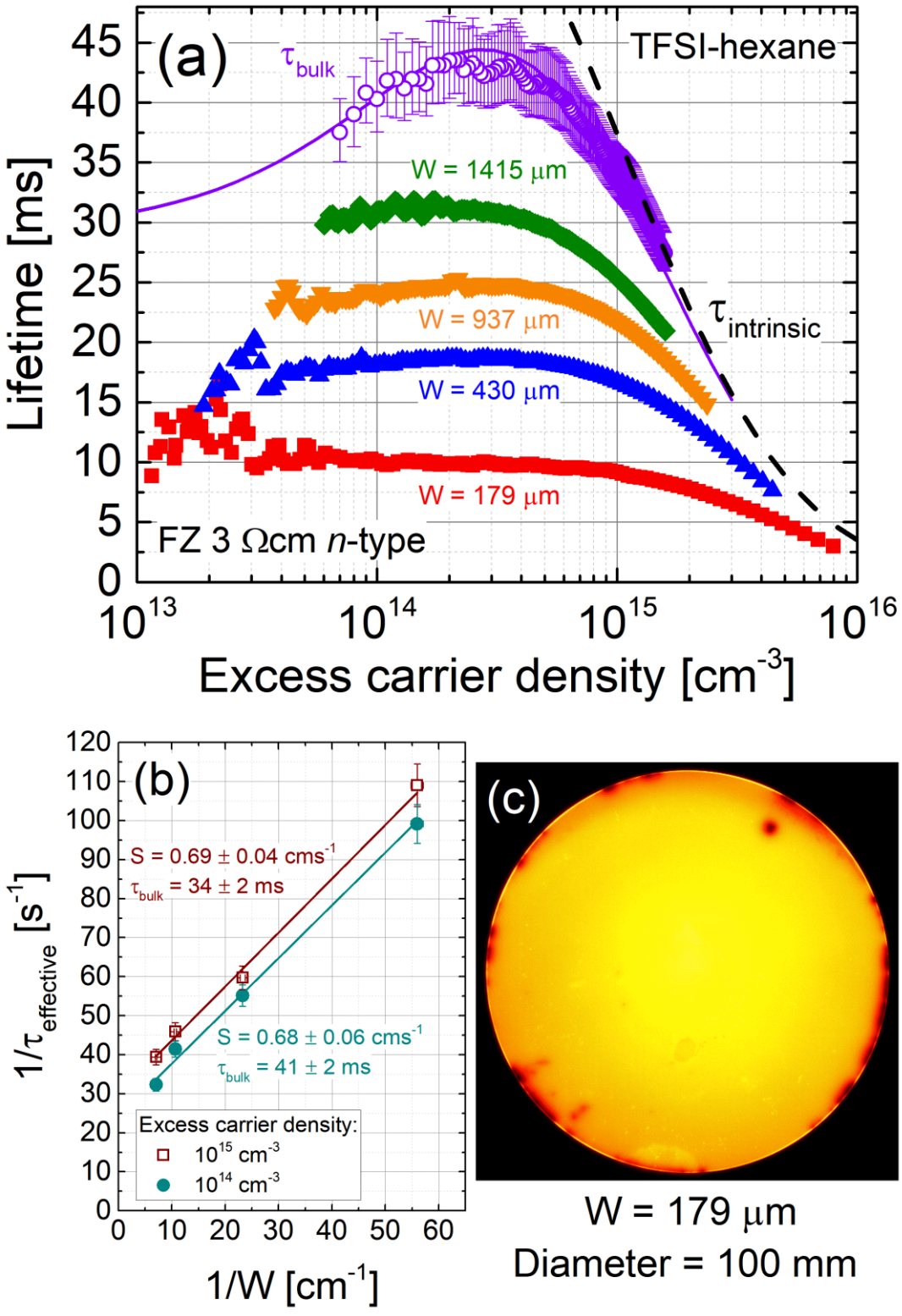

Figure 4.6 – (a) Effective lifetime measured in whole 100 mm diameter 3 Ωcm *n*-type FZ-Si wafers with different thicknesses from the same ingot passivated with TFSI-hexane using the best case results from a series of tests. Also shown are the current intrinsic lifetime limit [28] and the bulk lifetime extracted using Equation 4.1 as a function of injection. (b) Plot used to extract surface recombination velocity and bulk lifetime from the data in (a). (c) Uncalibrated photoluminescence image of the passivated 179 μm thick 100 mm diameter wafer to show the passivation and bulk lifetime uniformity.

4.2.5.1 Analysis of Achieved Surface Passivation

In general, the surface passivation of silicon arises from two possible mechanisms, which are chemical passivation (i.e. termination of dangling bonds) and field effect passivation, whereby carriers are repelled from the surface by the presence of a charge.

It is possible to relate the effective surface recombination velocity, S, to the unpassivated state density, N, according to:

$$S = \sigma v_{th} N \qquad \text{Equation 4.2}$$

where σ is the capture cross-section and v_{th} is the thermal velocity of carriers.

Taking typical values of σ as 10^{-15} cm^2 and v_{th} as 10^7 cm s^{-1} and using the best case S of around 0.7 cm s^{-1} for TFSI-hexane treatment (from Figure 4.6), gives N as low as 7×10^7 cm^{-2}. The methodology used in this study to determine the value of surface recombination velocity (S) was based on testing several variable thickness wafers from the same ingot and, as such, it is believed the results presented in Figure 4.6 are extremely robust, more so than typical practices used much more commonly in other passivation studies.

The value found for N would be about 3 to 4 orders of magnitude lower than typical AlO_x, SiO_x and AlO_x/SiN_x stack passivation [127-129]. However, this estimation assumes that there is zero interface charge, and it should be noted that for such low unpassivated state densities that a small amount of charge can have a huge impact on the level of surface passivation. Based on these assumptions, with the best case passivation found, the unpassivated dangling bonds would be separated by around 1.2 µm. Assuming S_n = 4.5 cm s^{-1} from the fitting procedure underpinning Figure 4.8, gives N as 4.5×10^8 cm^{-2}, which is a separation of around 470 nm.

Because of these results, it is not considered likely that the TFSI molecule itself passivates the silicon surface. Dangling bonds at the surface of silicon are separated by a lattice constant of 5.431 Å or less, and DFT calculations have shown that the TFSI molecule when maximally reduced to a sphere has a diameter of 10.7 Å or 10.96 Å [130], meaning that the TFSI molecule

is much larger than the atom spacing of silicon allows, and so is unlikely to give the ultra-low levels of unpassivated dangling bond densities that have been inferred from these tests.

Additionally, as TFSI is most likely to exist as a negatively charged anion in solution, which would be repelled away from any negatively charged dangling bonds at the surface. It seems most likely that the TFSI molecule breaks up in solution or during treatments and its constituents cause passivation of the silicon surface, although it could still be possible that a large part of the molecule attaches itself to the surface in a vertical orientation.

Finally, it should be noted that the effective surface recombination velocities achieved with TFSI-based passivation are similar to those achieved by HF immersion passivation, in which passivation is known to arise from hydrogen termination of dangling bonds [68]. It is, however, possible that other species (such as H or CF_3) are responsible for the passivation; this will remain under investigating in the following chapters.

The mechanism by which the solvent influences the level of passivation will be the subject of further study. There seem to be at least two ways in which it is possible for the solvent to affect the passivation. Firstly, the solvent could be incorporated into the thin film, which forms on the surface of the silicon. Secondly, the different solvents could change the pathway through which TFSI may break apart and hence a variety of species could be responsible for the surface passivation in each case.

4.2.6 Reproducibility of Passivation Treatment

An important consideration for any temporary surface passivation scheme is the extent to which it is reproducible. A series of reproducibility tests were conducted using TFSI-hexane on 3 Ωcm *n*-type FZ silicon wafers of variable thickness from the same ingot. The tests are referred to as Tests 1 to 5, with Test 4 giving the best-case results, presented previously in Figure 4.6. Figure 4.7 (a) shows the key results of the reproducibility experiments, with the reciprocal lifetime (at 10^{15} cm^{-3} injection) plotted as a function of the reciprocal wafer thickness according to Equation 4.1. As each passivation step involved a chemical etch, it should be noted that the samples become thinner each time they are tested.

The TFSI-DCE passivation scheme that developed in previous studies [101, 103] has been demonstrated to be an effective passivation technique used when gaining an understanding of

the origin of efficiency degradation of IBC cells [131] and also for separating bulk and surface passivation effects in investigations of light-induced degradation [132, 133].

However, the work presented in this chapter has shown that the TFSI-hexane treatment appears to be superior to the previous TFSI-DCE technique in many ways, including offering marginally improved surface passivation and thus higher lifetimes (presented in Figure 4.1), alongside better passivation stability over 1 to 3 hours (shown in Figure 4.2 and Figure 4.5) and improved prepared solution longevity (demonstrated in Figure 4.5) owing to the observed colour change that TFSI-DCE solutions undergo (seen in Figure 4.4), suggesting a reaction occurs in this solution mixture. These factors, combined with the knowledge that DCE is "possibly carcinogenic to humans" [102], mean that it is now possible to advocate the use of TFSI-hexane treatments for when temporary solution-processed surface passivation is needed, particularly for the purposes of measuring high lifetimes without affecting properties of the bulk lifetime of the material. It should still be noted however, that hexane is not completely benign; it too must be handled with care like most petrochemicals, although it is not currently known to be carcinogenic. An additional benefit to using hexane is that unlike DCE it does not contain chlorine, therefore it does not attack plastic in the same way DCE does, which helps during sample processing and storage.

It was shown in Figure 4.7 that TFSI-hexane superacid-derived passivation can be used reasonably reproducibly when the conditions of processing and treatment are kept clean and consistent but, as with any passivation scheme (including dielectric layers deposited by plasma enhanced chemical vapour deposition or atomic layer deposition), minor problems with surface preparation or even sample handling during processing can strongly influence the results achieved.

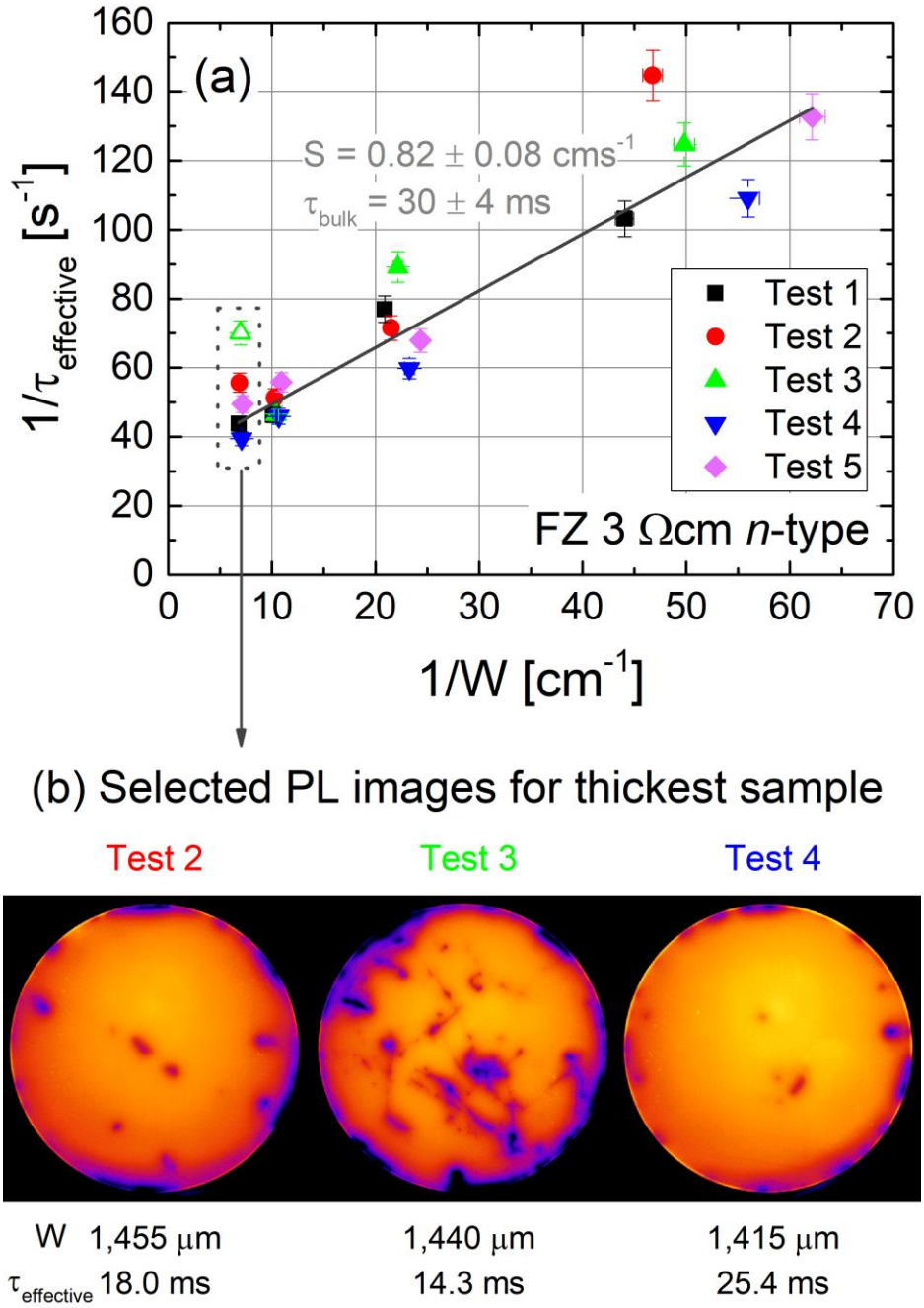

Figure 4.7 – Results of the reproducibility study on whole 100 mm diameter 3 Ωcm *n*-type FZ-Si wafers with different thicknesses from the same ingot passivated with TFSI-hexane. Lifetimes are extracted at an injection level of 10^{15} cm^{-3}. (a) Plot in accordance with Equation 4.1 to determine the effective surface recombination velocity and bulk lifetime. The open data point from Test 3 was excluded from the fit due to process-induced surface damage. (b) Selected uncalibrated PL images of the thickest sample for Tests 2 to 4, showing that surface damage during processing during Test 3 is removed by etching as part of Test 4.

A notable outlying point in Figure 4.7 (a) is in Test 3 for the thickest sample tested (marked with an open green triangle), for which the lifetime is substantially lower than might be expected. It was noted that at some point during processing (images shown in Figure 4.7 (b)) that the thickest sample became damaged between Test 2 and Test 3. The PL images shown in Figure 4.7 (b) shows why this is the case, with the centre of the wafer where the photoconductance lifetime measurement is made becoming damaged between Test 2 and Test 3, and recovering again for Test 4.The photoconductance lifetime measured in the sample was still very high (14.3 ms), but the PL imaging reveals scratches in the central area of the wafer, which are thought to be very shallow and were possibly introduced during handling of the whole wafer during the HF dip stage immediately prior to passivation. Other points in Figure 4.7 (a), such as Test 2 for the thinnest sample, show deviation from the expected trend but no damage was found in the PL images (not shown). In this case it is suspected that the variation arose due to a minor discrepancy during one of the cleaning procedures. The best results were achieved in Test 4, for which a brand new TMAH solution was used when etching, but this may be coincidental. A benefit of this technique that can be seen in these tests is the ease with which reprocessing (and surface passivation improvement) is possible with this technique, as can be seen in the PL images for tests 2, 3, 4 (in Figure 4.7 (b)), despite how damaged the surface appears to be in test 3. By doing nothing more than simplify re-running the sample through the outlined process again, it is possible to recover a damaged sample fully to its expected value and to excellent surface passivation uniformity. This would not have been as easily achieved if similar surface damage had been found after using a dielectric passivation method (such as AlO_x), as the re-processing to remove the dielectric layers could be much more aggressive and re-annealing of the sample could significantly alter its parameters. PL images for other possible outliers in Figure 4.7 (a), such as Test 2 for the thinnest sample, were also inspected, but no significant marks were found in other cases.

For a more detailed analysis of the passivation treatment, modelling was performed in collaboration with Trina Solar, with data provided by the author and worked on by Pietro Altermatt, the results of which are presented in Figure 4.8, in which, $\frac{1}{\tau_{bulk}}$ in Equation 4.1 is fitted with Shockley-Read-Hall (SRH) theory, the Auger lifetime [28] and the radiative lifetime [26, 134] as:

$$\frac{1}{\tau_{bulk}} = \frac{1}{\tau_{SRH}} + \frac{1}{\tau_{Auger}} + \frac{1}{\tau_{radiative}} \qquad \text{Equation 4.3}$$

in the whole measured injection range of Tests 1 to 5 and all wafer thicknesses.

The overall residuals are smallest if the hole lifetime is chosen for all wafers as $\tau_p = 0.035$ s, but if τ_p is left free during the fitting procedure it only deviates by a small amount from 0.035 s. As the samples were not measured at injection densities exceeding about 2×10^{15} cm^{-3}, the electron lifetime, τ_n, does not influence the fitting result as much as τ_p with τ_n between 0.01 s and 0.02 s giving good fitting results with the defect energy in the mid gap. The two thinnest wafers are most sensitive to the surface passivation quality, and their resulting S values are plotted in Figure 4.8. The analysis shown in Figure 4.7 (a) yielded $S = 0.82 \pm 0.08$ cm s^{-1} at an injection density of 1×10^{15} cm^{-3}, and this range indeed comprises about two thirds of all S values of Figure 4.8, as is expected from Gaussian error analysis.

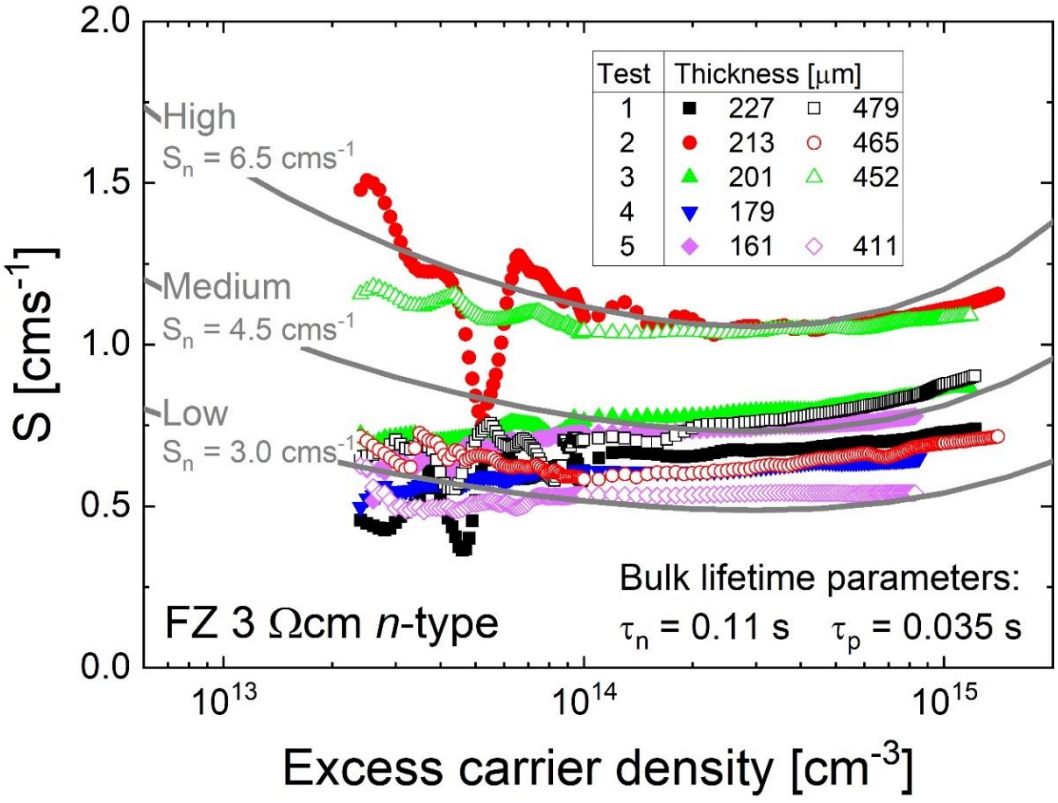

Figure 4.8 – Modelled effective surface recombination velocity (*S*) vs excess carrier density for whole 100 mm diameter 3 Ωcm *n*-type FZ-Si wafers from same ingot passivated with TFSI-hexane. The data shown are for the two thinnest wafers for Tests 1 to 5 (except Test 4 for the second thinnest sample) with the thinnest wafer being denoted with closed symbols and the next thinnest wafer denoted with open symbols. For these calculations $Q_f = -7 \times 10^{10}$ qcm^{-2} and three scenarios with different S_n values are shown. The author collected the experimental data while fitting was performed by Pietro P. Altermatt.

The S curves in Figure 4.8 were fitted with Equation 3 of Ref. [135] and obtained the best fit near a fixed surface charge density of $Q_f = -7 \times 10^{10}$ q cm^{-2} is denoted by the curves on the plot. The medium curve is obtained using a surface recombination velocity for electrons of $S_n = 4.5$ cm s^{-1}. The high and low curves have S_n values of 6.5 and 3 cm s^{-1}, respectively. For $Q_f > -6 \times 10^{10}$ q cm^{-2}, S increases sharply towards lower injection densities because no inversion is obtained anymore, while at $Q_f < -1 \times 10^{11}$ q cm^{-2} and at positive Q_f values, S increases more pronounced at higher injection densities. The fitting procedure is not expected to be a very reliable means to determine Q_f and therefore $Q_f = -7 \times 10^{10}$ q cm^{-2} should be taken as a mere indication. The negative value of Q_f is, however, also compatible with the decreasing lifetimes observed in Figure 4.1 towards lower excess carrier densities.

4.3 Superacid Treatment Applications

So far, this chapter has focused on improvements to the passivation technique through understanding of the implications of the solvents used in the passivation solution, and then investigation into the effect environmental factors have on the quality and degradation of the resulting passivation. The resulting improved processing techniques and solutions have led to a further reduction in effective surface recombination velocity. As the level of passivation that can be offered is able to compete with even high quality dielectric surface treatments, but without the resulting possible modifications in bulk lifetime during processing from the use of elevated temperatures, it is therefore possible to use this passivation scheme to measure the true bulk lifetimes of materials during and after cell processing.

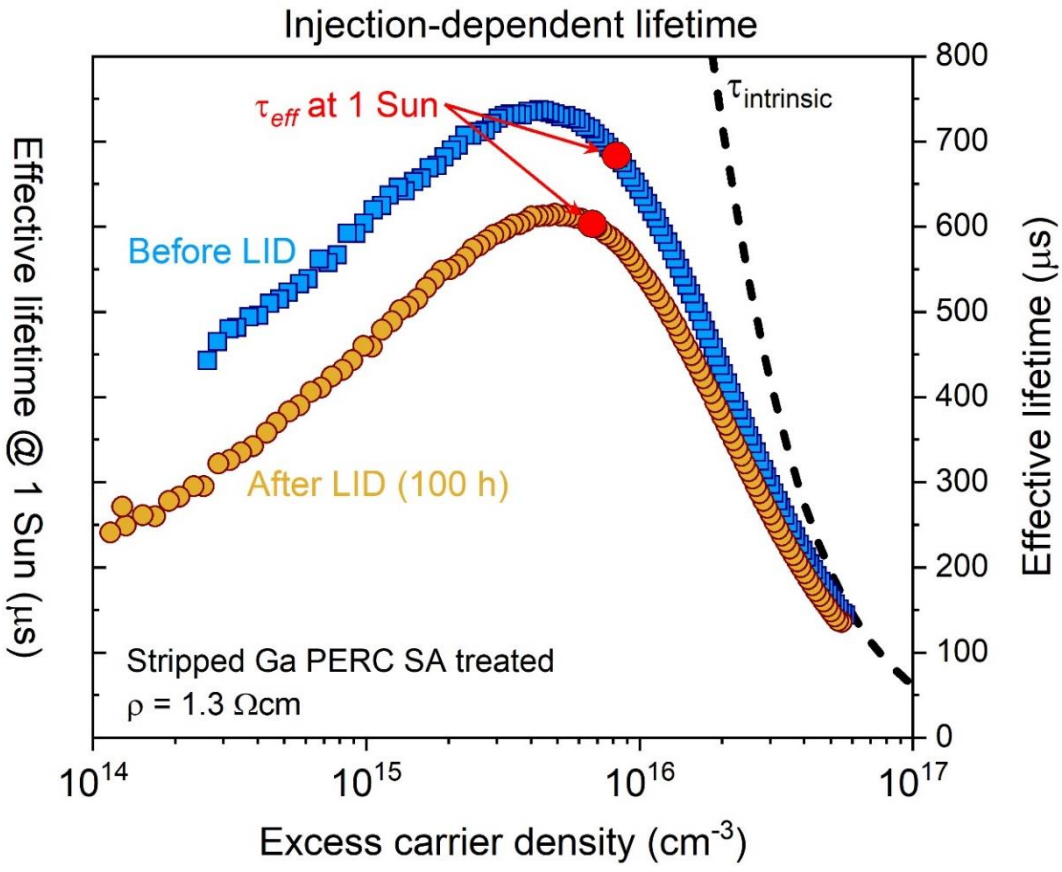

Figure 4.9 – Injection-dependent effective lifetime of Ga doped Silicon PERC devices treated with superacid-based passivation, showing results before and after light-induced degradation

In this section, the improved scheme of superacid derived passivation (TFSI dissolved in hexane) is used to analyse lifetime instabilities in an etch-back investigation on a selection of gallium-doped silicon monocrystalline PERC solar cells as an example of one of the lab uses for the treatment. The temporary surface passivation was used to correlate degradation results from PL imaging with bulk lifetime changes in the devices, it was therefore crucial bulk lifetime in the samples was unaffected by any passivation.

From the results obtained during this testing (displayed in Figure 4.9) it was evident that the PERC cell degradation was able to be attributed to the degradation of the bulk lifetime in the silicon wafers

One of the key benefits of the superacid treatment is the ease of ability to re-passivate samples that may become damaged during processing or when the results are not as expected, without changing any sample properties due to the low temperatures used during treatment. As discussed previously and demonstrated in the test images in (Figure 4.7(b)) – where the samples had been scratched during processing – this was another situation where the ease of retreatment giving the opportunity for passivation improvement (through additional reprocessing steps such as further etching or special chemical treatments) without affecting the properties of the bulk of the material was invaluable.

4.4 Summary

This chapter details a systematic study into the surface passivation of *n*-type silicon samples when treated with various TFSI solutions made with different anhydrous solvents.

All the solutions investigated were shown to passivate the Si surfaces to some extent, and the passivation quality was found not to correlate with the relative polarity of the solvent. Excellent initial surface passivation was achieved with several solvents, including hexane, DCE, toluene and DCM. TFSI solutions made with DCE and toluene are however unstable as evidenced by changes in colour of the prepared solutions, and, whilst DCM gives good results, the use of a chlorinated solvent is undesirable for safety reasons. It has been shown that TFSI-hexane gives better surface passivation than the previously used TFSI-DCE, whilst also providing better passivation stability and prepared solution longevity. Hexane is also considered safer than DCE,

which is a suspected carcinogen, so it can be concluded that TFSI-hexane is a better solution to use for superacid immersion passivation of silicon than TFSI-DCE used previously.

A series of investigations was then performed into the new TFSI-hexane passivation scheme. It was found that the stability of the passivation was strongly influenced by the storage humidity of the sample after passivation, the surface passivation being most stable when the samples are kept in a petri dish with the lid on. TFSI-hexane passivation was applied to a set of FZ silicon wafers cut with different thicknesses from the same ingot. This enabled the extraction of the bulk lifetime and surface recombination velocity. The best-case effective surface recombination velocity was 0.69 ± 0.04 cm s^{-1}. A series of five tests were then performed on the same sample set, demonstrating the reproducibility of the scheme.

In summary, the results presented in this chapter show that an improved superacid immersion treatment has been developed which consistently provides a very low surface recombination velocity with minimal test-to-test variation. This is an important step towards giving researchers the ability accurately to determine the bulk lifetime with good reliability whilst avoiding influencing the properties of the material being studied. This can allow the study and understanding of new passivation schemes, which will become ever more crucial as solar cell efficiencies become increasingly sensitive to surface and bulk recombination effects.

Chapter 4 has demonstrated that superacid-derived passivation can be extremely effective at passivating the surface of Si samples so, finally, in order to establish some of the possible real world uses of this relatively safe, low-temperature and solution-processed passivation technique, a study was performed into the lifetime degradation in gallium-doped PERC solar cells. The passivation method was demonstrated to have superior ease of processing and high quality surface passivation, crucially without effecting the properties of the materials under investigation, as can happen with processes requiring high temperature procedures. These data were included in the publication in Ref. [7].

Chapter 5 Evolution of Bis(trifluoromethanesulfonyl)-Based Passivating Solutions and their Effect on Surface Passivation

5.1 Introduction

Chapter 4 introduced the changes that can occur in the quality and longevity of the passivation when the solvents used to make the solutions, or the atmospheric storage conditions are changed. In this chapter, by altering the chemical that is being dissolved in the solvent, the aim is to gain a greater understanding of how the choice of solute that creates the solution affects the resulting passivation. A greater understanding of the molecular composition of the treatment solutions will aim to give a greater insight into the mechanisms behind the passivation scheme.

5.2 Motivation

Despite the empirical effects of the treatment being known [101], the mechanisms underpinning the passivating effects of the TFSI based treatments are not well understood. Therefore, the motivation for this chapter is the need to determine the mechanism by which the passivation works. Investigating and further understanding the chemical make-up of both the solution and the treated surface may make it possible to attain greater improvements in passivation lifetime and quality.

The main question to be answered is what chemical species from the bis(trifluoromethane)sulfonimide superacid solution explored by Bullock *et al.* [101] actually passivates the surface. It has been shown previously that it can be extremely difficult to determine what actually remains at or on the surface of the silicon being treated. Singular atomic bonds at the surface – particularly hydrogen-silicon bonds – are typically below the limit of detection for

most techniques. Due to this, an alternative approach needed to be taken. The approach is to gather empirical evidence that can be used to better clarify what chemical atoms or molecules may remain, that could explain the passivating effects of the treatment. Alongside this is the aim of determining whether the passivation attained is chemical and/or field effect in nature, also to discover, if as previously reported whether the superacidity of the solution is a requirement for good passivation.

With greater understanding, the intention is to then investigate whether it is possible to further improve passivation quality and/or longevity with the use of other chemicals, similar to the improvements previously found by altering the solvent used for the solution. The next step will be to use this insight to improve the stability of passivation, in the hope of converting what is currently only a temporary passivation into a permanent organic passivation scheme.

5.3 New Passivating Solutions and Molecule Dependence

The first tests were aimed at trying to understand the effects of the chemical molecules themselves. In order to do this, different chemicals for the solute were strategically chosen to mirror key properties of TFSI, that is already known to passivate, to try to infer from the results which parts of the molecule were important for passivation. All passivating chemicals were chemical analogues of TFSI, with key structural similarities, but also key differences so that the experimental results could be used to differentiate between the way in which passivation arises. The common group between all the chemicals chosen was the Triflyl chemical group (Figure 5.1) as from reviewing previous literature it was suspected that this might be one of the sources of the passivation, because passivation had been found to occur with several chemicals from this family (such as PFBS and TFMS).

Experiments were performed to passivate surfaces with different solutions formed by molecules with a bis-(trifluoromethanesulfonyl)-based structure. For these experiments hexane was used as the solvent as it has been previously shown to provide better stability [1] than 1,2-dichloroethane (DCE) used in other studies [96, 101, 103]. The molecules of the chemicals chosen are presented in Figure 5.1, and as discussed all have the common triflyl group structure, except with different functional groups in the position marked “X” at the center of the molecule.

For the purposes of this study and ease of interpretation they will be labeled according to the "X", with bis(trifluoromethane)sulfonimide (TFSI) designated "NH" (as originally discovered by Bullock *et al.* [101]). The three new treatment solutions under investigation being labelled as follows;

- trifluoromethanesulfonic anhydride designated "O"
- bis-(trifluoromethanesulfonyl)methane designated "CH_2"
- *N*-phenyl-bis(trifluoromethanesulfonimide) designated "N-benzene".

Minority carrier lifetime measurements made for 5 Ωcm *n*-type silicon, treated with the different solutions at room temperature are shown in Figure 5.1. Also presented is the data for a HF-dipped sample which was subjected to the same cleaning procedures as the other samples, but with no additional passivation treatment. For the purpose of providing a control reference for the lifetime of the silicon wafers used for the tests. The lifetime in the HF-dipped sample is substantially higher than a free silicon surface as the silicon bonds are temporarily terminated/passivated by hydrogen [68].

The excellent surface passivation from TFSI (labeled "NH" here) has previously been found for silicon [1, 101, 103] and other materials [96, 98-100, 108, 136, 137]. It is frequently referred to as "superacid passivation", because the properties of the TFSI-containing solution arise from the particularly labile hydrogen on the TFSI molecule [138], and the effects arising from TFSI treatments are often explained in terms of surface protonation [136]. As can be seen from the data presented in Figure 5.1, the room temperature treatment of silicon test samples with the three new solutions under investigation, also resulted in high effective lifetimes due to the improved surface passivation. Crucially, what the data in Figure 5.1 demonstrates is that the passivation effect arises more generally than with just a superacid.

The three newly tested chemicals, which do not have labile hydrogen (O, CH_2, and N-benzene) but have a similar molecular structure to TFSI (NH) give excellent surface passivation as well. This suggests that the super-acidic properties (*i.e.* high ionic hydrogen content) are not the reason for the exceptional passivation found previously for TFSI (NH).

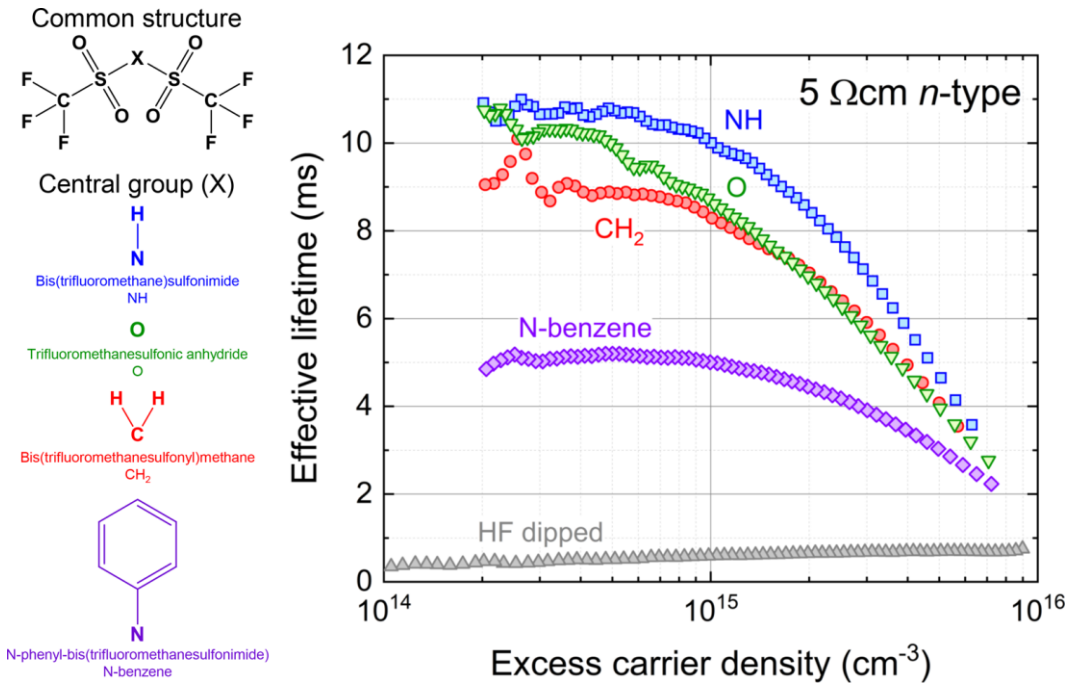

Figure 5.1 – (Left) The common structure of the molecules in the passivating solutions investigated, with the central group of the molecule varying (designated by "X"). (Right) Lifetime measurements performed in the high-specification glovebox on high-purity silicon wafers treated with different solutions in the same glovebox. The lifetime in the control sample which was only HF-dipped to have a hydrogen-terminated surface is also shown. Samples for this experiment were 5 Ω cm *n*-type float-zone silicon with a thickness of 750 μm.

5.4 Surface Chemistry and Passivating Species

In Section 5.3 it was reported that alternative chemicals, but from the same Triflic family of molecules, also result in a high level of surface passivation. This suggests that the superacidity offered by TFSI is not actually a requirement for good quality passivation, as previously suggested by other studies [101, 136]. In an effort to explain where the passivating effects of the treatments come from — now it has been shown it may not be protonation of the surfaces — supplementary tests need to be carried out for the purpose of resolving the factors that underpin the astonishingly low surface recombination rates offered by this family of simple room temperature surface treatments.

5.4.1 Nuclear Magnetic Resonance (NMR)

To understand the interactions in the chemical environment, it would be useful to identify possible atomic interactions that are occurring between the solutions and the surface of the prepared silicon. Solution state nuclear magnetic resonance (NMR) was used, to study the chemical environments in solution phase, formed by the mixtures of the passivating solutions (bis(trifluoromethanesulfonyl)-based molecules in hexane). The data collected from these experiments are presented below in Figure 5.2.

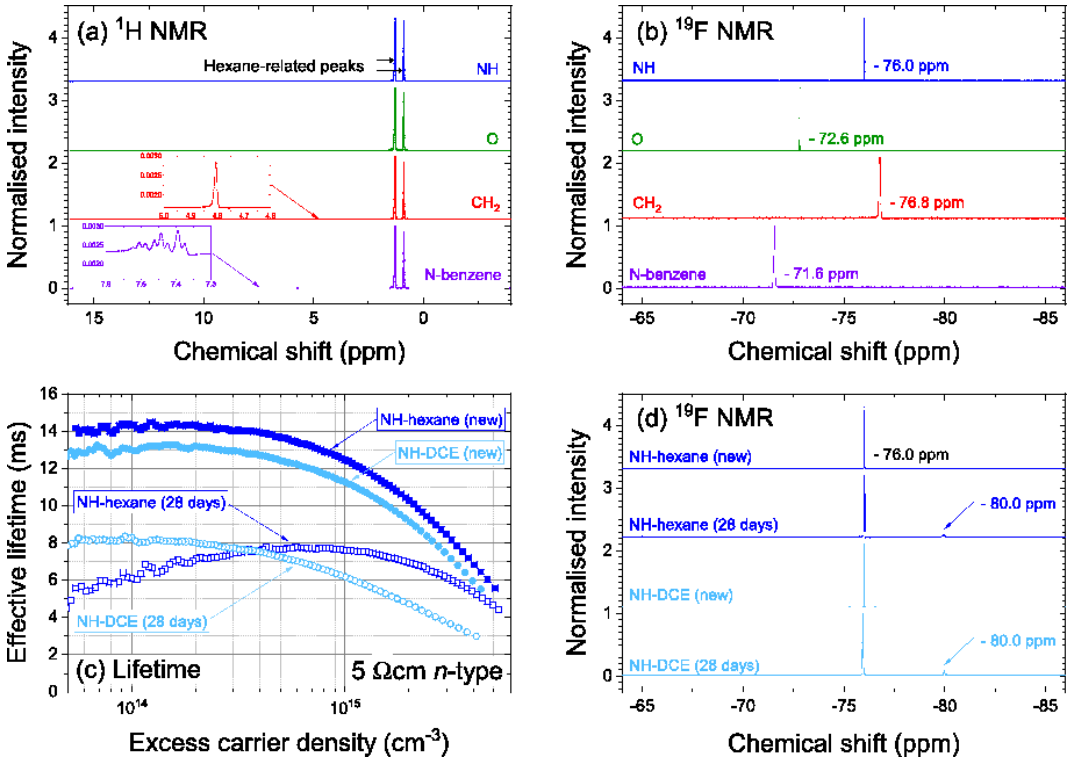

Figure 5.2 – (a) Proton NMR and (b) fluorine NMR performed on a range of passivating solutions formed from the molecules in Figure 5.1 dissolved in hexane. (c) Lifetime results for 5 cm *n*-type silicon treated with new and 28 days' old TFSI dissolved in hexane or DCE. (d) Fluorine NMR results for the solutions used in panel c showing the appearance of an additional fluorine-related shift due to degradation of the solutions.

Proton NMR results in Figure 5.2 (a) show a common pair of peaks arising from the hexane solvent. Weak signals (shown as insets) appear for the CH_2 and N-benzene solutions. No such

weak signal was found for the NH solution due to the labile central hydrogen in this super-acidic solution. Results from ^{19}F NMR are presented in Figure 5.2 (b), with peaks found in the −71 to −77 ppm range as expected for trifluoromethyl (CF_3) groups [139]. The measured values agree well with the previously measured values for NH (TFSI) of −76.0 ppm [140] and O of −72 ppm [139]. The results are also consistent with the known trend of the shift becoming more negative as the charge on the CF_3SO_2 increases [140]. Importantly, no other shifts are found in the fluorine NMR spectra than those shown in Figure 5.2 (b), which suggests no initial decomposition of TFSI in hexane affecting the fluorine atoms.

This does not necessarily mean that the chemical passivation of the silicon surface arises from the intact molecules, which seems unlikely due to molecular sterics and the number of terminated bonds [1], as was discussed in the results of Chapter 4. Studies [141, 142] have proposed mechanisms for the decomposition of the TFSI anion, and it is possible that the anion breaks-up in the vicinity of the silicon surface. In such a case, a component of the bis(trifluoromethanesulfonyl)-based molecule (e.g., CF_3 or SO_2CF_3) could play a role in chemically passivating the surface.

However, it is also possible that the chemical passivation arises mainly from hydrogen termination from the HF dip immediately prior to the treatment in the bis(trifluoromethanesulfonyl)-based solution, and that the film formed from the solution stabilises this chemical passivation. But from the extreme increase in lifetime this seems unlikely, without some further chemical reaction occurring.

The surface passivation level achieved with TFSI (NH) can depend on the solvent used [1, 101], with the level of passivation quality achieved, also affected by the age of the solution used [1], as was noted in Chapter 4. The lifetime results in Figure 5.2 (c) show superior passivation results with new solutions in hexane compared to 1,2-dichloroethane (DCE) as used in previous passivation studies of silicon [101, 103]. For solutions aged for 28 days, the hexane solution generally gives better results than the DCE solution, with the latter also experiencing a stronger injection-dependence. ^{19}F NMR results in Figure 5.2 (d) show the presence of an additional peak in both aged solutions with a shift of −80.0 ppm. This shift is in the range expected for a derivative of trifilic acid [139], and so this can be attributed to a CF_3SO_2 ion which has originated from the TFSI molecule which has degraded in the presence of the solvent, this provides evidence for the passivating solutions degrading chemically over time.

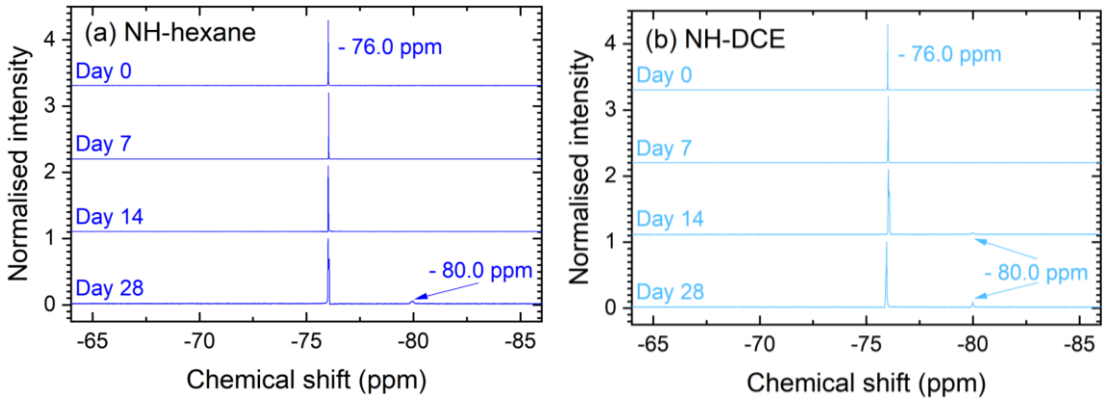

Figure 5.3 – 19F NMR spectra acquired for different solution ages for TFSI (NH) in (a) hexane and (b) DCE. The peak at – 80.0 ppm appears in the hexane solution after 28 days and in the DCE solution after 14 days.

A series of NMR experiments done over time (presented in Figure 5.3) show the –80.0 ppm peak to become detectable by NMR between 14 and 28 days for hexane, but much sooner for DCE becoming detectable between 7 and 14 days. It is noted that the DCE solution visibly changes color after 28 days but the hexane solution does not (shown in Figure 5.4). A similar injection-dependence in the aged DCE lifetime in Figure 5.2 (c) was previously observed with TFSI in acetone, which also undergoes a color change [1], Section 4.2.4.

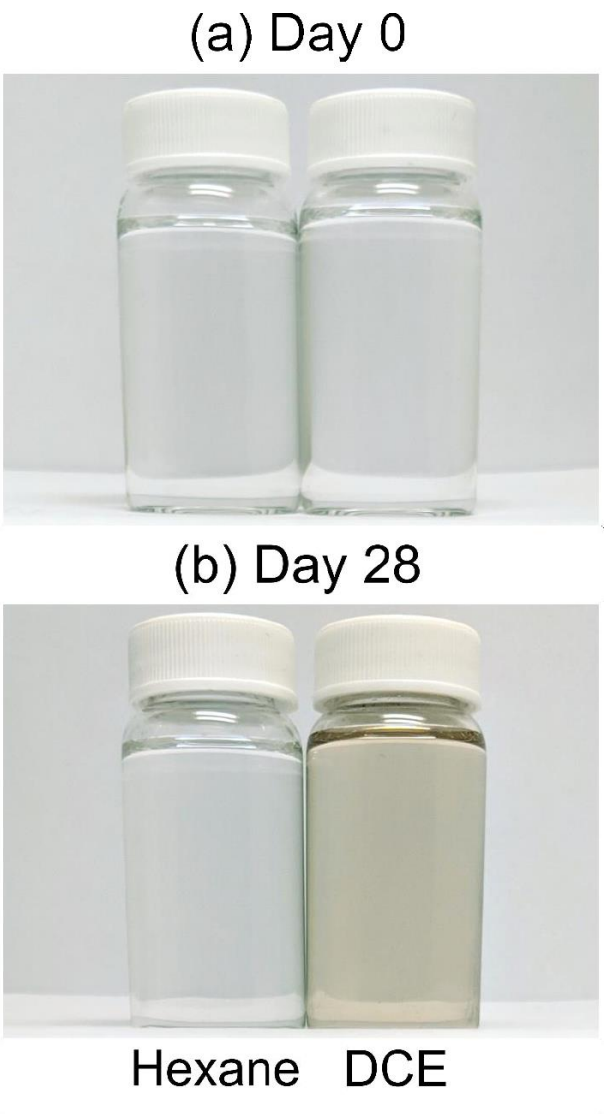

Figure 5.4 – Vials of passivation solutions of (NH) TFSI dissolved in hexane (left) or DCE (right) after (a) no days and (b) 28 days of sealed storage. A clear colour change is observed for DCE but not hexane.

5.4.2 Kelvin Probe – Surface Charge Measurement

In general, the passivation of surfaces occur by chemical passivation (i.e., termination of dangling bonds) and/or by field effect passivation whereby charge in a layer repels carriers away from the surface. Kelvin probe (KP) measurements were used to determine whether charge plays a role in our passivation process and how significant that role may be. Figure 5.5 shows the surface potential of an *n*-type silicon surface which has only been prepared to the HF-dipped

stage (to provide a baseline measurement), and a fully processed TFSI–hexane treated *n*-type silicon surface. Illumination of the HF-dipped *n*-type surface does not change the surface potential, whereas the surface potential of the treated surface becomes much less negative under illumination due to a reduction in the width of the depletion region.

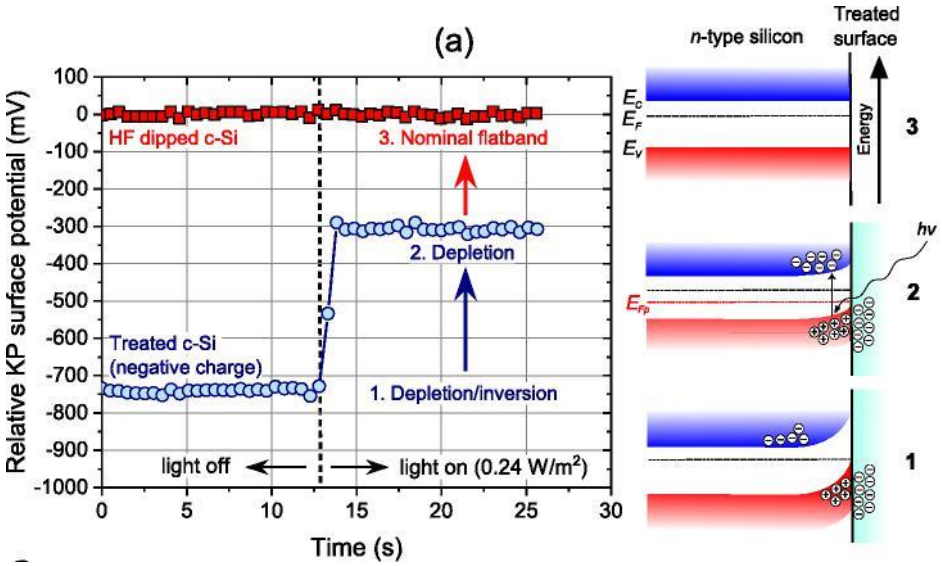

Figure 5.5 – Experiments to establish the role of field effect passivation on 5 Ωcm *n*-type silicon surfaces. The Kelvin probe (KP) measurements (left) show the relative effect of LED illumination on the surface potential for a HF-dipped sample and a TFSI-hexane treated sample, demonstrating that the passivating film is negatively charged. The band diagrams (right) illustrate the effects of illumination on the surface band structure.

Similar behavior is found for *p*-type silicon (as shown in Figure 5.6), although as *p*-type silicon is highly susceptible to bulk lifetime degradation [132], *n*-type silicon provides a better controlled system for studying thin film passivation mechanisms.

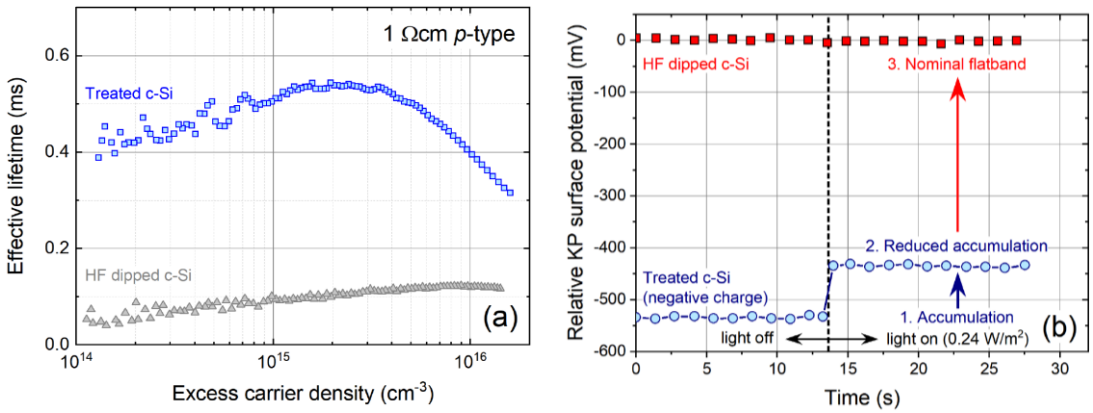

Figure 5.6 – Experimental results for HF dipped and TFSI-hexane treated 1 Ωcm 200 µm thick *p*-type silicon samples acquired following ~12 h in optimal storage conditions. Lifetime data in (a) show that the TFSI-hexane passivates the surfaces. Effective lifetimes are lower than in the *n*-type case but this may be because: (i) thinner samples were used; (ii) the passivation degrades slightly during storage prior to measurement; and (iii) the bulk lifetime is likely to be lower. The samples had not been subjected to a high temperature anneal to reduce bulk recombination [89] and light-induced degradation could have occurred [132]. Kelvin probe (KP) data in (b) show that LED illumination has the same effect as observed on *n*-type samples (Figure 5.5), confirming the presence of negative charge in the thin film.

The Kelvin probe results confirm the presence of a negative charge, similar to very recent work with Lewis acids [143]. As illustrated by the band diagrams (Figure 5.5), illumination generates electron–hole pairs in the silicon, which reduces the size of the depletion region and hence lowers the quasi-Fermi level for holes (EF_p).

While the solution based surface treatment is stable enough for short-term characterisation purposes (discussed in Chapter 4), the silicon surfaces passivated by TFSI–based solutions are known to decay over a time scale of hours [1, 101, 103]. The KP surface potential from a TFSI–hexane treated sample stored in air for >20 h was monitored. The results (presented in Figure 5.7 (a)) show that the KP surface potential became less negative with time. After an initial increase, the relative KP surface potential increases fairly slowly before increasing more rapidly after ~10 h, prior to stabilisation. The origin of the stabilisation is currently not clear, but there are likely to be chemical changes in the film during the degradation, and it is possible that a very thin negatively charged film remains at the surface. Photoconductance lifetime measurements

made on the same sample as in Figure 5.7 (a) in the initial state and after 20 h are shown in Figure 5.7 (b), the reduction in effective lifetime of the sample follows the pattern of a reduction in measured surface charge over the time period, possibly suggesting that the two are linked.

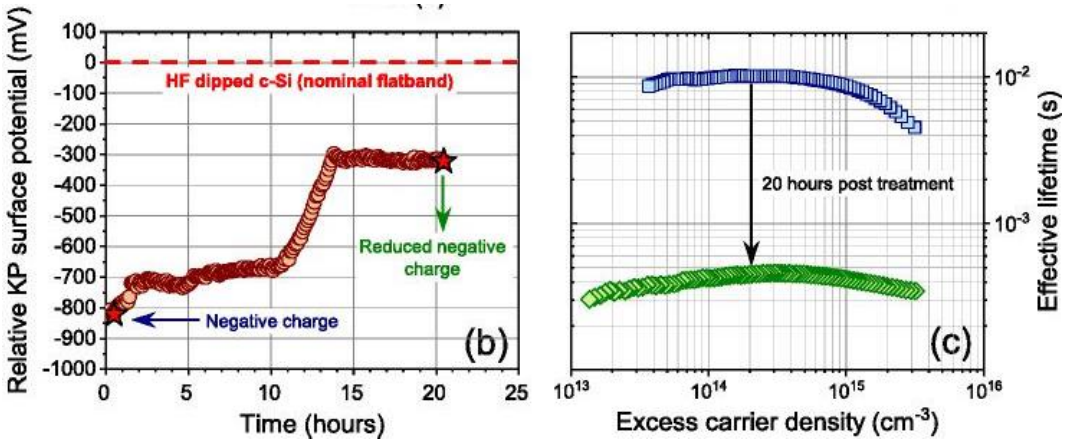

Figure 5.7 – Experiments to establish the role of field effect passivation on 5 Ωcm *n*-type silicon surfaces treated with TFSI-hexane. (b) Relative KP surface potential over an extended time period. (c) Lifetime measurements made in air on the same sample used for KP measurements in panel a showing the reduction in lifetime which has occurred.

Further data are presented in Figure 5.8, which provides simultaneous lifetime testing and relative KP surface potential measurements, on two samples from the same wafer, which have undergone identical treatment processes and were subjected to a TFSI-hexane passivation treatment. The lifetime reduces with time and the KP surface potential becomes less negative with time, as expected. However, it is found that differences in the measurement environment used for the different techniques have a strong impact on the degradation kinetics, the KP measurements were performed in an enclosed chamber and lifetime measurements were performed in an open laboratory environment. The charge appears to have reduced to a lower level in the lifetime sample than in the KP sample, which is consistent with previous work presented in Chapter 4 showing that the ambient atmospheric conditions the samples are exposed to affect the surface passivation stability.

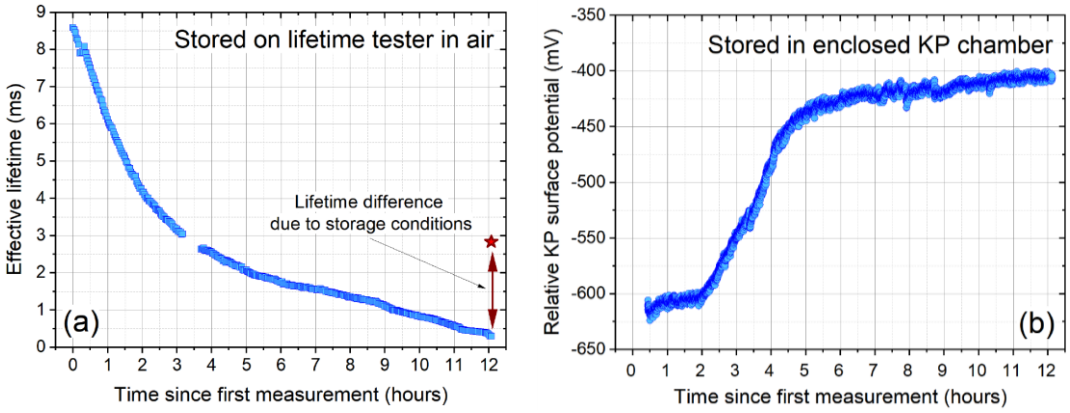

Figure 5.8 – (a) Lifetime and (b) KP measurements made on two different quarters of the same 700 µm thick 5 Ωcm *n*-type float-zone silicon wafer. The KP surface potential is plotted relative to an HF dipped sample at 0 mV. The lifetime measured in the KP sample at the end of the experiment is shown as a star, on plot (a).

Whilst the relative KP surface potential becomes less negative over time, seeming to coincide with a reduction in effective lifetime measured on the samples, that could lead to an assumption that the two are causally linked, a detailed analysis of the injection dependence of the effective lifetimes (Figure 5.9), shows that chemical passivation is likely to reduce too. The modelled fits to the measured data were performed by holding the interface charge density (Q_{eff}) constant and by varying the interface trap density (D_{it}). The bulk lifetime was held constant at 20 ms. It was not possible to fit the data without the inclusion of negative charge, and it was also not possible to fit the degradation data by varying the charge density alone.

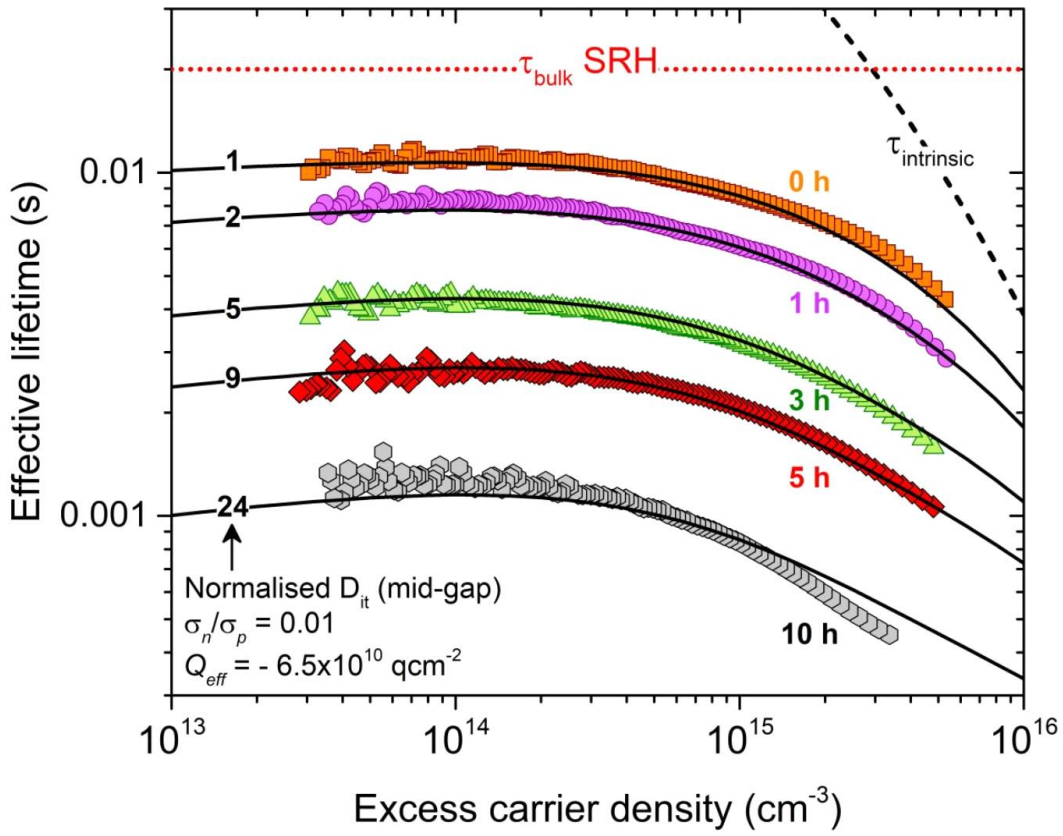

Figure 5.9 – Fitting of injection dependent lifetime data for 700 µm thick 5 Ωcm *n*-type float-zone silicon wafers passivated with TFSI-hexane at different stages of degradation in air. Interface charge density (Qeff) was held constant and the interface trap density (Dit) was varied for the fits presented. The author collected the experimental data while fitting was performed by Dr Nicholas E. Grant.

Therefore, while the film formed does appear to contain negative charge, the lifetime degradation is not just via reduction of charge in the external layer. This might occur by various mechanisms, including chemical changes (e.g., a reaction with water from the atmosphere), leakage of charge across the surface of the silicon, or accumulation of charged/polarisable species from the atmosphere which compensates the film's charge. Finally, it is noted that corona charging experiments were used in an attempt to modify the charge level in the passivating film, but both positive and negative polarity of the corona charging, resulted in a rapid (<60 s) reduction in lifetime (Figure 5.10). This is likely to be due to damage to the thin passivation layer from corona charge breakdown, as has been observed when an excessive electric field is applied to a dielectric-silicon system [106].

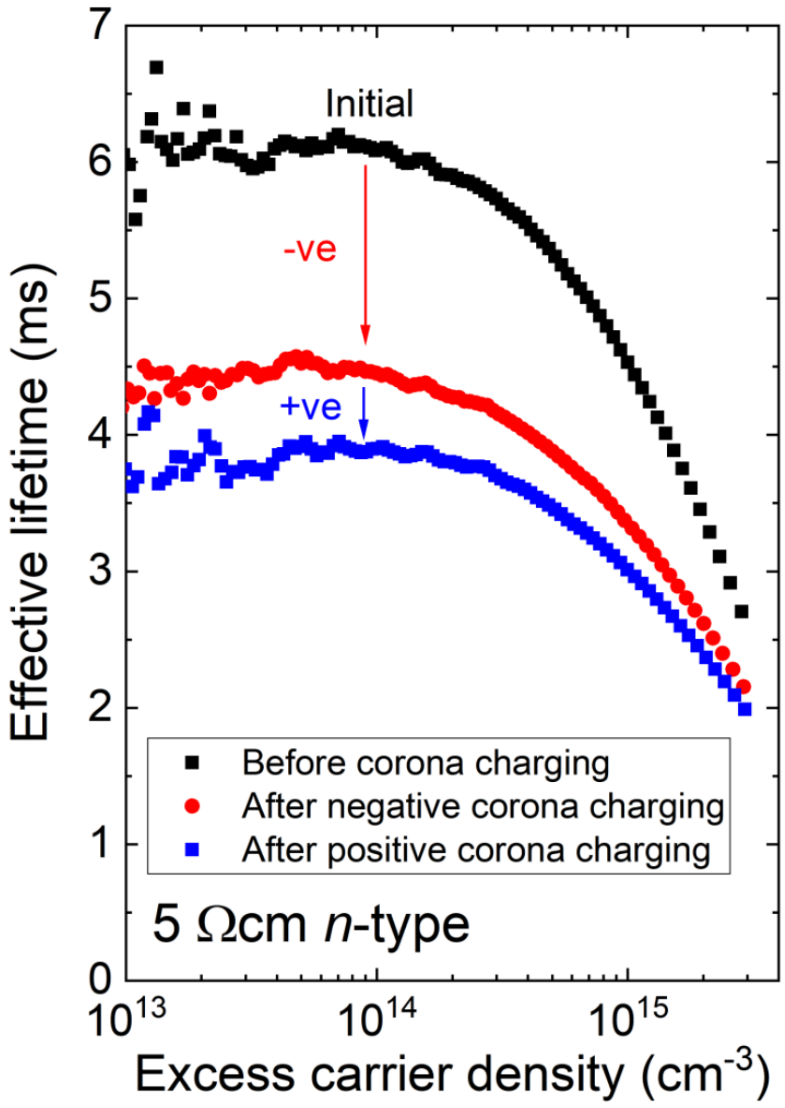

Figure 5.10 – Lifetime measurements made on the same 740 μm thick TFSI-hexane passivated sample subjected to corona charging. The lifetime reduces with negative and positive corona charging. Corona charging was attempted using a point-to-plane set up described previously [106] with the point electrode held at 30 kV and 20 cm away from the sample. Charges were applied for 30 to 60 s on both surfaces.

5.4.3 X-ray Photoelectron Spectroscopy (XPS)

X-ray photoelectron spectroscopy (XPS) is a highly sensitive surface technique that can help identify the elements that are covering a materials surface and what other elements they may be bonded to. In order to investigate the structure and chemical bonding at the silicon surface once the treatment has been performed, XPS was performed on just HF-dipped silicon and on TFSI–hexane treated silicon. The shallow takeoff angle (15°) F 1s and Si 2p spectra are shown in Figure 5.11 (a) and (b), respectively, with the 90° takeoff angle data shown in the Figure 5.12.

Although XPS has been used on TFSI–treated silicon surfaces before [101], as discussed in the literature view, extreme caution must be taken in the interpretation of the data gained, as during the experiments performed in this study it was found that the passivation lacks vacuum stability, which had not been noted before. Figure 5.11 (c) shows carrier lifetime for the same sample:

(i) after an HF dip [purple triangles]

(ii) then after TFSI-hexane passivation treatment [blue squares]

(iii) then after being exposed to a short subsequent vacuum treatment ($<6 \times 10^{-5}$ mbar) [red circles]

The vacuum treatment reverses the effects of the passivation treatment with the trifluoromethanesulfonyl-based solution, resulting in essentially the same lifetime as in the HF-dipped state, which is still substantially higher than for a non-hydrogen terminated surface. Furthermore, by performing the vacuum treatment in a chamber with an optical window, it was possible to physically observe the disappearance of a film from the silicon's surface while also experiencing a simultaneous decrease in chamber pressure. The XPS measurements performed were made under an ultrahigh vacuum level (down to 1×10^{-10} mbar) and consequently it seems probable that it is not possible to measure the true properties of the passivating film with this technique.

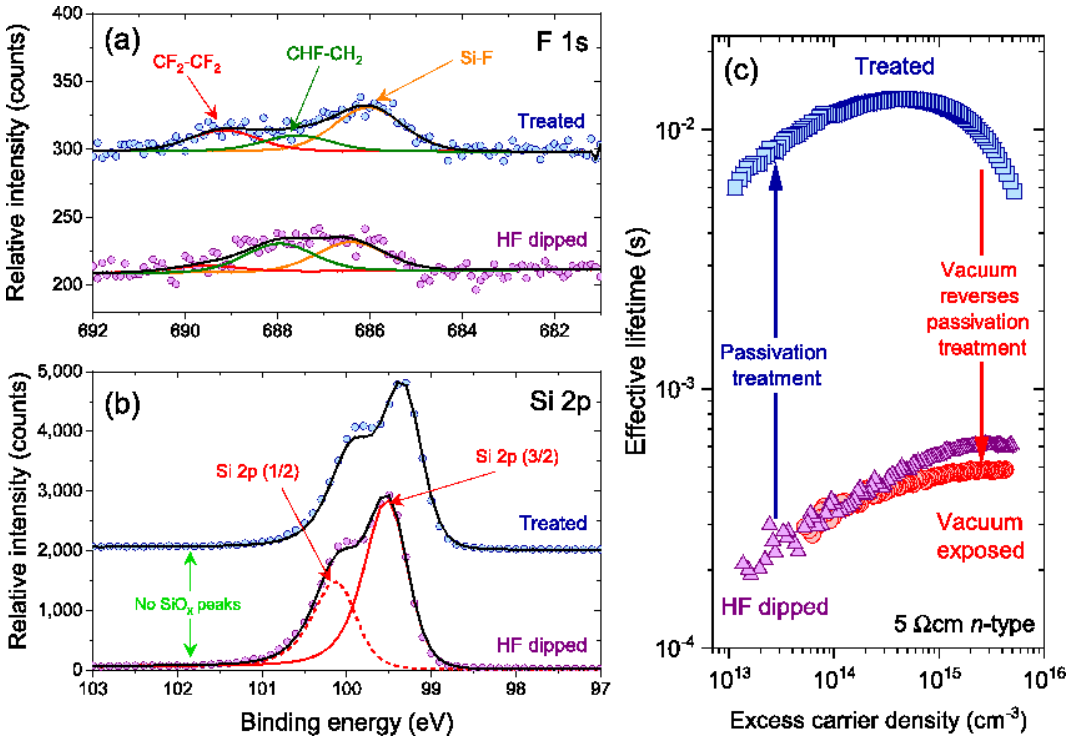

Figure 5.11 - (a) XPS F 1s spectra for HF-dipped and TFSI-hexane treated Si samples, with the treated data shifted upward by 100 counts for clarity. (b) XPS Si 2p spectra for HF-dipped and TFSI-hexane treated samples, with the treated data shifted upward by 2000 counts for clarity. Both sets of XPS spectra are for a takeoff angle of 15° to probe the near-surface region. (c) Lifetime measurements performed in air for a sample after an HF dip, after passivation with TFSI-hexane in the low specification glovebox, and after placing the passivated sample in a vacuum chamber.

Taking these new limitations into consideration, the XPS data can still provide some insight into the surface chemistry of the treatments. First, the F 1s spectra in Figure 5.11 (a) show evidence for Si–F bonding at the surface. Signals related to CF_2–CF_2 and CHF–CH_2 are required to fit the data. The same three peaks are required to fit the F 1s spectra for the HF-dipped and TFSI–hexane treated surfaces. This implies that the fluorine at the surface comes from the HF dip process (which is also performed before the TFSI–hexane treatment) and not necessarily from the fluorine-containing TFSI molecule. Second, the Si 2p spectra in Figure 5.11 (b) show no evidence for SiO_x peaks at the silicon surface. As SiO_x layers are likely to be vacuum stable this shows that SiO_x layers, such as a native oxide, do not play a role in the passivation.

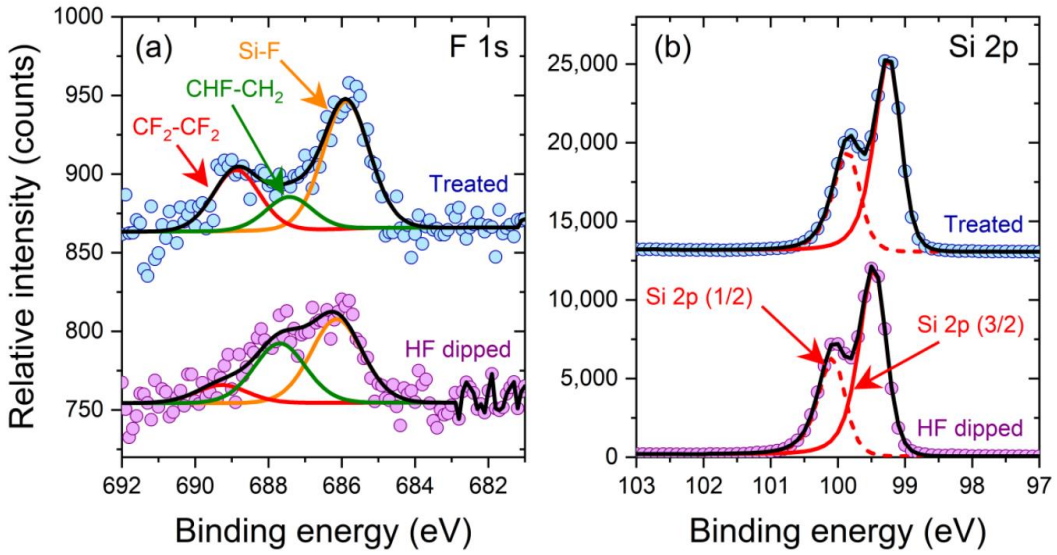

Figure 5.12 – XPS results for a take-off angle of 90°. (a) XPS F 1s spectra for HF dipped and TFSI-hexane treated Si samples, with the treated data shifted upwards by 80 counts for clarity (b) XPS Si 2p spectra for HF dipped and TFSI-hexane treated samples, with the treated data shifted upwards by 13,000 counts for clarity.

Using the new data presented here, it is possible to propose a model for the passivation of surfaces by trifluoromethanesulfonyl-based solutions, including TFSI. The results show there are at least two components to the passivation. The first is chemical passivation, similar to that which occurs for a hydrogen-terminated surface. HF-treated silicon surfaces are well-known to be hydrogen-terminated [68, 144, 145] and the HF pretreatment appears to provide a direct or indirect source of chemical passivation in combination with the trifluoromethanesulfonyl-based treatment. The second component is field effect passivation and this it is proposed to arise from a negatively charged thin film on the surface. The reversibility in carrier lifetime shown by the vacuum exposure experiment (Figure 5.11 (c)) implies that the film interacts with the surface by physical adsorption (physisorption), rather than chemisorption.

5.4.4 Raman Microscopy

When a silicon sample is treated with a bis(trifluoromethanesulfonyl)-based solution it is often observed that circular droplets remain on the surface (as can be seen on the micrograph images in Figure 5.13 (a,b). The droplets are not observed when the treatment is performed in a low relative humidity (RH) environment. When droplets are present they can be washed off with a solvent without substantially reducing the initial carrier lifetime and hence surface passivation level. Lifetime data presented in Figure 5.13 (d) show that similar high levels of initial passivation are achieved with and without droplets present, however the droplets may play an important role in stabilising the field effect passivation shown previously to be present at the surface of the treated samples. As shown in Figure 5.13 (d), samples with droplets present retain their high lifetimes for well over an hour, whereas the lifetime in samples without droplets decays very rapidly. The droplets seem to protect the passivation from being degraded by the ambient atmospheric environment the samples are in, but over time the droplets themselves disappear, and hence might explain the steady decay in passivation level. A speculative mechanism could be, that the droplets act as a reservoir to replenish the thin film adsorbed at the surface, which evaporates upon exposure to air, particularly when the relative humidity is low (leading to increased evaporation). The degradation in KP surface potential with time (previously presented in Figure 5.7 (b)) could therefore be explained in terms of charge loss, due to evaporation of the passivating film itself.

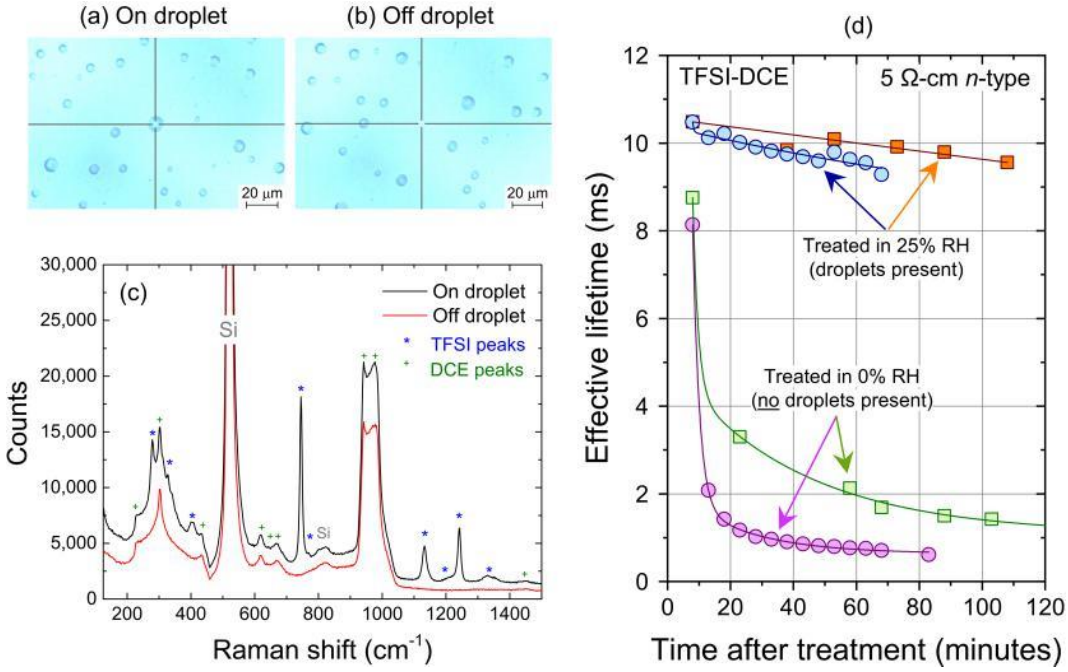

Figure 5.13 – (a and b) Optical micrographs of droplets of passivation solution on a silicon surface after TFSI-DCE passivation treatment. (c) Raman spectra acquired from the droplet in panel a and in a region between the droplets in panel b. Details of the peak assignments are given in Table 5.1. (d) Effective lifetime measured versus time in air for samples treated with TFSI-DCE in 25% RH (to have droplets present) and 0% RH (to have no droplets present), with curves plotted to guide the eye.

Finally, Raman spectroscopy was performed on a silicon sample treated with a bis(trifluoromethanesulfonyl)-based solution with the spectra plotted in Figure 5.13 (c). This study was performed using a TFSI–DCE solution as used in previous works [1, 101, 103]. The two spectra shown were acquired from the locations in Figure 5.13 (a,b), centering the acquisition area "on" a droplet and "off" a droplet, respectively. Dr Claire E. J. Dancer interpreted the Raman spectra which were acquired by the author. Many features are present in both spectra, with the large signal at 520 cm^{-1} arising from the silicon substrate and several peaks due to alkyl (C–Cl) and (C–C–Cl) bond vibrations originating from the DCE solvent used in the solution [146]. Clear additional peaks arising from the droplet are found at 744, 1132, and 1242 cm^{-1}, with less clear features observed at 279, 325, 402, 1206, and 1330 cm^{-1}. All these peaks can be assigned to various deformation modes of the CF_3 and SO_2 groups in the TFSI anion [147, 148]. Peaks are also present in both spectra at 119, 229, 302, 617, 640, 667, 942, 978, and 1447 cm^{-1}.

These peaks can all be assigned to known vibration modes in DCE [146]. In addition to the very intense bulk silicon vibration peak at 520 cm^{-1} found in both spectra as expected, a much weaker broad peak is observed around 821 cm^{-1} in both spectra. This is believed to be due to the HF-based cleaning procedure used on the silicon samples prior to the bis(trifluoromethanesulfonyl)-based solution treatment, as observed in Raman spectra taken from similar samples by Wang et al. [149] and Ren et al. [150]; however, it is not clear from this prior work exactly to what bond this peak should be attributed. Given the nature of the acid treatment it seems likely that an Si–H or similar vibration is the cause. A complete list of peaks and their assignment to bond vibrations in silicon, DCE, and TFSI based on existing information in the literature is provided in Table 5.1.

Peak assignment	Substance	Peak position (cm^{-1})	Peak description	Reference for assignment
δ (C-H)	DCE	1447	vw	[146]
υ SO_2	TFSI	1330	w	[147]
υ CF_3	TFSI	1243	w	[147]
υ CF_3	TFSI	1206	w	[147]
υ SO_2	TFSI	1132	w	[147]
ρ CH_2	DCE	977 (on) 979 (off)	vs	[146]
ρ CH_2	DCE	942	vs	[146]
	Etched silicon	820 (on) 822 (off)	vw	[149, 150]
δ CF_3	TFSI	766	vw	[147]
δ CF_3	TFSI	745	vs	[147, 148]
υ C-Cl	DCE	667	w	[146]
υ C-Cl	DCE	642 (on) 638 (off)	w	[146]
υ C-Cl	DCE	618 (on) 616 (off)	w	[146]
bulk (Si-Si)	Bulk silicon	520	vs	[149]
δ (C-C-Cl)	DCE	431 (on) 433 (off)	w	[146]
ω SO_2	TFSI	403	m	[147]
ρ SO_2	TFSI	326	m	[147]
δ (C-C-Cl)	DCE	301 (on) 303 (off)	s	[146]
ρ CF_3	TFSI	279	s	[147]
δ (C-C-Cl)	DCE	229	m	[146]
t (C-C)	DCE	119	m	[146]

Table 5.1 – Peak assignments for Raman spectrum on and off the droplets. Where peaks were observed in both spectra the peak position is given first for the "on droplet" spectrum then for the "off droplet" spectrum. Small variations in peak position are due to the variations in height for the on and off droplet positions. Symbols used are as follows: for relative peak intensity (compared to the maximum intensity peak observed in the spectrum for that substance); vs, strong; s, strong; m, medium; w, weak; vw, very weak [151]. Bond vibrations: υ, stretching; δ, bending; ω, wagging; ρ rocking; t, torsion [147]. Dr Claire E. J. Dancer interpreted the Raman spectra, which were acquired by the author.

The presence of TFSI in the droplets is consistent with the NMR data which show TFSI does not initially dissociate in the solvent (Figure 5.2 (a,b)). There are no additional peaks arising from the physisorbed thin film responsible for the field effect passivation, which suggests that the passivating film is very thin, and/or is made up of molecules and ions containing the same bonds as silicon, DCE, and TFSI. At this point it is difficult to assess, the thickness of the film from the Raman data without more knowledge of the composition of the film. Given that Raman micro spectroscopy has previously been used to detect polymer films of as little as 3 nm thickness and even monolayers and sub-monolayers of certain organic substances [152], it should in theory be possible.

5.5 Summary

While the benefits of TFSI–based surface treatments are clear, the mechanisms by which the effects arise are not well established. In this chapter, a series of experiments were performed to understand the origin of the passivation. The results presented have demonstrated that a range of solutions based on molecules with a bis(trifluoromethanesulfonyl)-based structure can give rise to excellent passivation of surfaces, with the common factor being the presence of CF_3SO_2 groups and not the solution's acidity.

Experimental work was conducted which found that the surface passivation achieved has both a chemical and a field effect component. Chemical passivation is thought to arise at least partially from hydrogen termination of the surface. The solution treatment adds a field effect element explainable by the existence of a negatively charged thin film physisorbed on the surface. This film is unstable in air and under vacuum, with the degradation in air being less severe when small droplets of solution help stabilise the film, the limited vacuum stability that the films have inhibits their reliable study with high vacuum techniques.

The finding that nonacidic solutions can offer excellent electrical passivation at room temperature, similar to levels of passivation using super-acidic solutions, opens up the possibility of using them on materials more sensitive to an acidic environment, meaning that these treatments could find future uses in materials systems sensitive to acidic environments, such as in perovskite solar cells [153].

In the following chapter the chemical treatments prior to passivation will be investigated in order to understand how maximising the silicon surface termination of the passivating treatments may help to improve the quality and longevity.

Chapter 6 Atomic Level Termination for Passivation and Functionalisation of Silicon Surfaces

6.1 Introduction

Chapter 5 investigated how the chemical used as the solute in the solution effected the treatment, in order to understand the mechanism of the passivation. It was discovered that the passivation arose from both field effect and chemical effects, it was also found that non-super-acidic solutions give similar levels of passivation to using super-acidic ones. In this chapter the relevance (and impact) of using a macroscopic analytical method to maximise silicon surface termination by optimising the HF treatment to enhance surface functionalisation will be investigated.

6.2 Motivation

Silicon materials lie at the heart of many electronic devices, including the vast majority of photovoltaic solar cells. Atomic level control of the interface between silicon and the materials deposited upon it, is vital for reliable and efficient device operation. Wet chemical processing, particularly cleaning and etching processes, have always been an intrinsic step of semiconductor processing, and are well established for the surface preparation of electronic device fabrication [110]. Hydrogen termination of the surface is usually the first step of subsequent functionalisation, and whether a surface has initially been well or poorly treated, can become apparent in subsequent device performance [154]. The importance of silicon surface termination extends well beyond the electronic device community with, for example, hydrogen termination being a necessary first step in attaching DNA to a silicon surface for analysis and modification [155], and for various optical devices, biomedical devices, and sensors [156].

An important factor in silicon's dominance as an electronic material is that its surface properties can be controlled precisely with simple thermal and chemical processing. A thin native oxide forms over time in air (or thermal oxides can be grown at elevated temperature), and oxides can be easily removed in hydrofluoric acid (HF). The science of silicon surfaces in the presence of

HF is covered in several reviews [157, 158], and there are a number of subtleties. It is already known that H-terminated semiconductor surfaces can be prepared through the use of wet chemical methods, by immersing silicon with a layer of native oxide into a dilute HF or NH_4F solution, to remove the native oxide and subsequently form a hydrogen terminated surface.

It is well established that a short treatment in a dilute HF solution results in a metastable hydrogen-terminated surface [69], however Si–F bonds are considerably stronger than Si–H bonds [69], and fluorine-terminated surfaces are known to result from treatments in concentrated HF [159, 160]. Control of the surface termination chemistry can be gained by adjusting the acidity of the solution [161], and the addition of hydrochloric acid (HCl) achieves hydrogen termination while not etching the bare silicon beneath [162].

While there have been a large number of studies regarding the science of HF treated surfaces [157, 158] – a reflection of its importance in semiconductor manufacturing – there are no known studies which address surface passivation at the macroscopic (e.g. centimetre) scale, once the sample is removed from the solution. Most analytical techniques employed to examine the silicon surface, post treatment, are performed on the nanometre to micron scale. Although these analyses help to determine what species are terminating the silicon surface post HF dip (e.g. H, F, OH) they do not quantify how many silicon bonds are terminated by these species, which in most device applications is crucial for increased functionalisation and spatial uniformity across the silicon surface. The aim, therefore, is to try to complement the currently known scientific insight, by quantifying the level of bond termination over a much larger area. It is currently thought this can only be done by measuring the rate of surface recombination at the terminated silicon surface by a carrier lifetime measurement (such as by photoconductance decay [42] or by photoluminescence imaging [114]) that can perform measurements on the timescale of milliseconds or longer. Providing that the measurement techniques give a sufficient level of sensitivity, it will be valuable in optimising the HF pre-treatment step in the process, and thus maximise functionalisation of the silicon surface. This could be of significant value when the silicon surfaces are treated with the triflyl-based solutions discussed in Chapter 5, including the superacid bis(trifluoromethane)sulfonimide (TFSI) [1-3, 101, 103], because the level of passivation achieved with these treatments is considerably greater than from just an HF dip. This is partly because of the existence of a charged layer on the surface which provides field effect passivation by repelling charge carriers away from the surface [2], as discussed in previous chapters of this thesis. The extent to which these triflyl-based passivation processes are affected

by the prior surface treatments are not well established, because the impact (and effectiveness) of the HF termination has not been clearly demonstrated on a macroscopic scale.

6.3 Effective Lifetime Experiments and Modelling

The extent to which a semiconductor surface is passivated can be quantified by measuring the effective carrier lifetime, $\tau_{effective}$, which for these experiments varies (by a good approximation) according to Equation 6.1.

$$\frac{1}{\tau_{effective}} = \frac{1}{\tau_{bulk}} + \frac{2S}{W} \qquad \text{Equation 6.1}$$

Where τ_{bulk} is the bulk carrier lifetime, S is the surface recombination velocity and W is the sample thickness. As τ_{bulk} and S are dependent on the excess carrier density, $\tau_{effective}$ is also dependent on the excess carrier density. As τ_{bulk} is unlikely to change with low temperature chemical treatments, $\tau_{effective}$ will increase with reducing S (i.e. improving surface passivation) and thus $\tau_{effective}$ is a measurement of the extent to which the surface is passivated.

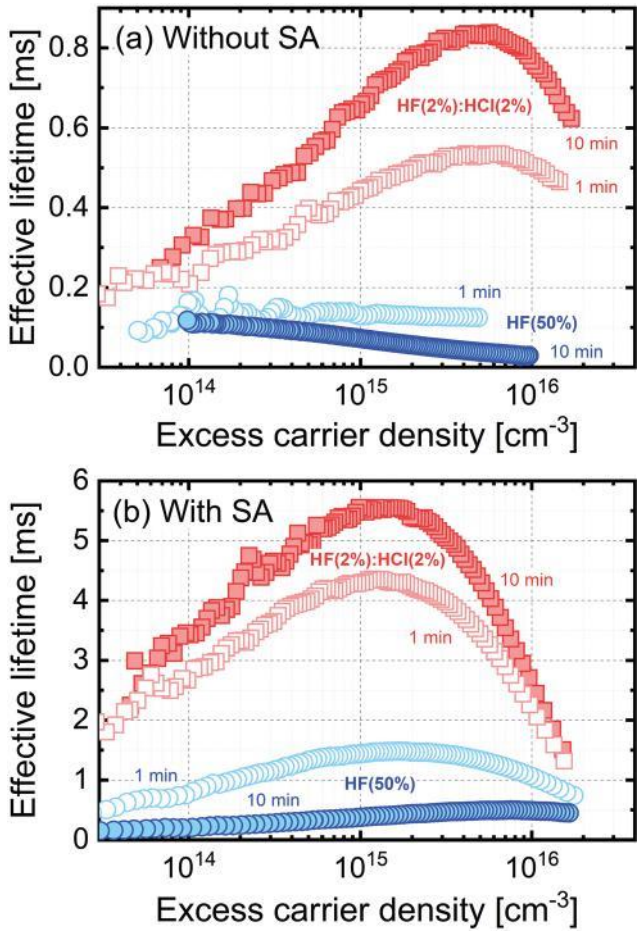

Figure 6.1 – Effective lifetime versus excess carrier density for 700 µm thick 5 Ω cm *n*-type TMAH etched silicon wafers. In (a) the samples are subjected to HF(2%) : HCl(2%) or HF (50%) treatments for the times stated, and in (b) a TFSI-pentane superacid-derived surface passivation scheme (SA) is applied in addition.

Effective carrier lifetime results for chemically treated TMAH etched 5 Ω cm *n*-type float-zone silicon (FZ-Si) are shown in Figure 6.1. Figure 6.1(a) shows that treatment with either HF (50%) or HF(2%) : HCl(2%) passivates the surface when the silicon samples are pulled dry from the solutions (i.e. no deionised water rinse is performed), which mitigates the formation of a hydroxylised surface when H and F related species are washed away during a rinse [163]. Therefore, samples were not rinsed in order to retain a well passivated surface.

In all cases the control samples, which had not received an HF-based treatment after cleaning, showed lifetimes well below the worst lifetimes which can be seen in both Figure 6.1 and Figure 6.2. Performing a longer treatment in HF(2%) : HCl(2%) resulted in better level of surface passivation than a shorter treatment did. Perhaps surprisingly, the passivating effect of a

HF(50%) treatment, gets worse with the length of treatment time, and the possible reasons for this will be explained later in this chapter.

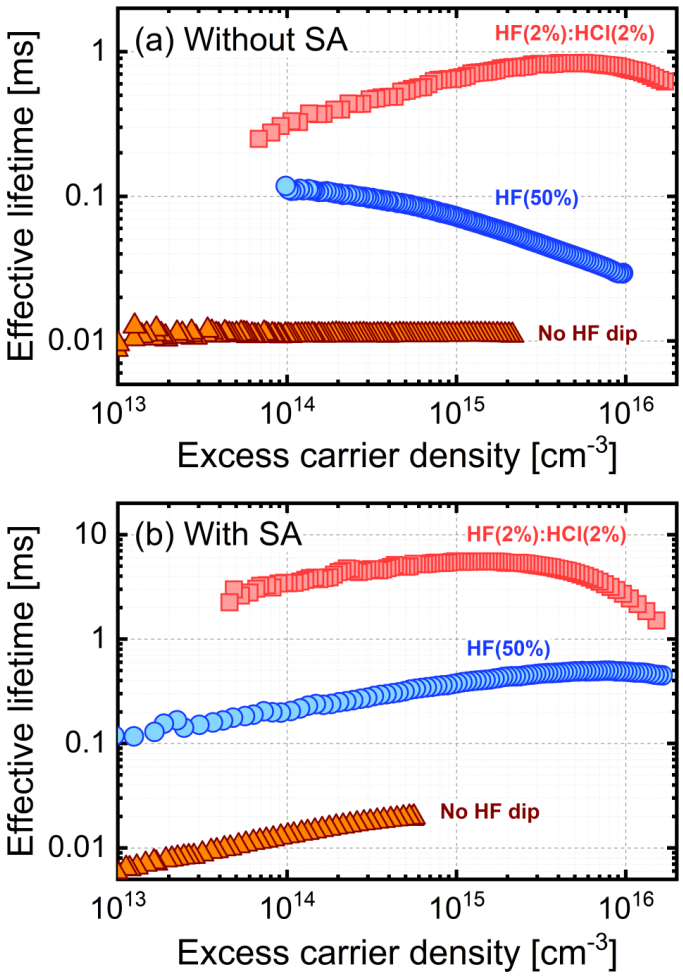

Figure 6.2 – Effective lifetime versus excess carrier density for 700 µm thick 5 Ωcm n-type TMAH etched silicon wafers. All samples were first subjected to the same cleaning process (HF dip, SC1 clean, HF dip, SC2 clean), then in (a) samples were subjected to either no HF dip, a 10 min HF(2%):HCl(2%) treatment, or a 10 min HF(50%) treatment. In (b) samples were subjected to the same processes in (a) plus an additional TFSI-pentane superacid treatment.

It was interesting to find that the effects observed were independent of the surface's starting condition, as similar trends were observed for smooth planar etched (process described in Section 3.2.2.4) silicon samples (see Figure 6.3) and for TMAH etched surfaces which are relatively rough at the nanometre scale [103].

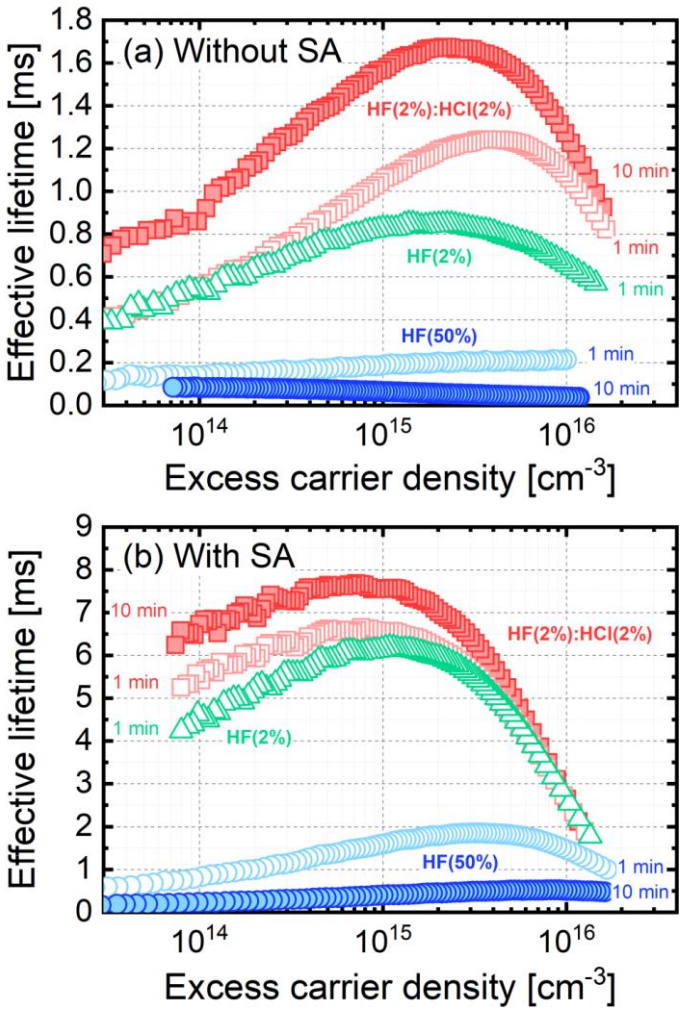

Figure 6.3 – Effective lifetime versus excess carrier density for 700 μm thick 5 Ωcm n-type planar etched silicon wafers. In (a) the samples are subjected to HF(2%):HCl(2%), HF(2%) or HF (50%) treatments for the times stated, and in (b) a TFSI-pentane superacid-derived surface passivation scheme (SA) is applied in addition.

The results found for planar etched surfaces, shown in Figure 6.3, also show that treatment with just HF(2%) without HCl, produce a lower lifetime than with HF(2%) : HCl(2%) showing that the presence of HCl in the solution results in better passivation.

The data shown in Figure 6.1 (b) show the effect of an additional superacid-derived passivation treatment (using the TFSI-pentane treatment, performed for a 60 s dip in all cases), which was applied after the same pre-treatments as discussed in Figure 6.1(a). The additional superacid-derived passivation increases the effective lifetimes showing that the values presented in Figure 6.1(a) are not limited by the bulk lifetime of the sample. Importantly, the contribution of the different pre-treatments is still apparent after the superacid-derived passivating treatment, with

the same trends observed as in Figure 6.1(a). This highlights the key importance of the chemical process history in producing a functionalised or passivated sample surface in the processes demonstrated here. These findings could also be applicable on a more wider scale for other wet based treatment cases. The lifetime in control samples which had not received an HF-based treatment after cleaning, remained low, as can be seen in Figure 6.2.

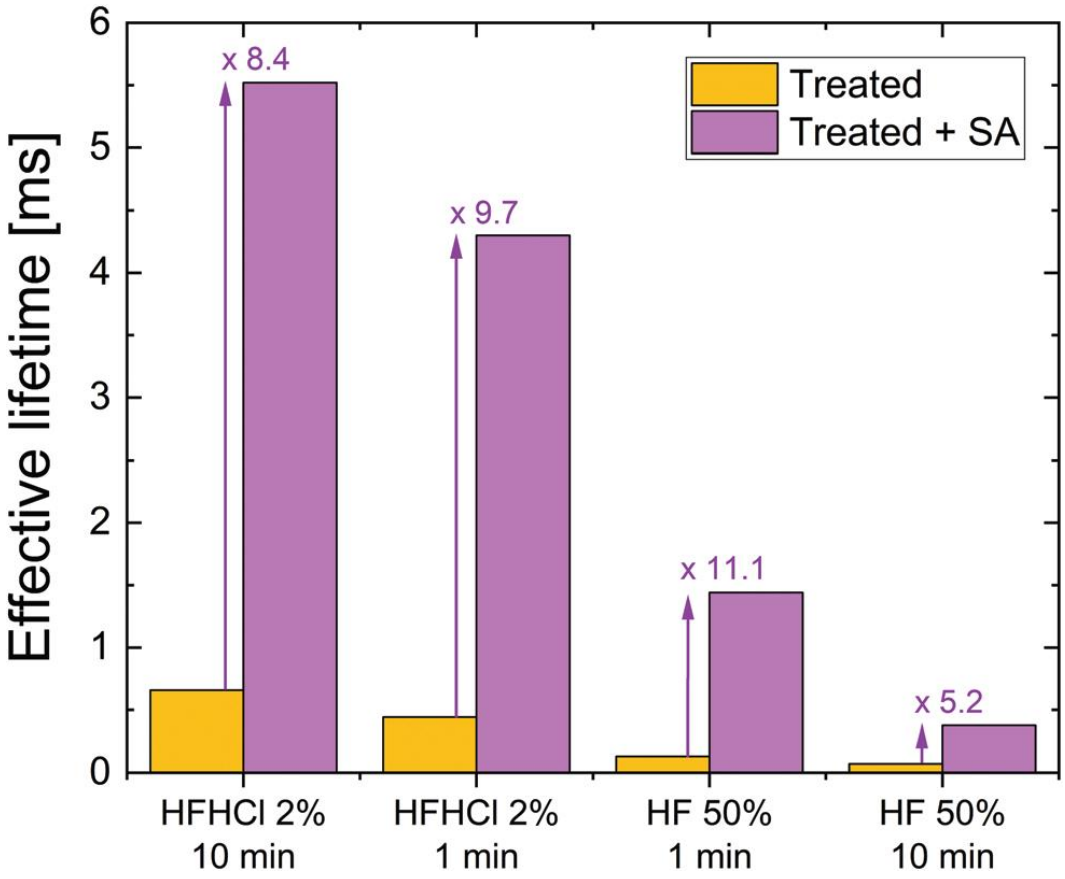

Figure 6.4 – Effective lifetime at an excess carrier density of 10^{15} cm^{-3} for 700 μm thick 5 Ω cm *n*-type TMAH etched silicon wafers. The left bar of each pair shows the effect of the stated treatment only, whereas the right bar shows the effect of the stated treatment plus an additional TFSI-pentane superacid-derived surface passivation scheme (SA). The factor by which the superacid-derived passivation enhances lifetime is stated. Data for planar etched silicon are shown in Figure 6.5.

Figure 6.4 summarises the effect on effective lifetime of the different treatments on TMAH etched silicon with and without superacid-derived surface passivation at a fixed excess carrier density of 1×10^{15} cm^{-3}. A similar plot for treated planar etched silicon is shown in Figure 6.5.

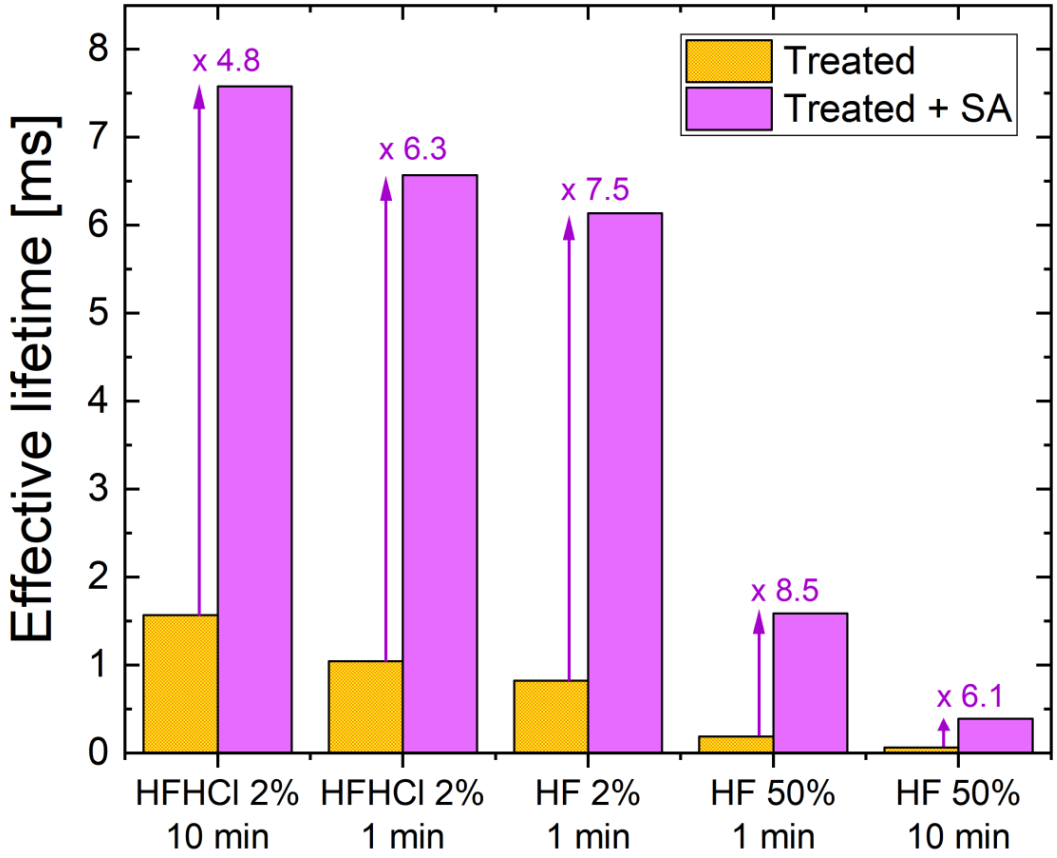

Figure 6.5 – Effective lifetime at an excess carrier density of 10^{15} cm^{-3} for 700 µm thick 5 Ωcm *n*-type planar etched silicon wafers. The left bar of each pair show the effect of the stated treatment only, whereas the right bar shows the effect of the stated treatment plus an additional TFSI-pentane superacid-derived surface passivation scheme (SA). The factor by which the superacid-derived passivation enhances lifetime is also stated.

As can be seen from the data in Figure 6.4, for each treatment it is clear that the superacid-derived passivation enhances lifetime substantially. The ratio of lifetime values at the chosen excess carrier density is between 5.2 and 11.1 times those seen after the initial acid dip treatment for the different conditions studied. It is noted that the interplay between the different passivation schemes and mechanisms is a complex one; however, more insight can possibly be gained by analysing the injection dependence of the effective lifetime, as presented next.

It is already well understood that surface passivation of semiconductors is governed by the extent to which dangling bonds are terminated ("chemical" passivation) and the level of charge in the passivating layer which modifies the distribution of carriers near the semi-conductor's surface ("field effect" passivation). Taking a set of fixed capture parameters, chemical passivation can be quantified by the reduction in interface state density (D_{it}), with the level of field effect passivation determined by the effective areal charge density (Q_{eff}). In high quality silicon samples with a low concentration of bulk recombination centres, such as those being used for this study, these parameters strongly influence the dependence of carrier lifetime on excess carrier density. Figure 6.6 shows the fitting of experimental lifetime curves using the calculators available from PV Lighthouse [164] based on a method described by Girisch et al. [165] which was extended by Aberle et al. [166]. When performing this fitting to the data it is assumed that surface recombination is governed by a single defect at mid-gap and use the intrinsic recombination parameterisation of Richter et al. [28]. The fit parameter for chemical passivation is a carrier type-specific surface recombination parameter, and for electrons is $S_{n0} = v_{tn} \times \sigma_n \times D_{it}$ and for holes is $S_{p0} = v_{tp} \times \sigma_p \times D_{it}$, where v_{tn} is the thermal velocity of electrons and v_{tp} is the thermal velocity of holes, and σ_n and σ_p are the capture cross-sections for electrons and holes, respectively. Unfortunately, it is not possible to separate the cross-section and interface state density terms from the analysis of lifetime data alone.

The data shown in Figure 6.6 presents the fits to the extreme datasets for the TMAH etched samples in Figure 6.1, i.e. those giving the highest and lowest lifetimes, Figure 6.6 (a) in the absence of, and those shown in Figure 6.6 (b) in the presence of additional superacid-derived passivation treatment. The fits to selected lifetime curves for planar silicon etched samples are provided in Figure 6.8. Good fits to the experimental data for both Figure 6.6 and Figure 6.8 can be made in all cases, with the parameters used given on each of the graphs presented.

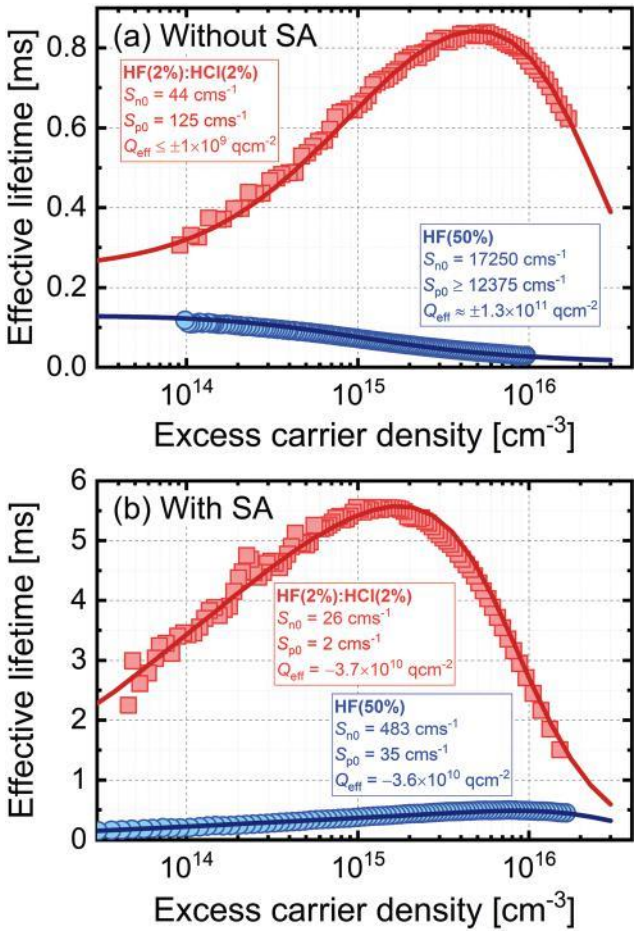

Figure 6.6 – Modelling of effective lifetime as a function of excess carrier density for 700 µm thick 5 Ω cm *n*-type silicon using the extrema of the experimental data for TMAH etched silicon in Figure 6.1 (all with 10 min treatment times). Plot (a) is for samples subjected to just HF(2%) : HCl (2%) or HF(50%) treatments, and samples for plot (b) also received a TFSI-pentane superacid-derived passivation scheme (SA). As described in the text, a model was used to produce the solid lines, which provided a good fit to the experimental data with the parameters stated.

In the absence of additional superacid-derived passivation as shown in Figure 6.6 (a), the 10 min HF(2%) : HCl(2%) treatment results in low values of Sn0 and Sp0, which is likely because the treatment gives rise to good chemical passivation by reducing D_{it}. Conversely when treated with HF(50%), but for the same 10 min treatment period, the fit has very high values of Sn0 and Sp0 which shows that this alternate treatment results in a poor level of chemical passivation. The level of field effect passivation arising from the HF(2%) : HCl(2%) treatment is low (Q_{eff} of order 10^{9} q cm^{-2}) and the experimental lifetime curves can be accurately modelled using either (positive or negative) charge polarity, indicating the surface charge is too low to have any

significant impact on the level of passivation in this case. The 10 min HF (50%) treatment has a much stronger field effect component, in this case, it is not possible to extract the charge polarity unambiguously, but a magnitude of Q_{eff} ~1×10^{11} q cm^{-2} is consistent with the lifetime data, as shown by fits for different charge densities provided in Figure 6.7.

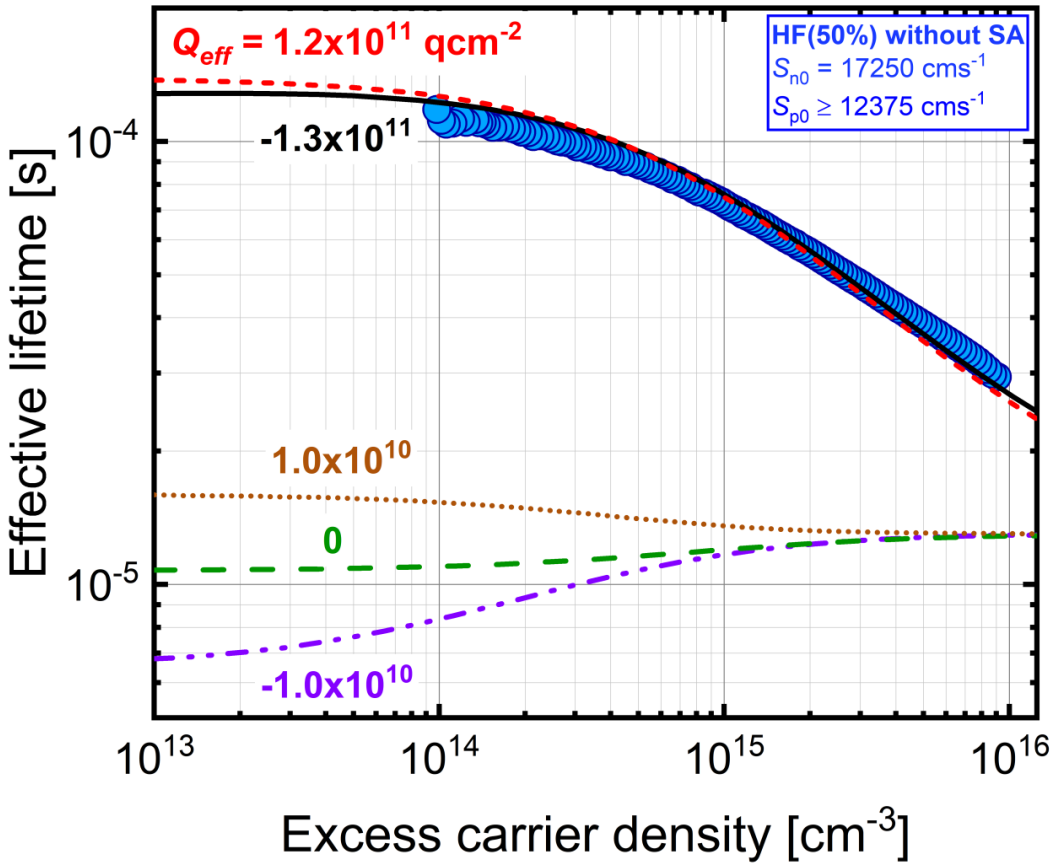

Figure 6.7 – Modelling of effective lifetime as a function of excess carrier density for 700 μm thick 5 Ωcm n-type TMAH etched silicon treated with HF (50%) for 10 min (without superacid-derived passivation). The experimental data (blue circles) are from Figure 1 (a). The values of Sn0 and Sp0 were fixed, and different values of Q eff were used to generate the curves shown.

The data presented in Figure 6.6 (b) shows the effects of adding an additional superacid-derived surface treatment following the initial acid dip with HF or HF/HCl, in order to understand the change adding the superacid passivating treatment made to the surface. For the sample first subjected to a 10 min HF(2%) : HCl(2%) treatment, the additional TFSI-pentane treatment improves both the chemical passivation (further reducing Sn0 and Sp0) and also the field effect passivation. For this case, a negative Q_{eff} is required with a magnitude of 3.7×10^{10} q cm^{-2}. The

inference of negative charge agrees with previous Kelvin probe studies of TFSI-based passivation of silicon [2], and the magnitude of the charge is similar to that found for silicon passivated with a range of bis(trifluoromethanesulfonyl)-based solutions which find negative values in the range 6–9 × 10^{10} q cm^{-2} [2, 3]. The results for the 10 min HF (50%) treatment in Figure 6.6 (b) show an improvement in chemical passivation (reduced Sn0 and Sp0) as a result of the TFSI-pentane passivation, and a similar level of field effect passivation to the HF(2%) : HCl(2%) case. In summary, the results in Figure 6.6 (b) show that the superacid-derived treatment provides a similar level of field effect passivation regardless of the pre-treatment performed on that sample, but the level of chemical passivation remains strongly influenced by the surface pre-treatment performed prior to the superacid-derived passivation step, demonstrating the key importance of the pre-processing of the samples. By measuring the effective lifetime directly after performing only the HF dip (the required pre-treatment step), the level and effectiveness of the surface termination of the bare Si can be assessed, and how this will subsequently impact the functionalisation of the silicon surface when then performing the superacid treatment step. The high lifetimes reported in Figure 6.6 (b) also confirms just how effective, superacid-derived treatments can be, as the thin film which forms after removal from the super-acidic solutions provide equivalent passivation to when silicon is fully immersed in liquid HF [67].

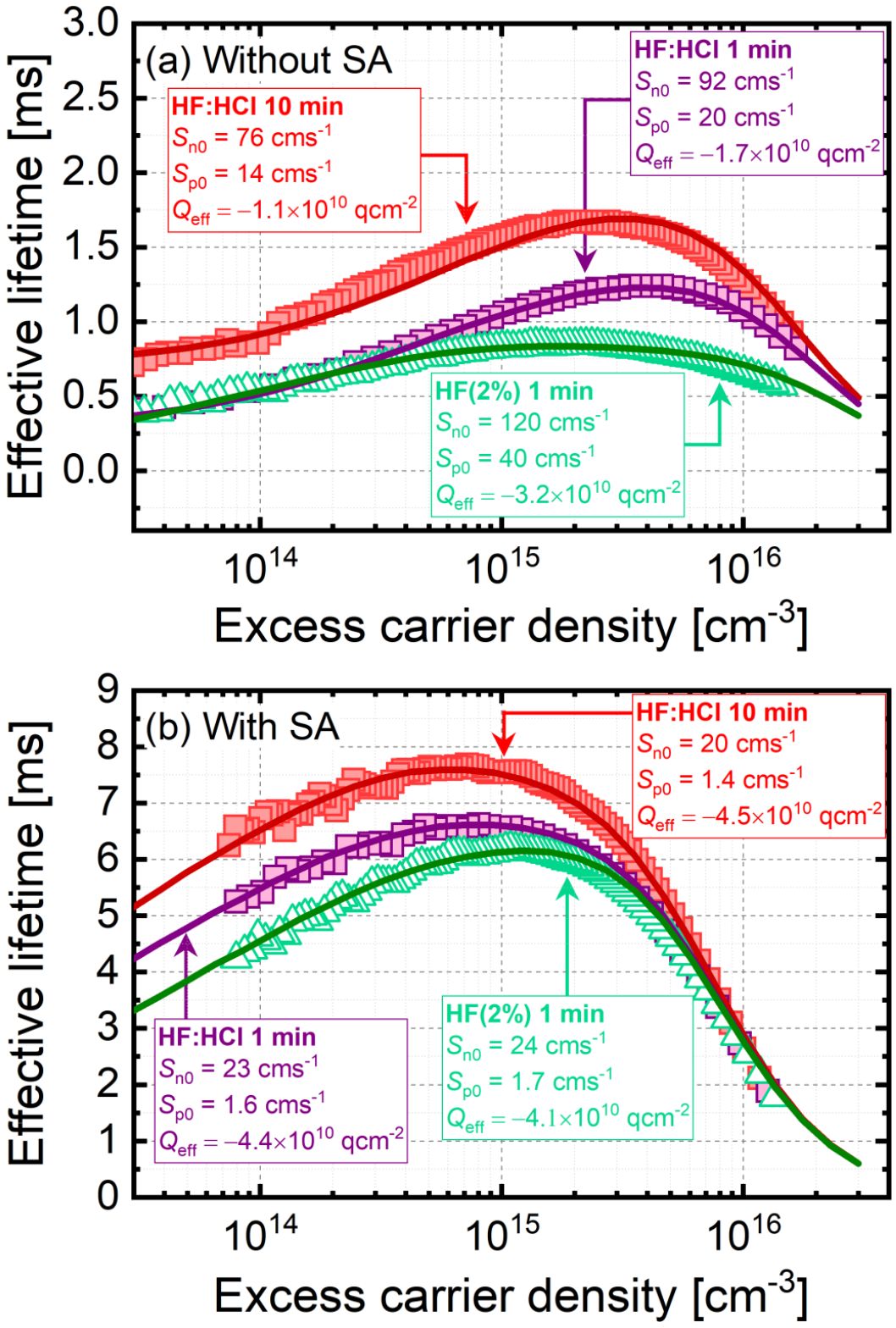

Figure 6.8 – Modelling of effective lifetime as a function of excess carrier density for 700 µm thick 5 Ω cm n-type silicon using experimental data for HF(2%):HCl(2%) and HF(2%) treated planar etched silicon. Plot (a) is for samples subjected to just HF(2%):HCl(2%) or HF(2%) treatments, and samples for plot (b) also were subjected to a TFSI-pentane superacid-derived passivation scheme (SA). The parameters used to fit the data are shown in the figure.

The fitting of lifetime curves for planar etched surfaces tells a similar story (as presented in Figure 6.8). The values for Sn0, Sp0 and Q_{eff} are slightly different to those for the TMAH etched case in the absence of superacid-derived passivation, but are very similar after the superacid-derived passivation is performed. In the planar etched case, a small density of negative charge is required to fit the data before the additional passivation, and such a difference is justifiable given the considerable differences between the types of etching.

6.4 Surface Characterisation

Cleaned silicon samples subjected to 10 min HF(50%) and HF (2%) : HCl(2%) treatments were characterised by XPS after being pulled dry from their respective solution, with key results shown in Figure 6.9. The data shown are for a shallow take-off angle of 15° with respect to the surface parallel as this gives a relatively good sensitivity for surface studies. Data for a 90° take-off angle are included in Figure 6.10, as is a table of elemental compositions in Table 6.1.

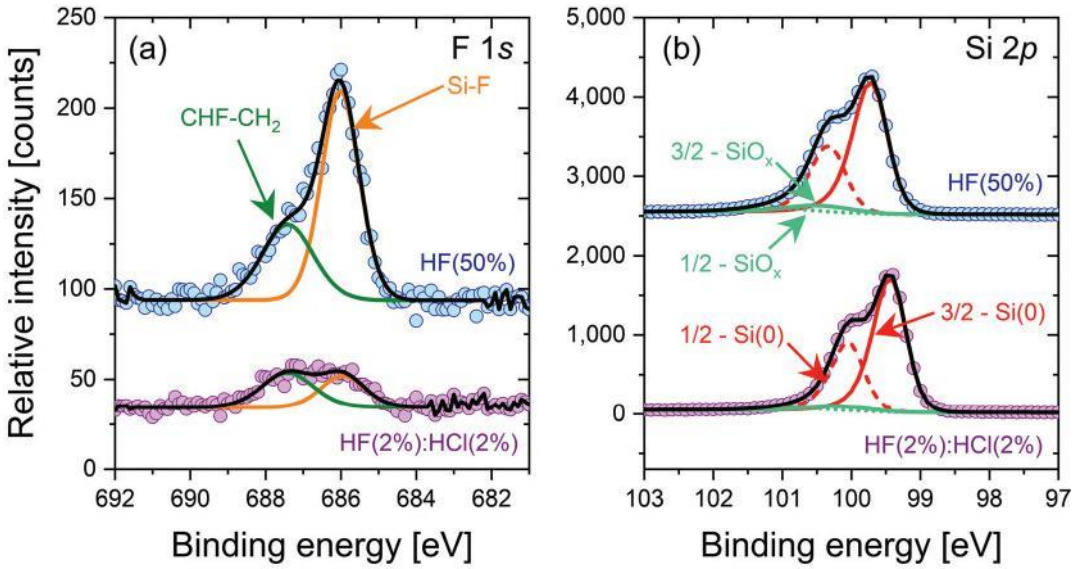

Figure 6.9 – XPS spectra at take-off angle of 15° with respect to the surface parallel for 5 Ω cm *n*-type FZ-Si treated for 10 min with HF(50%) at the top, and HF(2%) : HCl(2%) at the bottom. Spectra have been offset in the vertical direction for clarity. The F 1s spectra (left) show substantially enhanced fluorine termination in the HF(50%) case. The Si 2p spectra (right) are similar for both treatments, showing any SiO_x layer is thin. Additional superacid-derived passivation was not applied.

The F 1s spectra in Figure 6.9 (a) shows a substantially larger Si–F peak for a 10 min HF(50%) treatment compared to a 10 min HF(2%) : HCl(2%) treatment. The CHF–CH_2 peak is also larger. This shows that more fluorine termination occurs in the case of the HF(50%) treatment. Figure 6.9 (b) shows the Si 2p spectra, which are similar for both samples. There are small SiO_x-related peaks in both samples, which may arise from thin oxide layers formed during the transfer of the samples from the cleanroom to the XPS system. Cl 2s spectra were also recorded but showed no Cl-related peaks for either sample in the 260 to 280 eV binding energy range.

Treatment	Take-off angle	Si	C	O	F
HF(50%)	90°	80.8	15.5	1.9	1.8
HF(50%)	15°	53.8	41.3	3.4	1.5
HF(2%):HCl(2%)	90°	83.6	14.1	1.8	0.4
HF(2%):HCl(2%)	15°	50.1	46.1	3.4	0.4

Table 6.1 - XPS elemental composition data for chemically treated silicon surfaces (percentages).

A drawback of XPS experiments is that they are not able to provide reliable information on hydrogen termination. Direct detection is not possible because of hydrogen's small photo-ionisation cross-section, and any hydrogen-related change in the Si 2p peak position sometimes used to assess hydrogen termination [167] is likely to be affected by the co-existence of fluorine resulting from our HF-based wet chemical treatments.

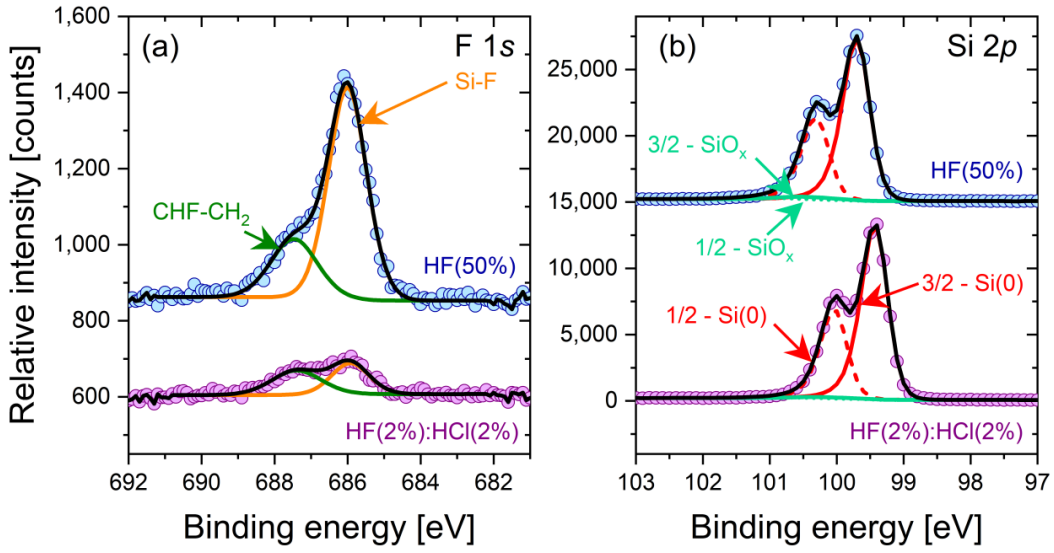

Figure 6.10 – XPS spectra at take-off angle of 90° with respect to the surface parallel for 5 Ωcm *n*-type FZ-Si treated for 10 min with HF(50%) at the top, and HF(2%):HCl(2%) at the bottom. Additional superacid-derived passivation was not applied. Spectra have been offset in the vertical direction for clarity.

To investigate the surface topology, AFM maps were acquired for samples subjected to 10 min HF(50%) and HF (2%) : HCl(2%) treatments and the results are shown in Figure 6.11. The sample treated with HF(50%) was found to be decorated with nano-particulates at the surface, whereas no such particles are found in the HF(2%) : HCl(2%) case. The particles have a typical dimension of 2 nm to 6 nm from the surface. It therefore appears that an extended etch in concentrated HF damages the surface in some way and this, as well as fluorine termination, may account for the lower levels of surface passivation achieved.

It is typically stated that HF etches silicon oxide, completely terminating the silicon surface with hydrogen [168]. This H-terminated Si is said to be stable towards further attack from HF, but it has been shown that this etching process is spatially anisotropic, with the (111) planes being considerably more stable than other faces [169]. Other silicon surface orientations do not exhibit this level of stability and have been shown to be slowly and selectively etched in solutions containing HF. This can change the initial morphology of the interface causing (100) Si surfaces to roughen, ultimately developing (111) facets [170]. This may be the cause of the roughening we have observed during this study, but the identification of the causes were not within the scope of this study.

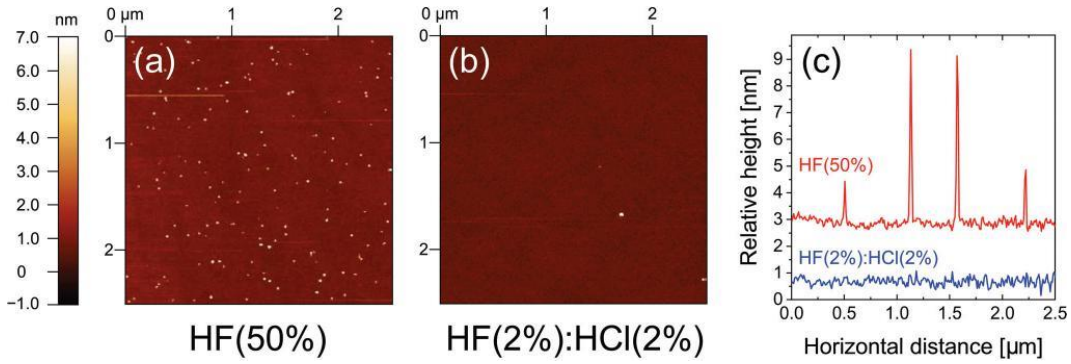

Figure 6.11 – Representative 25 µm × 25 µm AFM maps of 5 Ω cm *n*-type FZ-Si after (a) an HF(50%) treatment for 10 min and (b) an HF(2%) : HCl(2%) treatment for 10 min. Neither sample had been subsequently treated with superacid-derived passivation. The horizontal line scans in (c) show scans typical of both sample types.

6.4.1.1 Discussion - Surface Treatments and Termination

The method used here, of measuring lifetimes a few seconds after removal from the HF or HF : HCl solutions without rinsing enables the surface termination effects of the treatments to be assessed out of solution. Passivation arises in all cases (as seen in Figure 6.1 (a)), although the level of passivation is strongly dependent on the solution's composition and duration of treatment. Previous studies measured lifetimes with samples immersed in acidic solutions [68, 71, 171] and the differences between the chemical treatments are less apparent (reviewed in ref. [67]). Here the presented data clearly shows that out-of-solution HF(2%) : HCl(2%) treatments offer better passivation than HF(50%), and that this passivation improves with immersion time in the former but gets worse with time in the latter. The modelling results (presented in Figure 6.6 (a)) show that the superiority of HF(2%) : HCl(2%) over HF(50%) is because of lower S_{n0} and S_{p0} values, which is most likely because of better chemical passivation of the surface (lower D_{it} values assuming fixed capture parameters).

The presence of HCl in the HF solution affects the surface termination in at least three ways. Firstly, it cleans impurities (mostly metals) away from the silicon surface which is why it is used in Standard Clean 2 (SC2) as part of RCA cleaning [110]. Secondly, it reduces the pH of the solution as the ionic hydrogen concentration is higher [161], hence aiding Si–H surface

termination. Thirdly, it reduces the concentration of fluoride ions in the solution [161], and hence reduces the formation of bonds with fluorine species. The addition of HCl has also been found to be beneficial when the lifetime is measured with the sample immersed in an HF-containing solution [171], probably for the same reasons as these. It can therefore be suggested that the addition of HCl to HF-containing solutions could be beneficial for the creation of a high-quality hydrogen-terminated surface required for a range of applications (e.g. DNA attachment to a silicon surface [155]).

Treatments in concentrated HF solutions result in a different surface termination chemistry compared to HF : HCl solutions. Figure 6.1 (a) shows a 1 min treatment in HF(50%) results in better passivation than a 10 min treatment. The possible explanation is that the initial metastable hydrogen termination is reduced, as the level of fluorine termination increases with immersion time. The fluorine concentration will be much higher than in the HF(2%) : HCl(2%) solution and the hydrogen concentration lower [161]. There is clear evidence for Si–F bonding in HF(50%) samples treated for 10 min in the XPS data in Figure 6.9 (a), and similar findings have been published previously [159, 160], which supports the experimental data obtained during this research. The fact that Si–F bonds form over time is expected thermodynamically given the bond dissociation energies of Si–F are perhaps the strongest single bonds known [160], and are almost a factor of two higher than Si–H [69, 172].

As well as the surface termination, the results show that the material surfaces themselves are different as a consequence of the treatments as demonstrated in Figure 6.11, as expected from the findings of an earlier AFM study [162], HF-HCl treatments do not roughen the surface. Whereas, prolonged treatment in concentrated HF appears to result in a roughened surface, as has been found previously for silicon treated in strong HF solutions [161]. Trucks et al. explain the difference in surface behaviour in terms of polarisation of the Si–Si bonds, which can be broken by dipolar HF, whereas a hydrogen-terminated surface is stable due to the lack of polarisation of adjacent Si– Si bonds [69].

6.4.2 Surface Termination for Dielectric-based Passivating Films

For stable passivation in electronic devices, such as silicon solar cells, thin films of dielectric materials are typically used (see reference [19] for a more in-depth review). As it has been established that the effects of the chemical pre-treatment persists after superacid-derived passivation (see Figure 6.1 (b), Figure 6.4 and Figure 6.6 (b)), it is important to assess whether this might be the case for dielectric deposition. Using atomic layer deposition (ALD) 20 nm thick aluminium oxide films was deposited on the surface of *n*-type Cz-Si samples from the same wafer pre-treated with HF(50%) or HF(2%) : HCl (2%) for 10 min (where the samples were pulled dry from their respective solution). The process comprises a deposition step at 200 °C followed by a 460 °C activation anneal performed in a quartz tube furnace in air for 30 minutes. The injection-dependent effective lifetime results are shown in Figure 6.12.

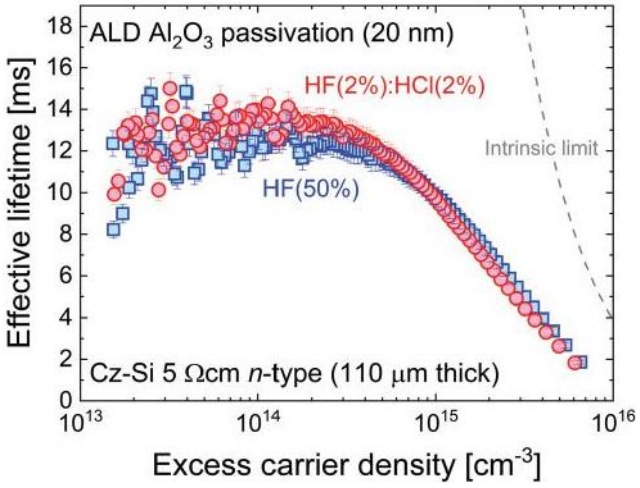

Figure 6.12 – Effective lifetime versus excess carrier density for 110 μm thick 5 Ω cm n-type Cz-Si samples from the same wafer treated with HF (2%) : HCl(2%) or HF(50%) for 10 min immediately before the ALD process (200 °C deposition with 460 °C activation). The level of surface passivation is the same within the 5% error shown, unlike for the superacid-derived passivation in Figure 6.1 (b). The intrinsic lifetime limit from Richter et al. [28] is also shown, as discussed in Section 2.1.3.

It is clear from Figure 6.12 that the pre-treatment makes no significant difference to the level of ALD passivation achieved within the typical errors of lifetime measurement (error bars of 5% are shown, guided by ref. [113]). The difference from the chemical pre-treatment appears to have been eliminated during the AlO_x growth and activation process. While this is an important

result, it is noted that the surface preparation prior to AlO_x deposition can still make a difference if the surface is not treated prior to deposition to remove SiO_x layers which form during sample cleaning. In Figure 6.13 it is shown that much worse surface passivation results when the samples are not treated with a HF-based solution after SC1 or SC2 cleaning.

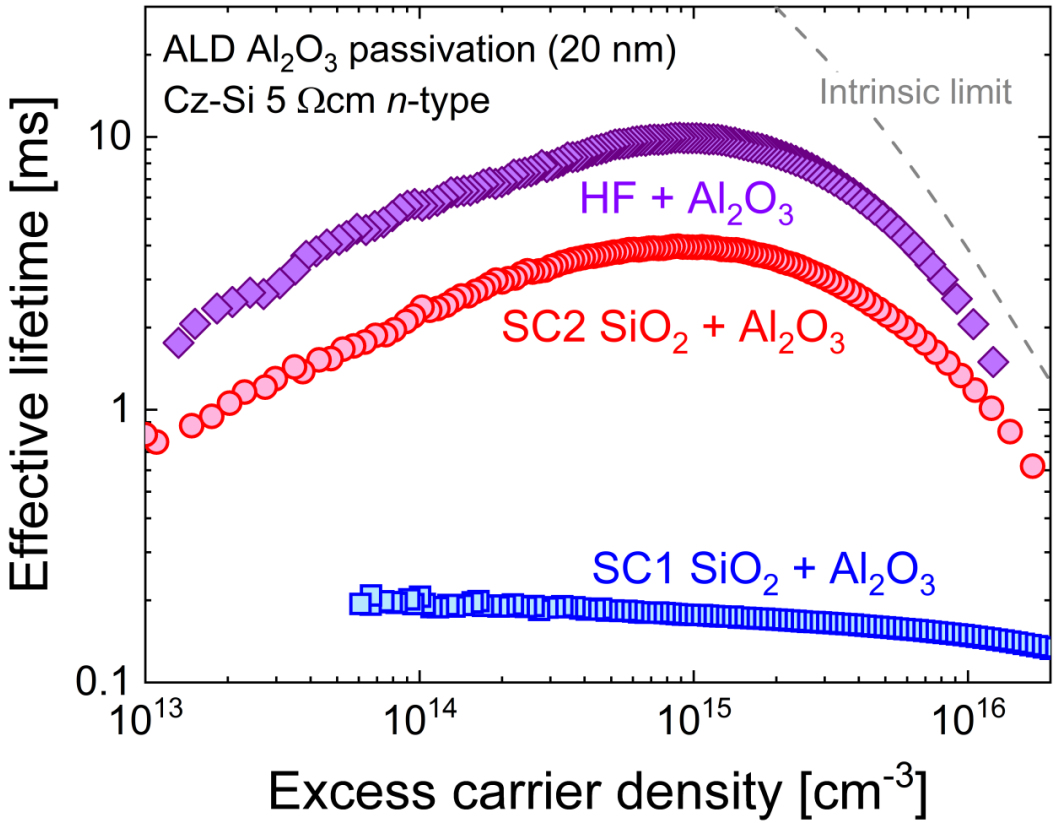

Figure 6.13 – Effective lifetime versus excess carrier density for 130 µm thick 5 Ωcm n-type Cz-Si samples from the same wafer passivated with ALD Al_2O_3 after different pretreatments. The wafer had been alkaline etched (KOH) by the supplier and samples were not subjected to TMAH or planar silicon etching. All samples were initially subjected to the same cleaning process (HF dip, SC1 clean, HF dip, SC2 clean, HF dip). One sample (blue) was then subjected to an additional SC1 cleaning step which grows a thin SiO_x layer and was not HF dipped prior to deposition. Another sample (red) was then instead subjected to an additional SC2 cleaning which also grows a thin SiO_x layer and was not HF dipped prior to deposition. The other sample (purple) was HF dipped and pulled dry immediately prior to deposition to remove any oxide formed during cleaning. For all samples, deposition was performed at 200 °C followed by a 30 min 460 °C activation anneal. The intrinsic lifetime limit of Richter et al. [28] is also shown. The results demonstrate that the presence of a pre-existing SiOx layer results in a lower level of passivation by ALD Al_2O_3.

It is worth noting that the level of passivation achieved in Figure 6.12 is state-of-the-art. At an excess carrier density of 1×10^{15} cm^{-3}, using Equation 6.1 with τ_{bulk} as the intrinsic limit from Richter et al. [28] gives S as 0.45 cm s^{-1}. Thus, although the HF(50%) chemical treatment appears not to give the optimal conditions initially, its effect is not relevant once a high quality dielectric has been deposited.

It is worth noting that most films deposited by ALD do exhibit a thin silicon dioxide layer sandwiched between the silicon substrate and thin film [64, 66, 173, 174], even when the dielectric being deposited does not use an oxygen containing precursor or co-reactant. An example of this can be seen in the Figure 6.14 which shows the existence of an approximately 1.5 nm thick SiO_2 film underneath a thin silicon nitride (Si_3N_4) layer by XPS.

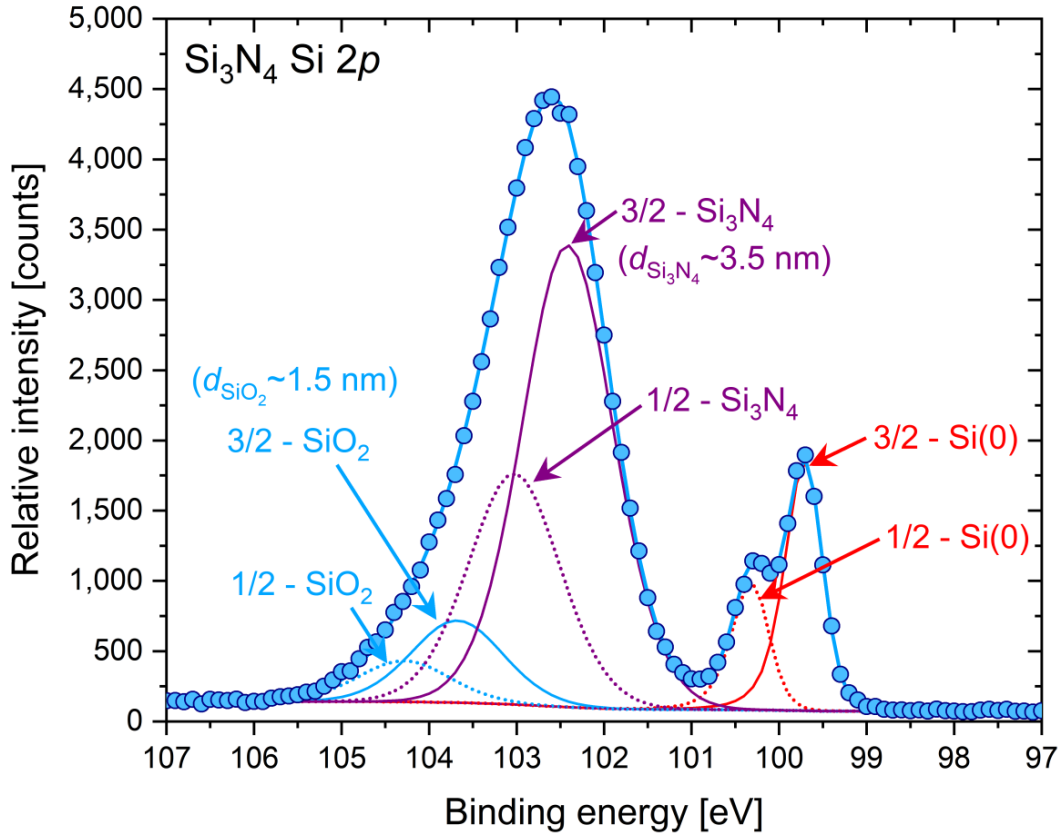

Figure 6.14 – Si 2p XPS spectra at take-off angle of 90° with respect to the surface parallel of an ALD Si_3N_4 coated silicon wafer. The solid and dashed lines are fits to the experimental data (blue circles).

Based on the results for ALD AlO_x surface passivation, it can be conclude that, despite the difference in surface termination by a HF(2%) : HCl(2%) and HF(50%) treatment, the growth of a thin silicon dioxide layer during the ALD deposition prohibits any variation of the electrical quality of the ALD film caused by the type of final dip treatment. However, other low temperature deposition techniques (e.g. plasma-enhanced chemical vapour deposition) may result in different behaviour.

6.4.2.1 Discussion - Additional passivation after chemical treatments

The application of two different surface passivation schemes after the different chemical surface treatments have been systematically studied, and substantial differences were found between the cases. For superacid-derived passivation, the passivation trends (Figure 6.1 (b)) follow those of the underlying surface treatment (Figure 6.1 (a)). For ALD-grown AlO_x passivation, the surface pre-treatment seems to be irrelevant after the passivation is applied. Figure 6.12 shows that excellent levels of passivation ($S < 0.5$ cm s^{-1}) can be achieved even with the poorest performing surface treatment.

The absence of a difference in ALD Al_2O_3 passivation when the surface is either fluorine or hydrogen terminated is an important finding of this study. As is usual for this passivation system [46], the ALD deposition was performed at low temperature (200 °C) and then perform a higher temperature (460 °C) ex situ anneal to “activate” the passivation. While it is possible that the surface termination affects the properties of the passivating film during the process (pre-hydrogenation affects the ALD growth [175], for example), the final outcome is that the passivation is independent of the initial surface treatment. Furthermore, ALD is an exceptionally good approach for coating silicon surface features at the nm scale [176], so any surface damage caused by the concentrated HF treatment seems to be equally well passivated as the undamaged surface. As ALD AlO_x passivation is widely used in silicon solar cell fabrication, the fact that the details of the HF treatment prior to passivation is relatively unimportant is convenient for cell manufacturers.

There could be a number of reasons why there is a difference in behaviour between superacid-derived passivation and ALD AlO_x passivation. The temperatures of the processes are very different, but this may not be the only factor. It is noted that Takahagi et al. studied room temperature oxidation of silicon pre-treated with HF(1%) and HF(50%) and found no difference in the growth rate [159], whereas in the room temperature superacid-derived process performed during these studies large difference were found in passivation behaviour with different surface treatments. In the ALD process the reactions with precursors could render the initial surface treatment irrelevant due to the formation of a thin silicon oxide layer.

6.5 Summary

A sensitive study was performed into whether surface treatments affect the passivation and subsequent functionalisation of (100)-orientation silicon wafers at the macroscopic scale. Treatment with HF(50%) leads to fluorine termination and a damaged surface, whereas treatment with HF(2%) : HCl(2%) leads to a damage-free surface which is likely to be hydrogen terminated. Differences in termination are relevant for some subsequent surface functionalisation processes, but not others. Importantly, whether the surface is hydrogen or fluorine terminated seems to be irrelevant from the perspective of achieving state-of-the-art surface passivation with ALD AlO_x, with surface recombination velocities of 0.45 cm s^{-1} achieved in both cases. It has been demonstrated, however, that the surface termination is of vital importance for other surface functionalisation using wet chemical treatments, such as when superacid-derived passivation is applied to the surface, with a weak aqueous solution of HF and HCl giving the best results.

Chapter 7 Conclusion

The work in this thesis focused on devising methods to improve the understanding and use of superacid-based passivation methods. Methods which could result in improved efficiency of Si solar cells through improved passivation techniques, and enable a better understanding of Si processing through providing a technique that is simple to perform in a lab setting. The aim was to gain extremely high quality passivation, that does not affect the bulk lifetime of the material under study due to the low temperatures used.

Chapter 4, introduced the results from tests on the solvent component of the treatment and went on to show the resulting passivation quality is heavily influenced by solvent choice and atmospheric conditions.

Chapter 5 followed this up by considering and testing different solutes used in the passivating solution and their effects on the treatment process and resulting passivation.

Finally, Chapter 6 aimed to understand the effects pre-treatments have on wet solution based treatments of silicon surfaces and the importance of these steps when trying to functionalise the bare Si surface.

The summary of these findings alongside other areas for further work are reviewed next.

7.1 Solvent Dependence of Superacid-derived Passivation

In Chapter 4 systematic study was performed into the surface passivation of *n*-type silicon samples treated with TFSI solutions made with various anhydrous solvents. All solutions investigated passivated the surface to some extent, and the passivation quality was not found to correlate with the relative polarity of the solvent. Excellent initial surface passivation was achieved with several solvents, including hexane, DCE, toluene and DCM. TFSI solutions made with DCE and toluene are however unstable as evidenced by colour changes, and, whilst DCM gives good results, the use of a chlorinated solvent is undesirable. TFSI-hexane gives better surface passivation than TFSI-DCE used previously and provides better passivation stability and

solution longevity. Hexane is also arguably safer than DCE, which is possibly carcinogenic, so it is concluded that TFSI-hexane is a better solution to use for superacid immersion passivation of silicon than TFSI-DCE used previously.

A series of investigations was performed into the TFSI-hexane passivation scheme. The stability of the passivation was strongly influenced by the storage humidity of the sample after passivation. The passivation was most stable when the samples are kept in a petri dish with the lid on. Further investigations are required to understand the composition of the passivating thin films on the silicon surface. TFSI-hexane passivated was applied to a set of FZ silicon wafers cut with different thicknesses from the same ingot. This enabled the extraction of the bulk lifetime and surface recombination velocity. The best case effective surface recombination velocity was 0.69 ± 0.04 cm s^{-1}. A series of five tests was performed on the same sample set, demonstrating the reproducibility of the scheme.

In summary, a superacid immersion treatment has been developed which consistently provides a very low surface recombination velocity with minimal test-to-test variation. This is an important step towards giving researchers the ability accurately to determine the bulk lifetime with good reliability and to ascertain the surface passivation quality of their desired passivation schemes, especially as cell efficiencies become more sensitive to surface and bulk recombination effects.

7.2 Evolution of Bis(trifluoromethanesulfonyl)-Based Passivating Solutions and their Effect on Surface Passivation

In Chapter 5 it was demonstrated that a range of solutions based on molecules with a bis(trifluoromethanesulfonyl)-based structure can give rise to excellent passivation of surfaces. While this includes the superacid TFSI, a high level of passivation also arises from solutions which are nonacidic, and so (super)acidity is not a prerequisite for the passivation. The surface passivation achieved has both a chemical and a field effect component. Chemical passivation arises at least partially from hydrogen termination of the surface. The solution treatment adds a field effect element being explainable by the existence of a negatively charged thin film physisorbed on the surface. This film is unstable in air and under vacuum, with the degradation

in air being less severe when small droplets of solution help stabilize the film. The finding that nonacidic solutions offer similar levels of passivation as super-acidic solutions means that these treatments could find future uses in materials systems sensitive to acidic environments, such as in perovskite solar cells.

7.3 Atomic Level Termination for Passivation and Functionalisation of Silicon Surfaces

In Chapter 6, the results of experiments to investigate the effects of surface termination of silicon at an atomic scale were reported. Injection-dependent carrier lifetime measurements on high lifetime float-zone silicon were used as a sensitive probe of the surface passivation arising from different chemical treatments. The terminated surfaces were then functionalised using a superacid-derived passivation process, and found that the different initial chemical treatments strongly affect the level of passivation subsequently achieved. By modelling the variation of carrier lifetime with excess carrier density, it was possible to separate contributions arising from chemical and field effect passivation. To understand the physical origins of the behaviour observed the treated surfaces were studied by X-ray photoelectron spectroscopy (XPS) and atomic force microscopy (AFM). Finally, it was demonstrated that the effects of the chemical treatments are not always apparent, and are lost entirely when AlO_x dielectric passivation is deposited on the treated surface by atomic layer deposition (ALD).

This study highlights that chemical pre-treatments can be extremely important in the creation of high quality functionalised surfaces. The removal of the native silicon dioxide layer is of crucial importance when performing wet chemical treatments to silicon surfaces. This can be achieved several different ways using both HF and NH_4F based solutions including NH_4F/HF mixtures, here it has been shown that it may be preferential to use a HF based solution including the use of HCl, removing the native silicon dioxide and hydrogen-terminating the surface in one step.

7.4 Future Work

While surface oxides have so far served as the main passivation route for solar PV, as devices get ever more complex there will be a greater interest on being able to tailor the interface properties. Molecular monolayers for passivation of silicon through functionalisation is a large area of research, but so far has mainly focused on the use of self-assembled monolayers (SAMs) on silicon for the creation of biosensor devices, and has not yet been significantly investigated for use as a passivating layer on silicon.

The formation of organic monolayers through the use of wet chemistry is an exciting avenue of research. Some of the current methods to assemble SAMs on silicon include the use of; organic radicals from decomposition of chemicals at elevated temperatures, halogenation of the surface followed by reaction with Grignard reagents, the use of ultraviolet light and the use of Lewis acids (like TFSI). Silicon wafers can be etched in hydrofluoric acid (HF) to remove the native oxide and form a hydrogen-terminated silicon surface. The hydrogen-terminated surfaces developed and used for pre-treatments in this thesis are known to be able to undergo hydrosilation with unsaturated compounds (such as terminal alkenes and alkynes), to form a stable monolayer on the surface. Following on from the work performed in this thesis, some research ideas to further this area of work are to investigate the possibility of assembling a SAM on the surface of silicon wafer but for the purposes of surface passivation.

Through the use of chemicals with molecules belonging to a wide class of terminally unsaturated organic molecules, but with the added key property, suggested by this research in Chapter 5, which are those containing a triflyl group or similar. Followed by either performing ultraviolet light activation or using Lewis acids to catalyse the surface reaction, it may then be possible to permanently passivate the surface of a silicon wafer using similar wet chemical processing techniques to those developed during this thesis. Two interesting chemicals of note for this process could be Ethenesulfonyl-fluoride and Hexafluoropropene, because of their similarity to chemicals that have been proven to passivate in this study whilst also containing unsaturated bonds suitable for undergoing substitution reactions.

Truly ordered functionalised Si surfaces have been shown to exhibit remarkable stability, by functionalising the silicon surfaces with molecules that provide chemical and field effect passivation like those used during this study. It may be possible to turn the currently temporary passivation scheme into something that is able to last for the 20+ years of operation under ambient conditions that todays devices are expected to withstand. This may additionally result in organic PV friendly passivation layers and such covalently bonded molecular layers on silicon may find novel uses in hybrids of inorganic and organic semiconductors such as multilayer hybrid solar cells.

A further valuable area of research would be to try and prolong the stability of the existing treatment proposed in this thesis, through the use of encapsulation techniques, similar to those used for other organic based passivation. Through the use of a capping layer for example, coating a treated sample with a liquid UV-Vis light curable resin immediately after passivation, by spin or dip coating, may protect the surface enough from the atmosphere for the passivating layer to remain stable. The main difficulty would be finding a chemical resin of a type that does not undergo a reaction with the prior surface treatment. Other areas of interest would be to investigate the use of the treatments, to add charge to existing oxides through immersion experiments.

To conclude wet chemical cleaning constitutes roughly 30% of all silicon processing and is performed on entire cassettes of wafers in standard cleanrooms. The possibility of making the surface passivation of silicon wafers simply an additional wet treatment step in the process, while achieving surface recombination levels that are competitive with the current leading silicon nitrides, could bring about large cost and time saving benefits. Due to these benefits, the transformation of these treatments into a permanent surface passivation is an extremely interesting area of future research.

References

1. A. I. Pointon, N. E. Grant, E. C. Wheeler-Jones, P. P. Altermatt, and J. D. Murphy, *Superacid-derived surface passivation for measurement of ultra-long lifetimes in silicon photovoltaic materials.* Solar Energy Materials and Solar Cells, 2018. **183**: p. 164-172.

2. A. I. Pointon, N. E. Grant, R. S. Bonilla, E. C. Wheeler-Jones, M. Walker, P. R. Wilshaw, C. E. J. Dancer, and J. D. Murphy, *Exceptional Surface Passivation Arising from Bis(trifluoromethanesulfonyl)-Based Solutions.* ACS Applied Electronic Materials, 2019. **1**(7): p. 1322-1329.

3. A. I. Pointon, N. E. Grant, S. L. Pain, J. T. White, and J. D. Murphy, *Sub-2 cm/s passivation of silicon surfaces by aprotic solutions.* Applied Physics Letters, 2020. **116**(12): p. 121601.

4. N. E. Grant, A. I. Pointon, R. Jefferies, D. Hiller, Y. Han, R. Beanland, M. Walker, and J. D. Murphy, *Atomic level termination for passivation and functionalisation of silicon surfaces.* Nanoscale, 2020. **12**(33): p. 17332-17341.

5. J. D. Murphy, A. I. Pointon, N. E. Grant, V. A. Shah, M. Myronov, V. V. Voronkov, and R. J. Falster, *Minority carrier lifetime in indium doped silicon for photovoltaics.* Progress in Photovoltaics: Research and Applications, 2019. **27**(10): p. 844-855.

6. M. Al-Amin, N. E. Grant, A. I. Pointon, and J. D. Murphy, *Iodine–Ethanol Surface Passivation for Measurement of Millisecond Carrier Lifetimes in Silicon Wafers with Different Crystallographic Orientations.* physica status solidi (a), 2019. **216**(17): p. 1900257.

7. N. E. Grant, J. R. Scowcroft, A. I. Pointon, M. Al-Amin, P. P. Altermatt, and J. D. Murphy, *Lifetime instabilities in gallium doped monocrystalline PERC silicon solar cells.* Solar Energy Materials and Solar Cells, 2020. **206**: p. 110299.

8. *Key World Energy Statistics*. 2021, International Energy Agency.

9. *Global Market Outlook for Solar Power 2022-2026*. 2022, European Photovoltaic Industry Association (EPIA): Belgium.

10. D. Chiras, R. Aram, and K. Nelson, *Power from the Sun: A Practical Guide to Solar Electricity*. 2009, Canada: New Society Publishers.

11. M. Bazilian, I. Onyeji, M. Liebreich, I. MacGill, J. Chase, J. Shah, D. Gielen, D. Arent, D. Landfear, and S. Zhengrong, *Re-considering the economics of photovoltaic power.* Renewable Energy, 2013. **53**: p. 329-338.

12. S. Reichelstein and M. Yorston, *The prospects for cost competitive solar PV power.* Energy Policy, 2013. **55**: p. 117-127.

13. *Technology Roadmap: Solar Photovoltaic Energy*. 2014, International Energy Agency.

14. S. Philipps and W. Warmuth, *Photovoltaics Report.* https://www.ise.fraunhofer.de/content/dam/ise/de/documents/publications/studies/Photovoltaics-Report.pdf, Updated 26th February 2018.

15. T. Saga, *Advances in crystalline silicon solar cell technology for industrial mass production.* NPG Asia Materials, 2010. **2**(3): p. 96-102.

16. C. Battaglia, A. Cuevas, and S. De Wolf, *High-efficiency crystalline silicon solar cells: status and perspectives.* Energy & Environmental Science, 2016. **9**(5): p. 1552-1576.

17. B. Min, M. Müller, H. Wagner, G. Fischer, R. Brendel, P. P. Altermatt, and H. Neuhaus, *A Roadmap Toward 24% Efficient PERC Solar Cells in Industrial Mass Production.* IEEE Journal of Photovoltaics, 2017. **7**(6): p. 1541-1550.

18. *International Technology Roadmap for Photovoltaic (ITRPV) - Ninth Edition.* September 2018.

19. R. S. Bonilla, B. Hoex, P. Hamer, and P. R. Wilshaw, *Dielectric surface passivation for silicon solar cells: A review.* physica status solidi (a), 2017. **214**(7): p. 1700293.

20. S. Rein, W. Warta, and S. W. Glunz. *Investigation of carrier lifetime in p-type Cz-silicon: specific limitations and realistic prediction of cell performance*. in *Conference Record of the Twenty-Eighth IEEE Photovoltaic Specialists Conference - 2000 (Cat. No.00CH37036)*. 2000.

21. J. Schmidt and A. Cuevas, *Electronic properties of light-induced recombination centers in boron-doped Czochralski silicon.* Journal of Applied Physics, 1999. **86**(6): p. 3175-3180.

22. M. J. Kerr, *Surface, Emitter and Bulk Recombination in Silicon and Development of Silicon Nitride Passivated Solar Cells*. 2002.

23. J. D. Murphy, K. Bothe, R. Krain, V. V. Voronkov, and R. J. Falster, *Parameterisation of injection-dependent lifetime measurements in semiconductors in terms of Shockley-Read-Hall statistics: An application to oxide precipitates in silicon.* Journal of Applied Physics, 2012. **111**(11): p. 113709.

24. P. T. Landsberg, *Recombination in semiconductors*. 1991: Cambridge University Press. 595.

25. H. Schlangenotto, H. Maeder, and W. Gerlach, *Temperature dependence of the radiative recombination coefficient in silicon.* physica status solidi (a), 1974. **21**(1): p. 357-367.

26. T. Trupke, M. A. Green, P. Würfel, P. P. Altermatt, A. Wang, J. Zhao, and R. Corkish, *Temperature dependence of the radiative recombination coefficient of intrinsic crystalline silicon.* Journal of Applied Physics, 2003. **94**(8): p. 4930-4937.

27. H. T. Nguyen, S. C. Baker-Finch, and D. Macdonald, *Temperature dependence of the radiative recombination coefficient in crystalline silicon from spectral photoluminescence.* Applied Physics Letters, 2014. **104**(11).

28. A. Richter, S. W. Glunz, F. Werner, J. Schmidt, and A. Cuevas, *Improved quantitative description of Auger recombination in crystalline silicon.* Physical Review B, 2012. **86**(16): p. 165202.

29. T. Niewelt, B. Steinhauser, A. Richter, B. Veith-Wolf, A. Fell, B. Hammann, N. E. Grant, L. Black, J. Tan, A. Youssef, J. D. Murphy, J. Schmidt, M. C. Schubert, and S. W. Glunz, *Reassessment of the intrinsic bulk recombination in crystalline silicon.* Solar Energy Materials and Solar Cells, 2022. **235**: p. 111467.

30. M. J. Kerr and A. Cuevas, *General parameterization of Auger recombination in crystalline silicon.* Journal of Applied Physics, 2002. **91**(4): p. 2473-2480.

31. E. Yablonovitch and T. Gmitter, *Auger recombination in silicon at low carrier densities.* Applied Physics Letters, 1986. **49**(10): p. 587-589.

32. W. Shockley and W. T. Read, *Statistics of the Recombinations of Holes and Electrons.* Physical Review, 1952. **87**(5): p. 835-842.

33. R. N. Hall, *Electron-Hole Recombination in Germanium.* Physical Review, 1952. **87**(2): p. 387-387.

34. I. Pelant and J. Valenta, *Luminescence Spectroscopy of Semiconductors*. 2012: Oxford University Press.

35. V. P. Markevich, A. R. Peaker, B. Hamilton, S. B. Lastovskii, and L. I. Murin, *Donor levels of the divacancy-oxygen defect in silicon.* Journal of Applied Physics, 2014. **115**(1): p. 012004.

36. M. J. Kerr, *Surface, Emitter and Bulk Recombination in Silicon and Development of Silicon Nitride Passivated Solar Cells - PhD Thesis*. 2002, The Australian National University: Australia.

37. S. Rein, *Lifetime spectroscopy: a method of defect characterization in silicon for photovoltaic applications*. Vol. 85. 2005, New York: Springer Series in Materials Science.

38. D. K. Schroder, *Semiconductor Material and Device Characterization*. 3rd ed. 2006: John Wiley and Sons.

39. R. A. Sinton, A. Cuevas, and M. Stuckings. *Quasi-steady-state photoconductance, a new method for solar cell material and device characterization*. in *Conference Record of the Twenty Fifth IEEE Photovoltaic Specialists Conference - 1996*. 1996.

40. R. A. Sinton and A. Cuevas, *Contactless determination of current–voltage characteristics and minority-carrier lifetimes in semiconductors from quasi-steady-state photoconductance data.* Applied Physics Letters, 1996. **69**(17): p. 2510-2512.

41. R. A. Sinton, A. Cuevas, and M. Stuckings. *Quasi-steady-state photoconductance, a new method for solar cell material and device characterization*. in *Photovoltaic Specialists Conference, 1996., Conference Record of the Twenty Fifth IEEE*. 1996.

42. H. Nagel, C. Berge, and A. G. Aberle, *Generalized analysis of quasi-steady-state and quasi-transient measurements of carrier lifetimes in semiconductors.* Journal of Applied Physics, 1999. **86**(11): p. 6218-6221.

43. J. Brody and A. Rohatgi, *Analytical approximation of effective surface recombination velocity of dielectric-passivated p-type silicon.* Solid-State Electronics, 2001. **45**(9): p. 1549-1557.

44. K. L. Luke and L. J. Cheng, *Analysis of the interaction of a laser pulse with a silicon wafer: Determination of bulk lifetime and surface recombination velocity.* Journal of Applied Physics, 1987. **61**(6): p. 2282-2293.

45. A. B. Sproul, *Dimensionless solution of the equation describing the effect of surface recombination on carrier decay in semiconductors.* Journal of Applied Physics, 1994. **76**(5): p. 2851-2854.

46. G. Dingemans and W. M. M. Kessels, *Status and prospects of Al2O3-based surface passivation schemes for silicon solar cells.* Journal of Vacuum Science & Technology A: Vacuum, Surfaces, and Films, 2012. **30**(4): p. 040802.

47. S. Rein, *Lifetime Spectroscopy vol. 85*. 2005: Springer Series in Material Science.

48. B. E. Deal, *The Current Understanding of Charges in the Thermally Oxidized Silicon Structure.* Journal of The Electrochemical Society, 1974. **121**(6): p. 198C-205C.

49. O. Schultz, A. Mette, M. Hermle, and S. W. Glunz, *Thermal oxidation for crystalline silicon solar cells exceeding 19% efficiency applying industrially feasible process technology.* Progress in Photovoltaics: Research and Applications, 2008. **16**(4): p. 317-324.

50. J. D. Murphy, R. E. McGuire, K. Bothe, V. V. Voronkov, and R. J. Falster, *Minority carrier lifetime in silicon photovoltaics: The effect of oxygen precipitation.* Solar Energy Materials and Solar Cells, 2014. **120**(Part A): p. 402-411.

51. J. Haunschild, I. E. Reis, J. Geilker, and S. Rein, *Detecting efficiency-limiting defects in Czochralski-grown silicon wafers in solar cell production using photoluminescence imaging.* physica status solidi (RRL) – Rapid Research Letters, 2011. **5**(5-6): p. 199-201.

52. B. E. Deal, M. Sklar, A. S. Grove, and E. H. Snow, *Characteristics of the Surface-State Charge (Qss) of Thermally Oxidized Silicon.* Journal of The Electrochemical Society, 1967. **114**(3): p. 266-274.

53. M. J. Kerr and A. Cuevas, *Very low bulk and surface recombination in oxidized silicon wafers.* Semiconductor Science and Technology, 2002. **17**(1): p. 35.

54. R. Singh, *Rapid isothermal processing.* Journal of Applied Physics, 1988. **63**(8): p. R59-R114.

55. L. L. Alt, S. W. Ing, and K. W. Laendle, *Low-Temperature Deposition of Silicon Oxide Films.* Journal of The Electrochemical Society, 1963. **110**(5): p. 465.

56. C. E. Chryssou and C. W. Pitt, *Al2O3 thin films by plasma-enhanced chemical vapour deposition using trimethyl-amine alane (TMAA) as the Al precursor.* Applied Physics A, 1997. **65**(4): p. 469-475.

57. T. Lauinger, J. Moschner, A. G. Aberle, and R. Hezel, *Optimization and characterization of remote plasma-enhanced chemical vapor deposition silicon nitride for the passivation of p-type crystalline silicon surfaces.* Journal of Vacuum Science & Technology A: Vacuum, Surfaces, and Films, 1998. **16**(2): p. 530-543.

58. T. Lauinger, J. Schmidt, A. G. Aberle, and R. Hezel, *Record low surface recombination velocities on 1 Ωcm p-silicon using remote plasma silicon nitride passivation.* Applied Physics Letters, 1996. **68**(9): p. 1232-1234.

59. A. G. Aberle, *Surface passivation of crystalline silicon solar cells: a review.* Progress in Photovoltaics: Research and Applications, 2000. **8**(5): p. 473-487.

60. J. K. Mark and C. Andres, *Recombination at the interface between silicon and stoichiometric plasma silicon nitride.* Semiconductor Science and Technology, 2002. **17**(2): p. 166.

61. A. G. Aberle, *Overview on SiN surface passivation of crystalline silicon solar cells.* Solar Energy Materials and Solar Cells, 2001. **65**(1): p. 239-248.

62. Y. Wan, K. R. McIntosh, A. F. Thomson, and A. Cuevas, *Low Surface Recombination Velocity by Low-Absorption Silicon Nitride on c-Si.* IEEE Journal of Photovoltaics, 2013. **3**(1): p. 554-559.

63. Y. Wan, K. R. McIntosh, and A. F. Thomson, *Characterisation and optimisation of PECVD SiNx as an antireflection coating and passivation layer for silicon solar cells.* AIP Advances, 2013. **3**(3): p. 032113.

64. B. Hoex, S. B. S. Heil, E. Langereis, M. C. M. v. d. Sanden, and W. M. M. Kessels, *Ultralow surface recombination of c-Si substrates passivated by plasma-assisted atomic layer deposited Al2O3.* Applied Physics Letters, 2006. **89**(4): p. 042112.

65. G. Agostinelli, A. Delabie, P. Vitanov, Z. Alexieva, H. F. W. Dekkers, S. De Wolf, and G. Beaucarne, *Very low surface recombination velocities on p-type silicon wafers passivated with a dielectric with fixed negative charge.* Solar Energy Materials and Solar Cells, 2006. **90**(18): p. 3438-3443.

66. B. Hoex, J. Schmidt, P. Pohl, M. C. M. v. d. Sanden, and W. M. M. Kessels, *Silicon surface passivation by atomic layer deposited Al2O3.* Journal of Applied Physics, 2008. **104**(4): p. 044903.

67. N. E. Grant and J. D. Murphy, *Temporary Surface Passivation for Characterisation of Bulk Defects in Silicon: A Review.* physica status solidi (RRL) – Rapid Research Letters, 2017. **11**(11): p. 1700243.

68. E. Yablonovitch, D. Allara, C. C. Chang, T. Gmitter, and T. B. Bright, *Unusually Low Surface-Recombination Velocity on Silicon and Germanium Surfaces*. Vol. 57. 1986. 249-252.

69. G. W. Trucks, K. Raghavachari, G. S. Higashi, and Y. J. Chabal, *Mechanism of HF etching of silicon surfaces: A theoretical understanding of hydrogen passivation.* Physical Review Letters, 1990. **65**(4): p. 504-507.

70. T. Takahagi, I. Nagai, A. Ishitani, H. Kuroda, and Y. Nagasawa, *The formation of hydrogen passivated silicon single-crystal surfaces using ultraviolet cleaning and HF etching.* Journal of Applied Physics, 1988. **64**(7): p. 3516-3521.

71. N. E. Grant, K. R. McIntosh, and J. T. Tan, *Evaluation of the Bulk Lifetime of Silicon Wafers by Immersion in Hydrofluoric Acid and Illumination.* ECS Journal of Solid State Science and Technology, 2012. **1**(2): p. P55-P61.

72. T. S. Horányi, T. Pavelka, and P. Tüttö, *In situ bulk lifetime measurement on silicon with a chemically passivated surface.* Applied Surface Science, 1993. **63**(1): p. 306-311.

73. M. Takao and S. Yasushi, *Effect of Steady Bias Light on Carrier Lifetime in Silicon Wafers with Chemically Passivated Surfaces.* Japanese Journal of Applied Physics, 1996. **35**(2A): p. L133.

74. H. M'saad, J. Michel, J. J. Lappe, and L. C. Kimerling, *Electronic passivation of silicon surfaces by halogens.* Journal of Electronic Materials, 1994. **23**(5): p. 487-491.

75. N. Batra, Vandana, S. Kumar, M. Sharma, S. K. Srivastava, P. Sharma, and P. K. Singh, *A comparative study of silicon surface passivation using ethanolic iodine and bromine solutions.* Solar Energy Materials and Solar Cells, 2012. **100**(Supplement C): p. 43-47.

76. N. A. Kotulak, M. Chen, N. Schreiber, K. Jones, and R. L. Opila, *Examining the free radical bonding mechanism of benzoquinone– and hydroquinone–methanol passivation of silicon surfaces.* Applied Surface Science, 2015. **354**: p. 469-474.

77. B. Chhabra, S. Bowden, R. L. Opila, and C. B. Honsberg, *High effective minority carrier lifetime on silicon substrates using quinhydrone-methanol passivation.* Applied Physics Letters, 2010. **96**(6): p. 063502.

78. T. Hidetaka, S. Isao, and S. Ryuichi, *Quinhydrone/Methanol Treatment for the Measurement of Carrier Lifetime in Silicon Substrates.* Japanese Journal of Applied Physics, 2002. **41**(8A): p. L870.

79. T. Hidetaka, S. Isao, and S. Ryuichi, *Surface Passivation Effect of Silicon Substrates due to Quinhydrone/Ethanol Treatment.* Japanese Journal of Applied Physics, 2001. **40**(10A): p. L1003.

80. R. Lago-Aurrekoetxea, I. Tobías, C. del Cañizo, and A. Luque *Lifetime Measurements by Photoconductance Techniques in Wafers Immersed in a Passivating Liquid.* Journal of The Electrochemical Society, 2001. **148**(4): p. G200-G206.

81. J. Schmidt and A. G. Aberle, *Easy-to-use surface passivation technique for bulk carrier lifetime measurements on silicon wafers.* Progress in Photovoltaics: Research and Applications, 1998. **6**(4): p. 259-263.

82. J. Chen, Y. Shen, J. Guo, B. Chen, J. Fan, F. Li, H. Liu, Y. Xu, and Y. Mai, *Silicon surface passivation by polystyrenesulfonate thin films.* Applied Physics Letters, 2017. **110**(8): p. 083904.

83. Y. Xia, K. Sun, and J. Ouyang, *Solution-Processed Metallic Conducting Polymer Films as Transparent Electrode of Optoelectronic Devices.* Advanced Materials, 2012. **24**(18): p. 2436-2440.

84. J. Schmidt, V. Titova, and D. Zielke, *Organic-silicon heterojunction solar cells: Open-circuit voltage potential and stability.* Applied Physics Letters, 2013. **103**(18): p. 183901.

85. D. Zielke, C. Niehaves, W. Lövenich, A. Elschner, M. Hörteis, and J. Schmidt, *Organic-silicon Solar Cells Exceeding 20% Efficiency.* Energy Procedia, 2015. **77**: p. 331-339.

86. T. Mueller, S. Schwertheim, M. Scherff, and W. R. Fahrner, *High quality passivation for heterojunction solar cells by hydrogenated amorphous silicon suboxide films.* Applied Physics Letters, 2008. **92**(3).

87. J. Cui, Y. Wan, Y. Cui, Y. Chen, P. Verlinden, and A. Cuevas, *Highly effective electronic passivation of silicon surfaces by atomic layer deposited hafnium oxide.* Applied Physics Letters, 2017. **110**(2).

88. C. T. Nguyen, K. Ohdaira, and H. Matsumura, *Control of solution wettability on fine-textured crystalline silicon surface to obtain high-quality passivation for solar cells.* Applied Physics Letters, 2019. **114**(13).

89. N. E. Grant, V. P. Markevich, J. Mullins, A. R. Peaker, F. Rougieux, D. Macdonald, and J. D. Murphy, *Permanent annihilation of thermally activated defects which limit the lifetime of float-zone silicon.* physica status solidi (a), 2016. **213**(11): p. 2844-2849.

90. B. Chhabra, S. Suzer, R. L. Opila, and C. B. Honsberg. *Electrical and chemical characterization of chemically passivated silicon surfaces*. in *2008 33rd IEEE Photovoltaic Specialists Conference*. 2008.

91. M. Ju, Y.-j. Lee, K. Lee, C. Han, Y. Jo, and J. Yi, *Effectiveness of Iodine Termination for Ultrahigh Efficiency Solar Cells as a Means of Chemical Surface Passivation.* Japanese Journal of Applied Physics, 2012. **51**(9S2): p. 09MA03.

92. J. W. Chen, L. Zhao, H. W. Diao, B. J. Yan, S. Zhou, Y. H. Tang, and W. J. Wang, *Surface Passivation of Silicon Wafers by Iodine-Ethanol (I-E) for Minority Carrier Lifetime Measurements.* Advanced Materials Research, 2013. **652-654**: p. 901-905.

93. R. L. Opila, D. Yang, N. Kotulak, L. Costello, and B. Chhabra. *Mechanism of electrical passivation of Si surfaces with quinhydrone*. in *2012 38th IEEE Photovoltaic Specialists Conference*. 2012.

94. M. Chen, J. H. Hack, A. Iyer, K. J. Jones, and R. L. Opila, *Radical-Driven Silicon Surface Passivation by Benzoquinone– and Hydroquinone–Methanol and Photoinitiators.* The Journal of Physical Chemistry C, 2017. **121**(39): p. 21364-21373.

95. J. Chen, Y. Shen, J. Guo, B. Chen, J. Fan, F. Li, H. Liu, Y. Xu, and Y. Mai, *Silicon surface passivation by polystyrenesulfonate thin films.* Applied Physics Letters, 2017. **110**(8).

96. M. Amani, D.-H. Lien, D. Kiriya, J. Xiao, A. Azcatl, J. Noh, S. R. Madhvapathy, R. Addou, S. Kc, M. Dubey, K. Cho, R. M. Wallace, S.-C. Lee, J.-H. He, J. W. Ager, X. Zhang, E. Yablonovitch, and A. Javey, *Near-unity photoluminescence quantum yield in MoS2.* Science, 2015. **350**(6264): p. 1065.

97. D. Himmel, S. K. Goll, I. Leito, and I. Krossing, *A Unified pH Scale for All Phases.* Angewandte Chemie International Edition, 2010. **49**(38): p. 6885-6888.

98. M. Amani, P. Taheri, R. Addou, G. H. Ahn, D. Kiriya, D.-H. Lien, J. W. Ager, R. M. Wallace, and A. Javey, *Recombination Kinetics and Effects of Superacid Treatment in Sulfur- and Selenium-Based Transition Metal Dichalcogenides.* Nano Letters, 2016. **16**(4): p. 2786-2791.

99. Y. A. Alemu, G. H. Albuquerque, and G. S. Herman, *Enhanced photoluminescence from CuInS2/ZnS quantum dots: Organic superacid passivation.* Materials Letters, 2018. **219**: p. 178-181.

100. H. Kim, D.-H. Lien, M. Amani, J. W. Ager, and A. Javey, *Highly Stable Near-Unity Photoluminescence Yield in Monolayer MoS2 by Fluoropolymer Encapsulation and Superacid Treatment.* ACS Nano, 2017. **11**(5): p. 5179-5185.

101. J. Bullock, D. Kiriya, N. Grant, A. Azcatl, M. Hettick, T. Kho, P. Phang, H. C. Sio, D. Yan, D. Macdonald, M. A. Quevedo-Lopez, R. M. Wallace, A. Cuevas, and A. Javey, *Superacid Passivation of Crystalline Silicon Surfaces.* ACS Applied Materials & Interfaces, 2016. **8**(36): p. 24205-24211.

102. *1,2 Dichloroethane - IARC Monographs on the Evaluation of Carcinogenic Risks to Humans*. Vol. 71. 1999, Lyon, France.

103. N. E. Grant, T. Niewelt, N. R. Wilson, E. C. Wheeler-Jones, J. Bullock, M. Al-Amin, M. C. Schubert, A. C. v. Veen, A. Javey, and J. D. Murphy, *Superacid-Treated Silicon Surfaces: Extending the Limit of Carrier Lifetime for Photovoltaic Applications.* IEEE Journal of Photovoltaics, 2017. **7**(6): p. 1574-1583.

104. T. Trupke, R. A. Bardos, F. Hudert, P. Wurfel, J. Zhao, A. Wang, and M. A. Green. *Effective Excess Carrier Lifetimes Exceeding 100 Milliseconds in Float Zone Silicon Determined from Photoluminescence*. in *European photovoltaic solar energy conference, pp. 758–761*. 2004.

105. T. C. Kho, K. Fong, K. McIntosh, E. Franklin, N. Grant, M. Stocks, S. P. Phang, Y. Wan, E.-C. Wang, K. Vora, Z. Ngwe, and A. Blakers, *Exceptional silicon surface passivation by an ONO dielectric stack.* Solar Energy Materials and Solar Cells, 2019. **189**: p. 245-253.

106. R. S. Bonilla, C. Reichel, M. Hermle, P. Hamer, and P. R. Wilshaw, *Long term stability of c-Si surface passivation using corona charged SiO2.* Applied Surface Science, 2017. **412**: p. 657-667.

107. R. S. Bonilla, N. Jennison, D. Clayton-Warwick, K. A. Collett, L. Rands, and P. R. Wilshaw, *Corona Charge in SiO2: Kinetics and Surface Passivation for High Efficiency Silicon Solar Cells.* Energy Procedia, 2016. **92**: p. 326-335.

108. A. Alharbi, P. Zahl, and D. Shahrjerdi, *Material and device properties of superacid-treated monolayer molybdenum disulfide.* Applied Physics Letters, 2017. **110**(3): p. 033503.

109. W. Zhao and J. Sun, *Triflimide (HNTf2) in Organic Synthesis.* Chemical Reviews, 2018. **118**(20): p. 10349-10392.

110. W. Kern, *The Evolution of Silicon Wafer Cleaning Technology.* Journal of The Electrochemical Society, 1990. **137**(6): p. 1887-1892.

111. M. Kessler, T. Ohrdes, P. P. Altermatt, and R. Brendel, *The effect of sample edge recombination on the averaged injection-dependent carrier lifetime in silicon.* Journal of Applied Physics, 2012. **111**(5): p. 054508.

112. L. E. Black and D. H. Macdonald, *Accounting for the Dependence of Coil Sensitivity on Sample Thickness and Lift-Off in Inductively Coupled Photoconductance Measurements.* IEEE Journal of Photovoltaics, 2019. **9**(6): p. 1563-1574.

113. A. L. Blum, J. S. Swirhun, R. A. Sinton, F. Yan, S. Herasimenka, T. Roth, K. Lauer, J. Haunschild, B. Lim, K. Bothe, Z. Hameiri, B. Seipel, R. Xiong, M. Dhamrin, and J. D. Murphy, *Interlaboratory Study of Eddy-Current Measurement of Excess-Carrier Recombination Lifetime.* IEEE Journal of Photovoltaics, 2014. **4**(1): p. 525-531.

114. T. Trupke, R. A. Bardos, M. C. Schubert, and W. Warta, *Photoluminescence imaging of silicon wafers.* Applied Physics Letters, 2006. **89**(4): p. 044107.

115. T. Trupke, B. Mitchell, J. W. Weber, W. McMillan, R. A. Bardos, and R. Kroeze, *Photoluminescence Imaging for Photovoltaic Applications.* Energy Procedia, 2012. **15**: p. 135-146.

116. L. Kelvin, *V. Contact electricity of metals.* Philosophical Magazine Series 1, 1898. **46**: p. 82-120.

117. D. K. Schroder, *Semiconductor Material and Device Characterization: 3rd Ed*. 2006: John Wiley and Sons.

118. C. Reichardt and T. Welton, *Solvent and Solvent Effects in Organic Chemistry*. 4th ed. 2011: Wiley-VCH.

119. C. Reichardt and T. Welton, *Solvents and Solvent Effects in Organic Chemistry, Fourth Edition*. 2010: Wiley-VCH.

120. B. Veith, T. Ohrdes, F. Werner, R. Brendel, P. P. Altermatt, N.-P. Harder, and J. Schmidt, *Injection dependence of the effective lifetime of n-type Si passivated by Al2O3: An edge effect?* Solar Energy Materials and Solar Cells, 2014. **120**: p. 436-440.

121. G. S. Salvapati, K. V. Ramanamurty, and M. Janardanarao, *Selective catalytic self-condensation of acetone.* Journal of Molecular Catalysis, 1989. **54**(1): p. 9-30.

122. T. Boudewijns, M. Piccinini, P. Degraeve, A. Liebens, and D. De Vos, *Pathway to Vinyl Chloride Production via Dehydrochlorination of 1,2-Dichloroethane in Ionic Liquid Media.* ACS Catalysis, 2015. **5**(7): p. 4043-4047.

123. B.-Q. Xu, D. Sood, A. V. Iretskii, and M. G. White, *Direct Synthesis of Dimethylbiphenyls by Toluene Coupling in the Presence of Palladium Triflate and Triflic Acid.* Journal of Catalysis, 1999. **187**(2): p. 358-366.

124. S. C. Sherman, A. V. Iretskii, M. G. White, C. Gumienny, L. M. Tolbert, and D. A. Schiraldi, *Isomerization of Substituted Biphenyls by Superacid. A Remarkable Confluence of Experiment and Theory.* The Journal of Organic Chemistry, 2002. **67**(7): p. 2034-2041.

125. J. R. Johnson, S. D. Christian, and H. E. Affsprung, *The molecular complexity of water in organic solvents. Part II.* Journal of the Chemical Society A: Inorganic, Physical, Theoretical, 1966(0): p. 77-78.

126. J. W. Roddy and C. F. Coleman, *Solubility of water in hydrocarbons as a function of water activity.* Talanta, 1968. **15**(11): p. 1281-1286.

127. J. Albohn, W. Füssel, N. D. Sinh, K. Kliefoth, and W. Fuhs, *Capture cross sections of defect states at the Si/SiO2 interface.* Journal of Applied Physics, 2000. **88**(2): p. 842-849.

128. L. E. Black, T. Allen, K. R. McIntosh, and A. Cuevas, *Effect of boron concentration on recombination at the p-Si–Al2O3 interface.* Journal of Applied Physics, 2014. **115**(9): p. 093707.

129. D. Schuldis, A. Richter, J. Benick, P. Saint-Cast, M. Hermle, and S. W. Glunz, *Properties of the c-Si/Al2O3 interface of ultrathin atomic layer deposited Al2O3 layers capped by SiNx for c-Si surface passivation.* Applied Physics Letters, 2014. **105**(23): p. 231601.

130. C.-J. Yu, U.-S. Ri, G.-C. Ri, and J.-S. Kim, *Revealing the formation and electrochemical properties of bis(trifluoromethanesulfonyl)imide intercalated graphite with first-principles calculations.* Physical Chemistry Chemical Physics, 2018. **20**(20): p. 14124-14132.

131. T. Rahman, A. To, M. E. Pollard, N. E. Grant, J. Colwell, D. N. R. Payne, J. D. Murphy, D. M. Bagnall, B. Hoex, and S. A. Boden, *Minimising bulk lifetime degradation during the processing of interdigitated back contact silicon solar cells.* Progress in Photovoltaics: Research and Applications, 2018. **26**(1): p. 38-47.

132. T. Niewelt, M. Selinger, N. E. Grant, W. Kwapil, J. D. Murphy, and M. C. Schubert, *Light-induced activation and deactivation of bulk defects in boron-doped float-zone silicon.* Journal of Applied Physics, 2017. **121**(18): p. 185702.

133. D. Sperber, A. Graf, D. Skorka, A. Herguth, and G. Hahn, *Degradation of Surface Passivation on Crystalline Silicon and Its Impact on Light-Induced Degradation Experiments.* IEEE Journal of Photovoltaics, 2017. **7**(6): p. 1627-1634.

134. P. P. Altermatt, F. Geelhaar, T. Trupke, X. Dai, A. Neisser, and E. Daub, *Injection dependence of spontaneous radiative recombination in crystalline silicon: Experimental verification and theoretical analysis.* Applied Physics Letters, 2006. **88**(26): p. 261901.

135. S. Steingrube, P. P. Altermatt, D. S. Steingrube, J. Schmidt, and R. Brendel, *Interpretation of recombination at c-Si/SiNx interfaces by surface damage.* Journal of Applied Physics, 2010. **108**(1): p. 014506.

136. D. Kiriya, Y. Hijikata, J. Pirillo, R. Kitaura, A. Murai, A. Ashida, T. Yoshimura, and N. Fujimura, *Systematic Study of Photoluminescence Enhancement in Monolayer Molybdenum Disulfide by Acid Treatment.* Langmuir, 2018. **34**(35): p. 10243-10249.

137. Y. Yu, G. Li, L. Huang, A. Barrette, Y.-Q. Cai, Y. Yu, K. Gundogdu, Y.-W. Zhang, and L. Cao, *Enhancing Multifunctionalities of Transition-Metal Dichalcogenide Monolayers via Cation Intercalation.* ACS Nano, 2017. **11**(9): p. 9390-9396.

138. S. N. Suarez, J. R. P. Jayakody, S. G. Greenbaum, T. Zawodzinski, and J. J. Fontanella, *A Fundamental Study of the Transport Properties of Aqueous Superacid Solutions.* The Journal of Physical Chemistry B, 2010. **114**(27): p. 8941-8947.

139. W. R. Dolbier, *Guide to Fluorine NMR for Organic Chemists, Second Edition*. 2016: Wiley.

140. J. Foropoulos and D. D. DesMarteau, *Synthesis, properties, and reactions of bis((trifluoromethyl)sulfonyl) imide, (CF3SO2)2NH.* Inorganic Chemistry, 1984. **23**(23): p. 3720-3723.

141. D. M. Piper, T. Evans, K. Leung, T. Watkins, J. Olson, S. C. Kim, S. S. Han, V. Bhat, K. H. Oh, D. A. Buttry, and S.-H. Lee, *Stable silicon-ionic liquid interface for next-generation lithium-ion batteries.* Nature Communications, 2015. **6**: p. 6230.

142. E. Markevich, R. Sharabi, V. Borgel, H. Gottlieb, G. Salitra, D. Aurbach, G. Semrau, and M. A. Schmidt, *In situ FTIR study of the decomposition of N-butyl-N-methylpyrrolidinium bis(trifluoromethanesulfonyl)amide ionic liquid during cathodic polarization of lithium and graphite electrodes.* Electrochimica Acta, 2010. **55**(8): p. 2687-2696.

143. W. Ji, Y. Zhao, H. M. Fahad, J. Bullock, T. Allen, D.-H. Lien, S. De Wolf, and A. Javey, *Dip Coating Passivation of Crystalline Silicon by Lewis Acids.* ACS Nano, 2019. **13**(3): p. 3723-3729.

144. V. A. Burrows, Y. J. Chabal, G. S. Higashi, K. Raghavachari, and S. B. Christman, *Infrared spectroscopy of Si(111) surfaces after HF treatment: Hydrogen termination and surface morphology.* Applied Physics Letters, 1988. **53**(11): p. 998-1000.

145. D. B. Fenner, D. K. Biegelsen, and R. D. Bringans, *Silicon surface passivation by hydrogen termination: A comparative study of preparation methods.* Journal of Applied Physics, 1989. **66**(1): p. 419-424.

146. S. Mizushima, T. Shimanouchi, I. Harada, Y. Abe, and H. Takeuchi, *Infrared and Raman Spectra of 1,2-Dichloroethane and its Deuterium Compound in the Gaseous, Liquid, and Solid States.* Canadian Journal of Physics, 1975. **53**(19): p. 2085-2094.

147. I. Rey, P. Johansson, J. Lindgren, J. C. Lassègues, J. Grondin, and L. Servant, *Spectroscopic and Theoretical Study of (CF3SO2)2N- (TFSI-) and (CF3SO2)2NH (HTFSI).* The Journal of Physical Chemistry A, 1998. **102**(19): p. 3249-3258.

148. L. J. Hardwick, M. Holzapfel, A. Wokaun, and P. Novák, *Raman study of lithium coordination in EMI-TFSI additive systems as lithium-ion battery ionic liquid electrolytes.* Journal of Raman Spectroscopy, 2007. **38**(1): p. 110-112.

149. J. Wang, H. Tu, W. Zhu, Q. Zhou, A. Liu, and C. Zhang, *A comparative Raman spectroscopy study on silicon surface in HF, HF/H2O2 and HF/NH4F aqueous solutions.* Materials Science and Engineering: B, 2000. **72**(2): p. 193-196.

150. B. Ren, F. M. Liu, J. Xie, B. W. Mao, Y. B. Zu, and Z. Q. Tian, *In situ monitoring of Raman scattering and photoluminescence from silicon surfaces in HF aqueous solutions.* Applied Physics Letters, 1998. **72**(8): p. 933-935.

151. P. Vandenabeele. Practical Raman Spectroscopy - An Introduction. 2013: Wiley.

152. B. M. Liszka, A. T. M. Lenferink, G.-J. Witkamp, and C. Otto, *Raman micro-spectroscopy for quantitative thickness measurement of nanometer thin polymer films.* Journal of Raman Spectroscopy, 2015. **46**(12): p. 1230-1234.

153. M. Abdi-Jalebi, Z. Andaji-Garmaroudi, S. Cacovich, C. Stavrakas, B. Philippe, J. M. Richter, M. Alsari, E. P. Booker, E. M. Hutter, A. J. Pearson, S. Lilliu, T. J. Savenije, H. Rensmo, G. Divitini, C. Ducati, R. H. Friend, and S. D. Stranks, *Maximizing and stabilizing luminescence from halide perovskites with potassium passivation.* Nature, 2018. **555**(7697): p. 497-501.

154. H. F. Okorn-Schmidt, *Characterization of silicon surface preparation processes for advanced gate dielectrics.* IBM Journal of Research and Development, 1999. **43**(3): p. 351-326.

155. Z. Lin, T. Strother, W. Cai, X. Cao, L. M. Smith, and R. J. Hamers, *DNA Attachment and Hybridization at the Silicon (100) Surface.* Langmuir, 2002. **18**(3): p. 788-796.

156. J. Veerbeek and J. Huskens, *Applications of Monolayer-Functionalized H-Terminated Silicon Surfaces: A Review.* Small Methods, 2017. **1**(4): p. 1700072.

157. K. Oura, V. G. Lifshits, A. A. Saranin, A. V. Zotov, and M. Katayama, *Hydrogen interaction with clean and modified silicon surfaces.* Surface Science Reports, 1999. **35**(1): p. 1-69.

158. J. M. Buriak, *Organometallic Chemistry on Silicon and Germanium Surfaces.* Chemical Reviews, 2002. **102**(5): p. 1271-1308.

159. T. Takahagi, A. Ishitani, H. Kuroda, and Y. Nagasawa, *Fluorine-containing species on the hydrofluoric acid etched silicon single-crystal surface.* Journal of Applied Physics, 1991. **69**(2): p. 803-807.

160. B. R. Weinberger, G. G. Peterson, T. C. Eschrich, and H. A. Krasinski, *Surface chemistry of HF passivated silicon: X-ray photoelectron and ion scattering spectroscopy results.* Journal of Applied Physics, 1986. **60**(9): p. 3232-3234.

161. V. Bertagna, R. Erre, F. Rouelle, and M. Chemla, *Ionic components dependence of the charge transfer reactions at the silicon/HF solution interface.* Journal of Solid State Electrochemistry, 1999. **4**(1): p. 42-51.

162. L. Li, H. Bender, T. Trenkler, P. W. Mertens, M. Meuris, W. Vandervorst, and M. M. Heyns, *Surface passivation and microroughness of (100) silicon etched in aqueous hydrogen halide (HF, HCl, HBr, HI) solutions.* Journal of Applied Physics, 1995. **77**(3): p. 1323-1325.

163. X. G. Zhang, *Electrochemistry of Silicon and Its Oxide*. 2001: Springer.

164. Calculator Map from PV Lighthouse http://www.pvlighthouse.com.au

165. R. B. M. Girisch, R. P. Mertens, and R. F. D. Keersmaecker, *Determination of Si-SiO/sub 2/ interface recombination parameters using a gate-controlled point-junction diode under illumination.* IEEE Transactions on Electron Devices, 1988. **35**(2): p. 203-222.

166. A. G. Aberle, S. Glunz, and W. Warta, *Impact of illumination level and oxide parameters on Shockley–Read–Hall recombination at the Si-SiO2 interface.* Journal of Applied Physics, 1992. **71**(9): p. 4422-4431.

167. C. J. Karlsson, F. Owman, E. Landemark, Y. C. Chao, P. Mårtensson, and R. I. G. Uhrberg, *Si $2p$ Core-Level Spectroscopy of the Si(111)-(1 \ifmmode\times\else\texttimes\fi{} 1):H and Si(111)-(1 \ifmmode\times\else\texttimes\fi{} 1):D Surfaces: Vibrational Effects and Phonon Broadening.* Physical Review Letters, 1994. **72**(26): p. 4145-4148.

168. Y. J. Chabal, *Etching of Silicon (111) and (100) Surfaces in HF Solutions: H-Termination, Atomic Structure and Overall Morphology.* MRS Online Proceedings Library, 1992. **259**(1): p. 349-360.

169. P. Dumas, Y. J. Chabal, and P. Jakob, *Morphology of hydrogen-terminated Si(111) and Si(100) surfaces upon etching in HF and buffered-HF solutions.* Surface Science, 1992. **269-270**: p. 867-878.

170. L. A. Jones, G. M. Taylor, F. X. Wei, and D. F. Thomas, *Chemical etching of silicon: Smooth, rough, and glowing surfaces.* Progress in Surface Science, 1995. **50**(1): p. 283-293.

171. N. E. Grant, J. Visualized Exp., 2016. **107**(e53614).

172. R. Walsh, *Bond dissociation energy values in silicon-containing compounds and some of their implications.* Accounts of Chemical Research, 1981. **14**(8): p. 246-252.

173. J. B. H.Ali, G.Gregory, X.Yang, M.Schneider, K.Weber, A.Javey and K. O.Davis in *IEEE 7th World Conference on Photovoltaic Energy Conversion (WCPEC) (A Joint Conference of 45th IEEE PVSC, 28th PVSEC & 34th EU PVSEC)*. 2018. p. 2192-2194.

174. B. W. H. v. d. Loo, B. Macco, J. Melskens, W. Beyer, and W. M. M. Kessels, *Silicon surface passivation by transparent conductive zinc oxide.* Journal of Applied Physics, 2019. **125**(10): p. 105305.

175. M. M. Frank, Y. J. Chabal, and G. D. Wilk, *Nucleation and interface formation mechanisms in atomic layer deposition of gate oxides.* Applied Physics Letters, 2003. **82**(26): p. 4758-4760.

176. H. Savin, P. Repo, G. von Gastrow, P. Ortega, E. Calle, M. Garín, and R. Alcubilla, *Black silicon solar cells with interdigitated back-contacts achieve 22.1% efficiency.* Nature Nanotechnology, 2015. **10**(7): p. 624-628.